

Selective catalytic reduction of NO_x over Ag/alumina

Dissertation

PETR SAZAMA

2005

University of Pardubice
Faculty of Chemical Technology
Department of Inorganic Technology

J. Heyrovský Institute of Physical Chemistry
Academy of Sciences of the Czech Republic
Department of Catalysis

Dissertation

Selective catalytic reduction of NO_x over Ag/alumina

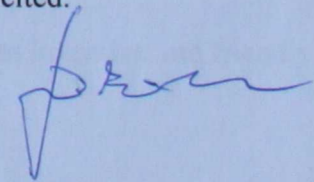
Scientific field – Inorganic Technology

Author: Ing. Petr Sazama
Supervisor: Ing. Blanka Wichterlová, DrSc.
Doc. Ing. Ladislav Svoboda, CSc.

2005

UNIVERZITA PARDUBICE	
Univerzitní knihovna	
Přir. č.	
Sign.	D 14 493
DT	

I declare that I worked out this Dissertation myself and the aid of other person is clearly stated.
All data, used from literature given in the Dissertation are cited.



This Dissertation was carried out at the Department of Catalysis of the J. Heyrovský Institute of Physical Chemistry, Academy of Sciences of the Czech Republic trough 2001-2005 years.

It is a great pleasure for me to acknowledge Dr. Blanka Wichterlová supervision and kind support during my PhD studies.

I also would like to thank to other colleagues for creating an inventive and friendly atmosphere during my studies.

Summary

The air pollution by nitrogen oxides remains a serious environmental problem in urban area. The conventional three-way catalysts used at stoichiometric engines are completely ineffective for NO reduction to N_2 under oxidizing atmosphere of lean-burn combustion at diesel engine exhausts. Selective catalytic reduction of nitrogen oxides (SCR-NO_x) into harmless nitrogen by hydrocarbons is believed to be the simplest and friendly to environment way to eliminate nitrogen oxides in diesel engine exhausts. However, the catalysts with sufficient activity, selectivity and durability under real conditions of automotive exhausts are still far from application. The silver/alumina is one of the most active and relatively stable catalysts. It exhibits high SCR-NO_x activity at high temperature region but at low temperatures it needs to be improved for practical application.

The object of the research work was analysis of the structure and operation of the most active Ag/alumina catalyst in SCR-NO_x by decane and that co-assisted by hydrogen. The study was focused on elucidation of the state of silver in Ag/Al₂O₃ catalyst and the effect of hydrogen in the enhancement of the rate of decane-SCR-NO_x reaction as well as the individual reactions steps. For that purpose a combination of reaction kinetic experiments and UV-Vis spectroscopy monitored at in-situ condition of the catalytic reactions was employed supplemented by ex-situ FTIR and TPR-H₂ techniques.

Ag⁺ ions were supported on γ -Al₂O₃ and ion exchanged into MFI zeolite with Ag loadings 1.3 - 2.88 wt.% and 1.41 - 5.91 wt.% respectively. Silver alumina possessed much higher SCR-NO_x activity than Ag-MFI catalyst. SCR-NO_x by decane and decane + O₂ and NO - NO₂ reaction steps over Ag/Al₂O₃ are greatly enhanced by hydrogen co-assistance. The effect is completely reversible. The NO_x conversion varied with reaction temperature, silver content of the catalysts, water vapor presence or absence in reactant stream, space velocity and decane, oxygen, nitrogen monoxide and nitrogen dioxide concentration in synthetic exhaust gas.

It has been concluded that Ag⁺ ions in highly active Ag/Al₂O₃ catalyst are active site in SCR-NO_x, stabilized by strong interaction with alumina support. Only a very small part of Ag⁺ is reduced to metallic charged Ag_n^{δ+} clusters ($n \leq 8$) during both the decane- and H₂/decane-SCR-NO_x reactions. The amount of the Ag_n^{δ+} clusters is related to NO_x conversion, regardless the increase of NO_x is achieved by increasing concentration of hydrogen, decane and oxygen, but they do not represent the active sites. Acceleration of the SCR-NO_x reaction by hydrogen has

been shown to originate mainly from the increased rate of oxidation of hydrocarbons and reaction intermediates, but not from the increased rate of the NO-NO₂ reaction. Hydrogen function in the C₁₀H₂₂-SCR-NO_x reaction is suggested to proceed via a radical reaction pathway. It is supposed that hydrogen dissociates, forms Ag-hydride, and then hydroperoxy and hydroxy radical species. Addition of H₂O₂ into the reactant stream, as source of radicals, has been shown to enhance also decane-SCR-NO_x over Ag/Al₂O₃. The requirement for the highly active and durable Ag/alumina is high dispersion of Ag⁺ ions stabilized on alumina surface with ability to be again re-dispersed if metallic Ag clusters are formed.

The high activity of silver alumina in C₁₀H₂₂-SCR-NO_x activated by hydrogen or H₂O₂ at low temperatures and short contact times provide promising results for further development of this catalytic system for its application at real diesel engine exhausts.

Keywords: Ag/alumina; Ag-MFI zeolite; SCR-NO_x; Hydrogen effect; Ag clusters; In situ UV-Vis

Souhrn

Znečištění vzduchu oxidy dusíku v městských aglomeracích zůstává závažným ekologickým problémem. Třícestné katalyzátory, které jsou používány pro motory se stechiometrickým spalováním, jsou zcela neefektivní pro redukcí oxidů dusíku na dusík v oxidační atmosféře chudého spalování dieselových motorů. Selektivní katalytická redukce oxidů dusíku na dusík (SCR-NO_x) uhlovodíky je považována za nejjednodušší a ekologicky šetrnou metodu pro odstranění oxidů dusíku z výfukových plynů dieselových motorů. Nicméně, katalyzátor s dostatečnou aktivitou, selektivitou a životností v podmínkách automobilových exhalátů není dostupný. Stříbro nanesené na alumině (Ag/Al₂O₃) je jeden z nejvíce aktivních a relativně stabilních katalyzátorů. Vykazuje vysokou aktivitu v oblasti vysokých teplot, ale pro praktické použití je nutné podstatně zvýšit aktivitu v nízkoteplotní oblasti.

Předmětem této práce byla analýza struktury a funkce vysoce aktivního Ag/Al₂O₃ katalyzátoru v selektivní katalytické redukci oxidů dusíku dekanem a analýza vlivu vodíku na tuto reakci. Práce byla zaměřena na objasnění stavu stříbra v Ag/Al₂O₃ katalyzátoru a vysvětlení efektu vodíku na dramatické urychlení SCR-NO_x i jednotlivých reakčních kroků. Pro tento účel byl použit komplexní přístup, který zahrnoval studium kinetiky reakce a současně stavu stříbra v katalyzátoru za reálných podmínek pomocí *in-situ* UV-Vis spektrometrie doplněný *ex-situ* FTIR, NIR a TPR-H₂ technikami.

1.3 až 2.9 hm.% stříbra bylo nanášeno v Ag⁺ formě na γ-Al₂O₃ a 1.4 až 5.9 hm.% stříbra bylo iontově vyměněno v zeolitu MFI. Katalyzátory Ag/Al₂O₃ vykazovaly mnohem vyšší aktivitu v SCR-NO_x než AgMFI katalyzátor. Konverze NO_x se mění s reakční teplotou, obsahem stříbra v katalyzátoru, přítomností vody v reakční směsi, zatížením katalyzátoru a koncentrací dekanu, kyslíku oxidu dusnatého a oxidu dusičitého v syntetických výfukových plynech. SCR-NO_x dekanem a oxidace dekanu a NO byly významně podporovány přítomností vodíku v reakční směsi. Tento efekt je zcela reverzibilní.

Aktivními centry ve vysoce aktivním Ag/Al₂O₃ katalyzátoru jsou Ag⁺ ionty stabilizované silnou interakcí s povrchem aluminu. Pouze malá část velmi aktivních Ag⁺ iontů je redukována na kovové nabitě klastry Ag_n^{δ+} ($n \leq 8$) během SCR-NO_x dekanem nebo dekanem za přítomnosti vodíku. Množství Ag_n^{δ+} ($n \leq 8$) přítomných na katalyzátoru je spojeno s NO_x konverzí, nezávisle na tom zda je vyšší konverze dosaženo zvýšenou koncentrací vodíku, dekanu nebo kyslíku, ale tyto klastry nerepresentují aktivní centrum pro SCR-NO_x. Efekt vodíku na SCR-NO_x má původ

zejména v propagaci oxidačních reakcí uhlovodíku a reakčních intermediátů, ale ne ve zvýšené oxidaci NO na NO₂. Je navržena funkce vodíku v mechanismu SCR-NO_x spočívající v propagaci radikálových reakcí. Předpokládáme, že vodík disociuje, tvoří Ag-hydrid a hydroperoxy a peroxy radikály. Dávkování peroxidu vodíku, jako zdroj radikálů, do reakční směsi také významně podporuje SCR-NO_x dekanem.

Podmínkou pro katalyzátor s vysokou a trvalou aktivitou je vysoká disperzita Ag⁺ iontů stabilizovaných na povrchu aluminy se schopností zpětné redispergace, jestliže vznikají kovové klastry.

Vysoká aktivita Ag/Al₂O₃ katalyzátoru v SCR-NO_x dekanem aktivované za nízké teploty nebo krátké doby zdržení přítomností vodíku nebo peroxidu vodíku poskytuje slibný výsledek pro další vývoj tohoto katalytického systému pro jeho aplikaci pro dieselové motory.

Klíčová slova: Ag/alumina; Ag-MFI zeolit; SCR-NO_x; Efekt vodíku; Ag klastry; In situ UV-Vis

Content

Summary.....	1
Souhrn.....	3
Content.....	5
1 Introduction.....	9
1.1. Nitrogen oxides	9
1.2 NO _x abatement.....	9
1.2.1 NO _x abatement in reducing atmosphere	9
1.2.2 NO _x abatement in oxidising atmosphere	10
1.3 NO _x emission from lean burn engines.....	11
1.4 NO _x emission control for lean burn engines.....	12
1.4.1 Decomposition of NO to N ₂ and O ₂	14
1.4.2 NO _x Storage catalysts	14
1.4.3 Selective catalytic reduction of NO _x by urea	14
1.4.4 Selective catalytic reduction of NO _x by hydrocarbons	15
1.4.4.1 Reducing agents for selective catalytic reduction of NO _x by hydrocarbons	15
1.4.4.2 Catalysts for selective catalytic reduction of NO _x by hydrocarbons	16
1.4 Selective catalytic reduction of NO _x by hydrocarbons over silver catalysts	17
1.4.1 Supports for silver catalysts.....	17
1.4.2 Preparation of silver catalysts.....	20
1.4.3. Activity of the silver catalysts at SCR-NO _x by hydrocarbons	20
1.4.4 Reducing agents at selective catalytic reduction of NO _x over silver catalysts	21
1.4.5 State of silver on silver/alumina catalysts	22
1.4.6 Active sites at selective catalytic reduction of NO _x by hydrocarbons over silver/alumina	23
1.4.7 Reaction mechanism of selective catalytic reduction of NO _x by hydrocarbons over silver/alumina	24
1.5 Enhancement of decane-SCR-NO _x over silver catalyst by hydrogen.....	25
Aim	26
2 Experimental.....	27
2.1 Catalysts preparation	27

2.1.1	Silver zeolite catalysts	27
2.1.2	Silver alumina catalysts	27
2.2	Catalyst testing in the C ₁₀ H ₂₂ -SCR-NO _x reactions, and NO, H ₂ and C ₁₀ H ₂₂ oxidation	28
2.2.1	Catalytic apparatus	28
2.2.2	Product analysis	29
2.3	H ₂ -TPR	34
2.4	FTIR spectroscopy	34
2.6	Diffuse reflectance UV-Vis-NIR spectroscopy	35
2.4.1	Ex-situ diffuse reflectance UV-Vis-NIR spectroscopy	35
2.4.2	In-situ diffuse reflectance UV-Vis-NIR spectroscopy	35
3	Results	37
3.1	Characterisation of the silver catalyst structure	37
3.1.1	UV-Vis spectra of silver alumina	37
3.1.2	UV-Vis spectra of silver MFI	38
3.1.3	H ₂ -TPR of silver catalysts	39
3.1.4	Interaction of silver with the support at the silver catalysts	41
3.1.4.1	NIR spectra of silver MFI	41
3.1.4.2	NIR spectra of silver alumina	42
3.1.4.2	FTIR spectra of d ₃ -acetonitrile	44
3.2	Activity of silver catalysts in selective catalytic reduction of NO _x	46
3.2.1	Selective catalytic reduction of NO _x by decane over silver alumina catalyst	46
3.2.2	Selective catalytic reduction of NO _x over silver alumina catalyst by decane and hydrogen	52
3.2.3	Selective catalytic reduction of NO _x over silver zeolite catalyst by decane and co-assisted by hydrogen	57
3.3	Effect of hydrogen on selective catalytic reduction of NO _x over silver alumina catalyst	59
3.3.1	Effect of hydrogen concentration on selective catalytic reduction of NO _x	59
3.3.2	Reversibility of the hydrogen effect on selective catalytic reduction of NO _x	60
3.3.3	Effect of hydrogen on selective catalytic reduction of NO _x as a function of GHSV	61

3.3.3	Effect of hydrogen on selective catalytic reduction of NO _x as a function of GHSV	61
3.3.4	Effect of water vapour on selective catalytic reduction of NO _x by decane and hydrogen	63
3.3.5	Oxidation of hydrogen, and effect of hydrogen on oxidation of NO and decane	63
3.3.6	Effect of NO vs. NO ₂ on selective catalytic reduction of NO _x by decane and hydrogen	67
3.3.7	Effect of H ₂ vs. CO as a co-reactant on selective catalytic reduction of NO _x by decane	67
3.4	State of silver at silver alumina catalyst at the conditions of the catalytic process	68
3.4.1	Reduction of Ag/alumina by hydrogen	68
3.4.2	Oxidation of H ₂ and CO by oxygen	71
3.4.3	Oxidation of NO to NO ₂ by molecular oxygen and the effect of hydrogen presence	76
3.4.4	Adsorption of NO _x species on silver alumina catalyst	77
3.4.5	Selective catalytic reduction of NO _x depending on H ₂ /C ₁₀ H ₂₂ /O ₂ compositions	79
3.4.5.1	Effect of hydrogen concentration	79
3.4.5.2	Effect of decane and oxygen concentration	83
3.4.6	Rate of growth and redispersion of Ag _n ^{δ+} clusters at SCR-NO _x	86
3.4.7	Selective catalytic reduction of NO _x by decane at CO vs. H ₂ presence	88
3.5	Selective catalytic reduction of NO _x enhanced by hydrogen peroxide over silver alumina catalyst	90
4	Discussion	93
4.1	Structure of the silver catalyst	93
4.1.1	State of silver in alumina and MFI zeolite	93
4.1.2	Reducibility of silver catalysts	94
4.1.3	Interaction of silver with the supports	96
4.1.4	Relationships among the Ag state, interaction with the support and reducibility of silver species	97
4.2	Selective catalytic reduction of NO _x by decane over silver catalysts	97
4.2.1	General features of the SCR-NO _x reactions over silver alumina catalysts	97

4.2.2	Activity of silver catalysts	98
4.2.3	Effect of reactant composition on SCR-NO _x over silver alumina	99
4.3	State of silver at the reaction conditions.....	102
4.3.1	Analysis of Ag species by UV-Vis spectra	102
4.3.2	Ag species under the reaction conditions of oxidation of H ₂ and NO by molecular oxygen	104
4.3.3	Ag species under the decane-SCR-NO _x reaction and that co-assisted by hydrogen and carbon monoxide.....	105
4.6	Function of hydrogen at SCR-NO _x over silver alumina catalyst.....	109
4.7	Enhancement of SCR-NO _x over silver alumina catalyst by hydrogen peroxide	110
4.8	Active site at SCR-NO _x over silver alumina catalyst	111
5	Conclusions.....	113
	References.....	115
	Index to abbreviations and symbols	119
	Publications.....	122

1 Introduction

1.1. Nitrogen oxides

Nitrogen has six different oxides NO, N₂O, NO₂, N₂O₃, N₂O₄ and N₂O₅. The most populated nitrogen oxides are nitric oxide (NO) and nitrogen dioxide (NO₂). The generic term nitrogen oxide/s (NO_x) is usually used to refer to NO and NO₂ or a mixture of them [1].

The source of NO_x in exhaust gases of combustion processes is oxidation of molecular nitrogen from air at high temperature (thermal NO_x) and of nitrogen compounds present in fuel (fuel NO_x), i.e. in the coal and oil. The rate of formation of NO_x is primary function of temperature and the residence time. During combustion, the nitrogen bound in the fuel is released as a free radical and ultimately forms free N₂ or NO. Fuel NO_x can contribute as much as 50% of total emissions when combusting oil and as much as 80% when combusting coal [2].

The primary manmade sources of NO_x are motor vehicles, electric utilities, and other industrial, commercial, and residential sources that burn fuels. Mobile sources are responsible for more than half of all nitrogen oxide emissions in the United States [2]. Chemical industry particularly nitric acid plants are also significant sources of NO_x emission.

NO_x causes a wide variety of health and environmental impacts. It is one of the main ingredients involved in the formation of ground-level ozone, nitrate particles and acid aerosol, which can trigger serious respiratory problems. It also contributes to atmospheric particles that cause visibility impairment and formation of acid rain [2,3].

While there are strong limits for NO and NO₂ emissions there is no limit for N₂O; N₂O₃, N₂O₄ and N₂O₅ are unstable [2]. Therefore, various processes have been developed to abate NO_x and further advanced processes are under development.

1.2 NO_x abatement

1.2.1 NO_x abatement in reducing atmosphere

A three-way catalytic converters are now standard equipment in cars with stoichiometric gasoline engine. A three-way catalytic converter has three simultaneous tasks:

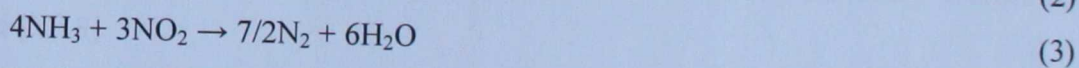
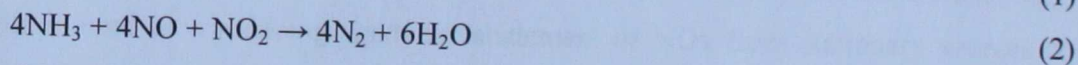
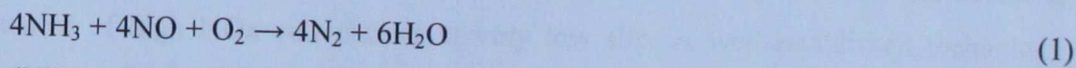
- Oxidation of carbon monoxide to carbon dioxide.
- Reduction of nitrogen oxides to nitrogen.
- Oxidation of hydrocarbons (unburned fuel) to carbon dioxide and water.

These three processes are most balanced at the stoichiometric point, where there is a balanced amount of oxygen to fuel in the engine. When there is more oxygen than required, then the system is said to be running lean, and the system is in oxidizing conditions. The above two oxidation reactions (of CO and hydrocarbons) are favoured at this conditions, but reduction of nitrogen oxides to nitrogen becomes ineffective. When there is more fuel than oxygen (stoichiometrically), then the engine is running at rich conditions and the reduction of NO_x is favoured [4].

1.2.2 NO_x abatement in oxidising atmosphere

Nitric acid tail gas

Waste gas from nitric acid plants downstream from the absorption column typically contains 200 – 3,000 ppm NO_x, 1,000 – 2,000 ppm N₂O and 1 – 4% O₂. Since the mid-seventies, selective catalytic reduction of NO_x by ammonia has been installed at nitric acid plants for NO_x abatement [2]. But as there is no limit for N₂O, no one takes care for N₂O pollution, although N₂O is more dangerous greenhouse gas compared to NO_x. NO_x at selective catalytic reduction reacts with ammonia, which is provided as a reducing agent. NH₃ is adsorbed on the catalyst and reacts with NO₂ and NO to give N₂ and H₂O. The majority of commercial installations use the V₂O₅/TiO₂ or V₂O₅-WO₃/TiO₂ catalyst as extruded monoliths. Some installations use a Cu-zeolite catalyst technology [5], advantage of which is operation at much lower temperature. The main reactions of the SCR-NO_x with ammonia are



These reactions implies 1:1 stoichiometry for NH₃ and NO and a participation of oxygen.

Exhaust from power plants

The NO_x emissions are primarily reduced by advanced system of fuel burning [6]. There are also installations where selective catalytic reduction systems selectively reduce NO_x by ammonia to form molecular nitrogen and water using V₂O₅/TiO₂ catalyst.

Exhaust from lean burn engines

Lean burning is an internal combustion of lean air-fuel mixtures. It occurs at high air-fuel ratio (typically 22:1), so the mixture has considerably less amount of fuel in comparison to

stoichiometric combustion ratio (14.6:1 for gasoline engines). The engines with lean burning provide much better performance with respect to efficiency of fuel use and thus low exhaust emissions of carbon oxides than those in conventional gasoline engines. The diesel engine operating at lean conditions is one of the most efficient energy converters of today, with up to 50% of the chemically bound fuel energy transformed into kinetic energy. Its high efficiency results in a low emission of carbon dioxide, nevertheless others emission characteristics such as emission of nitrogen oxides are high. The main drawback of lean burning is large amount of NO_x being generated, so a complex catalytic converter system is required (see Chapters 1.3 and 1.4). The three-way catalyst cannot remove nitrogen oxides in lean-burn engine exhausts containing oxidizing atmosphere [2,3,4].

1.3 NO_x emission from lean burn engines

There are two types of applications of lean burn engines - stationary and mobile diesel engines.

Stationary sources

A stationary diesel engine such as power generators or irrigation pumps is operated at constant load and there is actually no restriction concerning of the size of the SCR catalyst. That allows high values of contact time, simple control for the dosage of reducing agents and thus achievement of high NO_x conversions at very low slip. A well-established technology where ammonia is used as a reducing agent for abatement of NO_x from stationary sources could be applied [5,7,8].

Mobile sources

The requirements for NO_x abatement in a mobile diesel engine in a personal car or truck are completely different to the stationary sources of NO_x emissions. Firstly, load and engine speed vary often and abruptly, and this cause permanent changes of flow and temperature of the exhaust gas. A sophisticated control for the dosage of reducing agent is therefore necessary. In addition a catalyst has to be effective at broad temperature region. Moreover, the space available for a mobile De-NO_x system is very limited; therefore, typical space velocities (GHSV) are being

high, ranging from 30,000 to 60,000 h⁻¹, in short period to 120,000 h⁻¹. Further problems are represented by high concentration of water vapour (up to 12%) and presence of sulphur oxides in exhaust gases, which both by strong interaction with the catalyst causes its deactivation [1,2,7,8].

1.4 NO_x emission control for lean burn engines

The desire to reduce NO_x emission has been driven by legislation [3]. An indication of the extent to which legislation has been tightened in recent years is given by the fact that since the uncontrolled emissions level in 1966 the NO_x emissions have had to be reduced by more than 95%, of which the final most difficult part has come since the early 1990s (Table 1-1) [7].

In principle, there might be several possible ways from chemical viewpoint how eliminate nitrogen oxides from exhaust of diesel engines: Decomposition of NO to N₂ and O₂, NO_x storage with subsequent NO_x reduction in reducing atmosphere, selective catalytic reduction of NO_x by urea and selective catalytic reduction of NO_x by hydrocarbons in oxidizing atmosphere.

One of the main problems of diesel emissions is also particulate matter (PM). To eliminate the PM from exhaust gases various types of filter are used with high efficiency. The filters can contain Pt and/or Pd to oxidise trapped soot particles as well as NO. Provided NO₂ is much more effective oxidant than O₂, so it removes PM with high efficiency [7].

The opportunities of approaches for NO_x abatement at diesel exhaust by catalytic processes are described in the following paragraphs.

Table 1-1 Development of European emissions requirements [2,3,7].

Gasoline engine vehicles

Year	Mass CO g.km ⁻¹	Mass HC g.km ⁻¹	Mass HC + NOx g.km ⁻¹	Mass NOx g.km ⁻¹
1996 (EURO II)	2.2		0.5	
2000 (EURO III)	2.3	0.20		0.15
2005 (EURO IV)	1.0	0.10		0.08

Light duty diesel engine vehicles

Year	Mass CO g.km ⁻¹	Mass HC + NOx g.km ⁻¹	Mass NOx g.km ⁻¹	Particulates g.km ⁻¹
1996 (EURO II)	1.00	0.7		0.08
2000 (EURO III)	0.64	0.56	0.50	0.05
2005 (EURO IV)	0.50	0.30	0.25	0.025

Heavy duty diesel vehicles

Year	Mass CO g.kWh ⁻¹	Mass HC + NOx g.kWh ⁻¹	Mass NOx g.kWh ⁻¹	Particulates g.kWh ⁻¹
1996 (EURO II)	4.00	1.10	7.0	0.25
2000 (EURO III)	2.10	0.66	5.0	0.10
2005 (EURO IV)	1.50	0.46	3.5	0.02
2008 (EURO V)	1.50	0.46	2.0	0.02

1.4.1 Decomposition of NO to N₂ and O₂

Nitrogen monoxide is the simplest thermally stable odd-electron molecule and it is well known that NO decomposition to N₂ and O₂ is thermodynamically feasible at temperatures below 1200 K. Catalytic NO decomposition would be the simplest and most elegant method for its removal. However, the rate of decomposition is very low due to very high activation energy, therefore, highly efficient catalyst would be necessary [9]. Cu-MFI catalyst developed by Iwamoto [10] provides relatively high decomposition activity. But to-date, however, no catalyst with durable high activity in oxidizing atmosphere has been developed. This is due to fact that oxygen contained in the feed or produced in the decomposition of NO, oxidizes the active sites and competes with NO for adsorption sites. Also water vapor present in the exhaust gases decreases substantially the activity. As a result, high temperature and/or reducing agents are required to remove surface oxygen and regenerate catalytic activity [9].

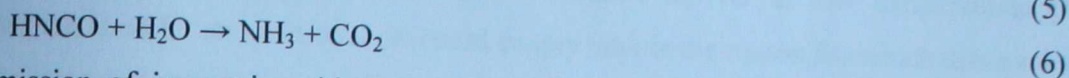
1.4.2 NO_x Storage catalysts

A commercial NO_x storage-reduction (NSR) catalyst system first appeared in the marketplace in Japan in 1994 [7]. The air/fuel ratio (A/F) in an engine feed is alternated between the stoichiometric value and lean value. NO_x is trapped when the engine is running lean, through the conversion of surface barium carbonate to nitrate, and it is transferred back when the engine is running rich by the reverse reaction coupled with NO_x reduction through a conventional TWC reaction. A typical NSR catalyst comprises Pt, to oxidize NO to NO₂ in order to enhance the efficiency of the trapping reaction, barium, which is present as a carbonate because the high levels of CO₂ in the normal exhaust, is used to trap NO₂, and frequently Rh is added to facilitate the reduction of NO, mainly by CO, under rich regeneration conditions [7]. A problem of NSR catalyst is its poisoning by SO₂. SO₂ in exhaust is readily oxidized to SO₃ on Pt component of the NSR catalyst and this SO₃ reacts rapidly with barium compounds to form a sulphate that is much more stable than either nitrate or carbonate. Regeneration of sulphate-poisoned catalyst requires very high temperature (with an associated fuel penalty).

1.4.3 Selective catalytic reduction of NO_x by urea

Selective catalytic reduction of NO_x using urea as reducing agent (urea-SCR-NO_x) is commercially accessible technology, which can fulfil present NO_x emission limit. The standard

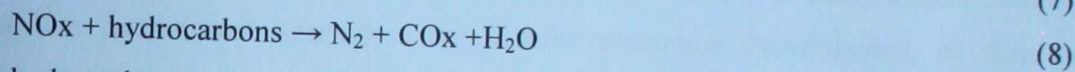
catalyst systems are based on $V_2O_5-WO_3$ or $V_2O_5-MoO_3$ supported on TiO_2 similar to that used in $NH_3-SCR-NO_x$ technology. If urea is used instead of ammonia the de- NO_x chemistry involves isocyanic acid as an intermediate.



The emission of isocyanic acid may occur producing ammonia slip at low temperature. In addition, isocyanic acid may react to higher products like biuret, melamine, cyanuric acid etc. [8]. Possible formation of all these compounds is the reason why the EPA in USA in 2002 has not approved the urea technology for applications at diesel engines [2].

1.4.4 Selective catalytic reduction of NO_x by hydrocarbons

In selective catalytic reduction of NO_x by hydrocarbons (HC-SCR- NO_x), hydrocarbon is used as the reducing agent and is injected into the flue gas stream, passing over a catalyst. Overall reactions of the SCR- NO_x process are



The temperature window in the diesel engine exhaust is usually between 473 and 723 K. The non-selective oxidation of hydrocarbons by oxygen causes losses of reducing the agent [3].

Research of HC-SCR- NO_x for lean NO_x after-treatment system began in the early 1980s. So far there is no catalyst, which could fulfil the requirements for NO_x abatement at lean-burn conditions. Thus, HC-SCR- NO_x in the oxygen-rich exhaust stream of lean-burn engines remains one of the major challenges for environmental catalysis.

1.4.4.1 Reducing agents for selective catalytic reduction of NO_x by hydrocarbons

Efficiency of HC-SCR- NO_x depends markedly on the nature of the reducing agent. Academic studies have tended to focus on the use of C1-C3 alkenes and alkanes as reductants [11,12,13,14]. Longer chain hydrocarbons (e.g. C8-C10), like those typically found in diesel fuels already on board, have attracted less attention [15,16]. The long chain alkanes usually give higher conversion of NO to N_2 at low temperatures. The greater enthalpy of adsorption of the longer

alkane chains and the weaker C-H bond strength of their methylene groups explain their higher reactivity and thus ability to react at lower temperature [3].

The oxygenated molecules as reducing agents have also been investigated. Alcohols and esters appear to give advantageously high conversion of NO at low temperatures [17,13]; however, the need for an additional on-board supply tank is the reason for which these substances are not considered as reductants of NO_x at exhaust gases of diesel engines [3].

1.4.4.2 Catalysts for selective catalytic reduction of NO_x by hydrocarbons

The first catalysts for HC-SCR-NO_x under oxidizing conditions were reported Cu-MOR and Cu-MFI [7]. Among various metal zeolite catalysts investigated the Cu-MFI was tolerant to water vapor but at long-term hydrothermal conditions it exhibited declination in activity. Low activity or a severe decline in the NO conversion was observed on chromium, iron, manganese, vanadium, cobalt, nickel ion exchanged several types of zeolites. Introduction of noble metals (platinum, rhodium, iridium) into MFI zeolite gave catalysts with low conversion in a rather narrow temperature range, with formation of N₂O and NO₂ [7]. Many others zeolite based catalyst have been found to catalyse the SCR-NO_x reaction. Nevertheless, all these catalyst proved to be inferior in comparison to Cu-MFI.

An alternative to the zeolite-based catalysts is development of non-zeolite based catalysts with high activity and durability for lean-NO_x reduction. Alumina is widely used as support in current automotive catalysts and is naturally the first choice as a support. Various alumina-supported metal oxide catalysts has been studied. However, the addition of Sn, Ga, Co, Ni oxides supported on alumina did not lead to high activity [15]. Pt/Al₂O₃ catalysts exhibited high activity for the NO_x reduction but only in the low-temperature range (473–523 K). Moreover, all the platinum-based catalysts present a serious drawback, i.e. formation of N₂O as a by-product. In 1993, Miyadera [18] found that an alumina-supported silver (Ag/Al₂O₃) catalyst is highly effective for SCR-NO by C₃H₆ and C₂H₅OH. Ag/Al₂O₃ exhibited considerably higher activity for the SCR-NO_x than Cu/Al₂O₃, especially at high temperature region [19].

At present, it is recognized that Ag/Al₂O₃ is one of the most active alumina-based catalyst for NO_x reduction with hydrocarbons or oxygenated hydrocarbons. It exhibits high activity at the conditions of real exhaust gas from diesel engine at temperatures above 620 K. But this catalyst

needs to be substantially improved at low temperatures (470-620 K), which is important for diesel engine exhaust.

1.4 Selective catalytic reduction of NO_x by hydrocarbons over silver catalysts

After more than 10 years of research on the Ag/alumina system, a breakthrough has not yet been achieved proving the significance of a silver-containing catalyst for commercial exhaust gas cleaning of gasoline or diesel engines under road conditions [20]. The complex process of the SCR-NO_x reaction over Ag/Al₂O₃ is not completely understood from the viewpoint of the reaction mechanism as well as the structure of active sites. The potential of silver-based supported catalysts for the selective catalytic reduction (SCR) of nitrogen oxides to nitrogen has recently been reviewed by Burch et al. [3] and Satsuma and Shimizu [21] summarized the present knowledge on mechanistic details of NO reduction over alumina-based catalysts.

1.4.1 Supports for silver catalysts

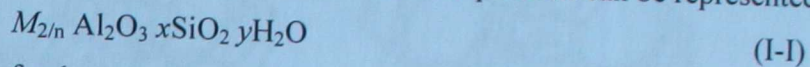
It has been recognized that silver on γ -Al₂O₃ alumina or located in MFI zeolite represent the most active silver catalysts for NO reduction with hydrocarbons or oxygenated hydrocarbons at lean conditions [3,21].

γ -Al₂O₃

Among various requirements, an effective automotive catalyst for lean NO_x reduction must be able to withstand both high temperatures and high concentrations of water vapor. As γ -Al₂O₃ can be prepared in a hydrothermally stable form, a γ -Al₂O₃-supported metal or metal oxide may be a practical lean NO_x reduction catalyst [14]. The γ -Al₂O₃ has a spinel-like structure; the oxygen lattice is built up by a cubic close-packed stacking of anions and aluminum atoms occupy both octahedral and tetrahedral sites. The surface of γ -Al₂O₃ can be regarded as an extended defect and therefore can be easily covered by various types of adsorbed species [22]. The alumina surface has acid-base character, however, the basicity is rather low. In general, alumina provides possibility for stabilization of small metal particles and/or metal ions [23].

MFI zeolite

Among high silica zeolites, rather stable at hydrothermal conditions, a zeolite of MFI structure exhibits advantageous pore architecture, more stable structure and well accessible cationic sites. MFI zeolite is crystalline aluminosilicates with well-defined crystallographic 10-member ring intersecting channels with distinct size of pores. This provides large inner surface area and low atomic density of the unit cell. Chemical composition can be represented as:



Where M is a cation of valency n ; x has value equal to or greater than ca 25. The aluminosilicates consist of SiO_4 tetrahedra in which each silicon is joined to four oxygen situated at the corners of a tetrahedron. The SiO_4 tetrahedra are linked to the other tetrahedra through shared oxygen atoms forming three dimensional framework structures. The framework structure of MFI is depicted in Fig. 1-1 [24,25].

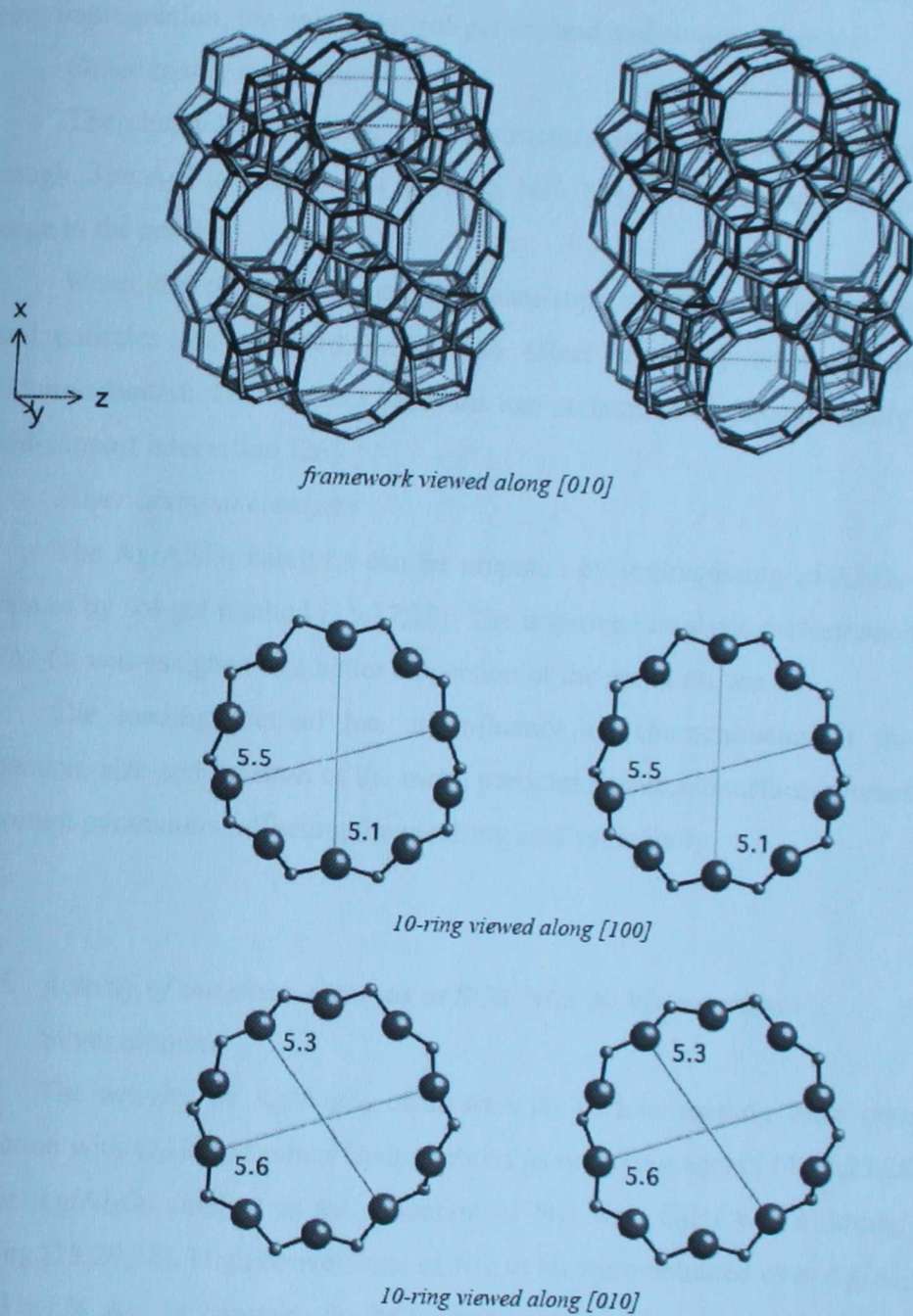


Fig. 1-1 Structure of zeolite MFI with the indication of pore diameter (Å).

1.4.2 Preparation of silver catalysts

Silver can be loaded into alumina and zeolite by various methods, the most widely used being impregnation, ion exchange, sol-gel method and co-precipitation.

Silver zeolite catalysts

The channels within the zeolite structure are large enough for the Ag^+ ions to diffuse through. The Ag^+ ion exchanges ion (e. g. Na^+ , NH_4^+), which neutralise the negative framework charge in the zeolite.

When impregnation is used, the metal-support interaction in zeolites is weaker, and large metal particles are obtained, which can affect secondary reactions, namely those that are structure-sensitive. On the other hand, the ion-exchange technique normally brings about a strong metal-support interaction [26].

Silver alumina catalysts

The $\text{Ag}/\text{Al}_2\text{O}_3$ catalysts can be prepared by impregnating of Al_2O_3 by solution of silver nitrate or by sol-gel method [15,27,28]. The improved catalytic performances of sol-gel-prepared $\text{Ag}/\text{Al}_2\text{O}_3$ was assigned to a better dispersion of the metal cations.

The loading method has an influence on characteristics of the catalysts as metal dispersion, size and location of the metal particles and metal-surface interactions. All of them are important parameters, affecting the resulting catalyst activity.

1.4.3. Activity of the silver catalysts at SCR-NOx by hydrocarbons

Silver alumina

The activity of $\text{Ag}/\text{Al}_2\text{O}_3$ catalysts with various loading were compared for lean NO reduction with C_3H_6 and others hydrocarbons as reducing agent [14,18,29,28]. The effectiveness of the $\text{Ag}/\text{Al}_2\text{O}_3$ catalyst in the reduction of NO with C_3H_6 was a strong function of the Ag loading [18,29,28]. High conversions of NO to N_2 were obtained over $\text{Ag}/\text{Al}_2\text{O}_3$ with loadings of 2 – 3 wt.% Ag. In contrast, the NO conversions to N_2 were much lower over highly loaded $\text{Ag}/\text{Al}_2\text{O}_3$ (~6 wt.%), and this catalyst formed a substantial amount of N_2O [14]. Jen [30] has shown that the de-NOx efficiency for $\text{Ag}/\text{Al}_2\text{O}_3$ varies significantly with the type of Al_2O_3 support used. In some case high activity was observed for silver loading up to ca 5 wt.% Ag [27,30]. Surface area as well as narrow distribution of pore-size appears to be important [30]. The

methods of introduction of silver into Al_2O_3 have also an effect on activity of $\text{Ag}/\text{Al}_2\text{O}_3$ (see chapter 1.4.2).

Silver zeolite catalysts

The conversion of NO_x to N_2 at CH_4 -SCR- NO_x over Ag-MFI catalysts increases with silver loading up to 11 wt.%. Further increase in loading (>11 wt.%) decreased the NO conversion [31]. Silver ions in the zeolite cation sites are inevitable necessary for the SCR-NO by methane. Without presence of isolated silver ions (only nano-sized silver particles exist on the outer surface of zeolite), the catalyst showed much lower activity and selectivity in the SCR reaction. Nevertheless, the activity was significantly enhanced by the nano-sized silver particles, besides isolated Ag^+ ions, if methane was used as reducing agent [31].

Among $\text{Ag}/\text{Al}_2\text{O}_3$, Ag-MFI and Ag-MOR studied in Ref. [32], the $\text{Ag}/\text{Al}_2\text{O}_3$ catalyst showed superior activity in comparison with the Ag-MOR and Ag-MFI catalysts in the temperature range 623-723 K. Within zeolite based catalysts Ag-MFI displays higher activity compared with Ag-MOR [47].

1.4.4 Reducing agents at selective catalytic reduction of NO_x over silver catalysts

The efficiency of HC-SCR- NO_x strongly depends on the reductant type. In general using more reactive reductants yields higher NO_x conversion at low temperatures. Especially C_3H_6 as a reducing agent has been investigated at selective catalytic reduction of NO_x over silver catalysts [27,28,32]. E.F. Iliopoulou et al. [33] tested C_2H_4 , C_2H_6 , C_3H_8 , C_4H_{10} , 1- C_4H_8 and 1,3- C_4H_6 as reducing agents. 1- C_4H_8 was the most efficient reductant not only increasing the maximum NO_x conversion, but exhibiting the lower and wider active temperature window as well. Miyadera reported [18] that also oxygen-containing organic compounds such as ethanol and acetone were more effective than propene in reducing nitric oxide over $\text{Ag}/\text{Al}_2\text{O}_3$ in the presence of water and excess oxygen. The most suitable reductant from practical viewpoint would be Diesel fuel. The high activity and durability of the $\text{Ag}/\text{Al}_2\text{O}_3$ catalyst for the NO_x reduction could be achieved by using the fuel injected before the catalyst [34].

1.4.5 State of silver on silver/alumina catalysts

Data concerning the electronic states of silver on surfaces of oxide supports are important for obtaining an insight into the nature of active sites for the catalytic reactions at the SCR-NO_x process. The state of silver was studied by various methods, FTIR [35], XRD [35,36], ESR [37, 38], ¹H MAS NMR and ¹²⁹Xe NMR [39, 40], XPS [41], UV-Vis [42,43,44,45]. The results of these studies show that silver can be supported on Ag/Al₂O₃ at different states: silver ions Ag⁺, silver charged clusters Ag_n^{δ+} and silver metallic particles.

Stabilization of Ag⁺ ions on γ-alumina depends on silver loading. Highly dispersed Ag⁺ ions are dominant Ag species on the low loading samples (ca 2 wt.%) [14,16,34,42,43,44,45, 46,47]. However, the local structure of species, containing Ag⁺ ions has not been ascertained. Supported Ag₂O clusters [20] or silver aluminate [29, 34] were observed in high active Ag/Al₂O₃. The formation of silver aluminate was confirmed by EXAFS and X-ray diffraction [29, 34].

In generally, reduction of silver ions in Ag/Al₂O₃ yields metallic silver with particle diameters of several nanometers. When a partial reduction is carried out oligomeric silver charged clusters Ag_n^{δ+} various nuclearity and charge could be formed. These Ag_n^{δ+} clusters could be stabilized in Ag/Al₂O₃ [14,16,45]. Crystalline Ag phases and large silver clusters are detectable in highly loaded Ag/Al₂O₃ (≥ 6 wt.% Ag) catalysts [14,16, 29,45,46] at the reaction conditions of the SCR process. The 2 wt.% Ag/Al₂O₃ was supposed to contain silver in the +1 oxidation state under reaction conditions, while the 6 wt.% Ag/Al₂O₃ catalyst contained Ag⁰ particles.

Bethke and Kung [14] showed that the oxidation states of Ag in Ag/Al₂O₃ were different under reaction conditions. The structure of a silver catalyst is very dynamic and readily transforms among Ag⁺, Ag_n^{δ+} clusters and metallic particles when changing the oxidative and reductive environment over the catalyst. As a consequence, *ex-situ* studies of the catalyst structure are of small relevance for elucidating the active site and the catalysts should be characterized under relevant catalytic conditions. To fulfil this condition, i.e. to find optimal conditions for measuring at the same conditions the catalyst performance and spectroscopic data, is not an easy task. This experimental gap has led, in some cases, to contradictory or, at least, confusing conclusions on the type and nature of active sites (see chapter 1.4.6). The appropriate approach is therefore to study silver catalysts inside a reactor by spectroscopic means at the same conditions, i.e. temperature, contact time, pressure and reactor design.

1.4.6 Active sites at selective catalytic reduction of NO_x by hydrocarbons over silver/alumina Ag⁺ ions

High dispersion of Ag⁺ ions, preserved as a result of a strong interaction with alumina support has been suggested to be indispensable for HC-SCR-NO_x to N₂ [14,16]. The difference in de-NO_x activity of the 2 wt.% and 6 wt.% Ag/Al₂O₃ were attributed to the much higher Ag dispersion for the 2 wt.% than the 6 wt.% of Ag, where also metallic particles were formed.

However, nature of active species, which contain Ag⁺ ions, has not been yet ascertained. Small Ag-aluminate "clusters" [14,34,45] or Ag₂O clusters of appropriate size [20] were suggested as the active sites.

Metallic silver

The low NO_x conversion during SCR-NO_x was reported over the highly loaded samples of Ag/Al₂O₃ [14,16,45,46]. Therefore, it was suggested that metallic silver is not active site for SCR-NO_x. The presence of Ag⁰ resulted in a high rate of C₃H₆ combustion at the expense of NO_x reduction [14]. The presence of Ag⁰ in the catalyst resulted also in formation of a substantial amount of N₂O [14].

Silver clusters - Ag_n^{δ+}

In recent work [48] Satokawa and co-workers suggested that the active sites are small silver clusters. They observed same structure-activity relationship and supposed that the small silver clusters, probably the Ag₄²⁺, are responsible for the selective reduction of NO by C₃H₈ [49].

It can be concluded that the definite conclusion on the structure of active site in Ag/Al₂O₃ at SCR-NO has not been made.

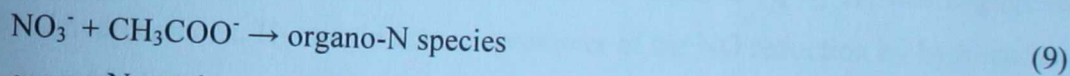
1.4.7 Reaction mechanism of selective catalytic reduction of NO_x by hydrocarbons over silver/alumina

The reaction mechanism of HC-SCR-NO_x over Ag/Al₂O₃ catalyst, including several reaction steps, is extremely complex. Much attention has been devoted to elucidation of the reaction mechanisms but so far it is not completely understood.

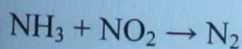
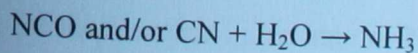
The *in-situ* FTIR spectroscopy investigations under the HC-SCR-NO_x reaction were used to try to identify key reaction intermediates [16,50,51,52]. From these extensive studies, it is clear that several intermediates are present under reaction conditions – nitrates and nitrites, cyanides and isocyanates, carboxylates and acetates and organo-nitrogen species. However, it is less clear which species are true intermediates or spectator species in the NO reduction to N₂. Shimizu et al. [16] on the basis of their results, and those given in the literature proposed a set of reaction steps (not elementary) for SCR-NO by hexane. They suggested that the reaction starts with formation of adsorbed nitrates via NO oxidation by O₂ (7) and formation of acetates by partial oxidation of a hydrocarbon with O₂ (8).



The acetate, which acts as a surface reductant, reduces nitrates via several steps to N₂. N-containing hydrocarbon species, Ag⁺-NCO and -CN adspecies, are formed, possibly via organo-nitrogen species (9,10) [12,50]. Ag⁺-NCO and -CN adspecies react with nitrates and O₂ to produce N₂, (12) [51,52].



NH₃ may be easily produced through hydration of NCO⁻ and CN⁻ species (12) [12,53] and can further react with NO₂ to produce N₂ (13) [12,53,54].



However He et al. [55] showed that C₃H₆ at C₃H₆-SCR-NO over Ag/Al₂O₃ and Cu/Al₂O₃ can be partially oxidized into enolic species and acetate species on the catalysts. The enolic species is more reactive intermediate for the formation of NCO species via the reaction with NO + O₂ than acetate species. However, the C₃H₆ can only be partially oxidized into acetate species

and then CO_2 on the $\text{Cu}/\text{Al}_2\text{O}_3$ catalyst. This has been indicated as the main reason why the activity of the $\text{Cu}/\text{Al}_2\text{O}_3$ catalyst for NO reduction is much lower than that of the $\text{Ag}/\text{Al}_2\text{O}_3$ catalyst.

In addition to the clearly surface reactions, Eränen et al. [56] showed that the formation of a part of N_2 , might take place in the gas phase in a short distance after the catalyst bed [56,57]. They showed that gas-phase reactions are initiated on the catalyst surface and proceeds in the free gas volume in the reactor behind the catalyst. Matrix isolation combined with EPR and FTIR technique at low temperature revealed formation of radicals of low molecular weight at the gas phase involved in SCR- NO_x over a highly active $\text{Ag}/\text{Al}_2\text{O}_3$ catalyst.

It should be emphasis that the details of the reaction mechanism depend on gas composition, loading of silver, choice of reductant, choice of support and can vary with temperature.

1.5 Enhancement of decane-SCR- NO_x over silver catalyst by hydrogen.

In 2000 was discovered that the NO reduction by C_3H_8 over $\text{Ag}/\text{Al}_2\text{O}_3$ could be dramatically increased by adding H_2 into the feed in the presence of excess of oxygen and water vapor [58]. The positive effect of hydrogen on NO_x conversion was predominantly observed at lower temperature region (590–760 K). Since NO_x reduction to N_2 by H_2 was negligible in the absence of hydrocarbons, H_2 should act as a promoter of the NO reduction by hydrocarbons over $\text{Ag}/\text{Al}_2\text{O}_3$ [58]. NO_x conversion at the low temperature region increased with increasing concentration of H_2 [58]. This discovery has not attracted attention in scientific community until 2003. Later, during performance of this study, this positive hydrogen-effect has invoked a high interest [20,49,59,60,61,62,63,64,65,66,67,68]. There have been proposed a mechanism and reason for the increase in the rate of NO_x reduction and individual reaction steps of SCR- NO_x . However, up to now there has not been given a definite conclusion.

Aim of the study

The aim of the study has been understanding of the structure and operation of silver alumina catalyst in transformation of NO_x to N₂ in exhaust gases of diesel engines by using selective catalytic reduction of NO_x with decane, as main component of diesel fuel, and under co-assistance of hydrogen.

To analyse the state and behaviour of silver species in Ag/alumina catalyst at the SCR-NO_x process and the dramatic positive effect of co-fed hydrogen, the individual reaction steps, i.e. oxidation of NO, decane and H₂ were also investigated. The purpose of co-feeding of carbon monoxide and hydrogen peroxide was to bring about an additional insight into the function of hydrogen in the SCR-NO_x process.

FTIR, UV-Vis-NIR and TPR by H₂ techniques were used to obtain relevant information on the state of silver. Of high importance was performance of the *in-situ* UV-Vis study carried out at the H₂/C₁₀H₂₂-SCR-NO_x reactions and its steps, monitoring real behaviour of silver species on alumina at true reaction conditions.

The study was a part of the European project "Advanced nanostructured metal/metal-oxo/matrix catalysts for redox processes. Application for NO_x reduction to nitrogen" carried out through 2001-2004 to solve abatement of NO_x in exhausts of diesel engines.

2 Experimental

2.1 Catalysts preparation

2.1.1 Silver zeolite catalysts

A MFI zeolite provided by IIC (Na^+ form, $\text{Si}/\text{Al} = 12.5$, crystal size $0.5 \mu\text{m}$) was used for preparation of silver zeolite catalysts. To obtain an NH_4^+ form, the zeolite was ion exchanged repeatedly (4x) with 1 M NH_4NO_3 solution at RT for 12 h^{-1} (1,000 ml of solution per 20 g of zeolite), washed several times with distilled water, filtered and dried in open air at room temperature. Silver zeolite catalysts were prepared by ion exchange of the MFI zeolite with a solution of AgNO_3 (100 ml of solution per 1 g of zeolite). The Na^+ and NH_4^+ forms of the MFI zeolite were used to prepare AgNa-MFI and $\text{AgNH}_4\text{-MFI}$ catalysts, respectively. After the Ag^+ ion exchange the silver zeolites were filtered, washed several times by distiller water and dried in open air at RT. The conditions of preparation and composition of silver zeolite catalysts are given in Tab. 2-1.

Table 2-1 Preparation and composition of silver zeolite catalysts

Sample	Conditions of preparation		Composition of Ag-zeolites	
	Concentration of AgNO_3 solution ($\text{mol}\cdot\text{dm}^{-3}$)	Time (h)	Ag (wt.%)	Na (wt.%)
$\text{AgNH}_4\text{-MFI-1.4}$	0.002	24	1.41	<0.1
$\text{AgNH}_4\text{-MFI-4.2}$	0.01	24	4.20	<0.1
AgNa-MFI-5.9	0.01	24	5.91	0.76

2.1.2 Silver alumina catalysts

Alumina supported silver catalysts were supplied by Laboratory of Industrial Chemistry, Abo Akademi University, Turku. The catalysts were prepared by impregnation of a commercial alumina support ($< 250 \mu\text{m}$, LaRoche, specific surface area $289 \text{ m}^2\text{g}^{-1}$) with aqueous silver nitrate solution. The conditions of preparation and composition of the catalysts are given in Tab. 2-2.

Table 2-2 Preparation and composition of silver alumina catalysts.

Sample	Conditions		Composition
	Concentration of AgNO ₃ solution (mol.dm ⁻³)	Time (h)	Concentration of Ag (wt.%)
Ag/Al ₂ O ₃ -1.3	0.011	24	1.28
Ag/Al ₂ O ₃ -1.8	0.022	24	1.76
Ag/Al ₂ O ₃ -2.9	0.033	24	2.88

Chemical analysis of all the above catalysts was carried out after their dissolution by Atomic Absorption Spectrometry at the Institute of Inorganic Chemistry Academy of Sciences, CR.

2.2 Catalyst testing in the C₁₀H₂₂-SCR-NO_x reactions, and NO, H₂ and C₁₀H₂₂ oxidation

2.2.1 Catalytic apparatus

The silver based catalysts were tested in selective catalytic reduction of NO and NO₂ with decane (C₁₀H₂₂-SCR-NO, C₁₀H₂₂-SCR-NO₂). Decane as a main component of diesel fuel, considered as a model hydrocarbons reductant. A fixed-bed through-flow quartz reactor placed in a catalytic apparatus (Fig. 2-1) was used to investigate the catalyst activity in C₁₀H₂₂-SCR-NO and C₁₀H₂₂-SCR-NO₂ and in oxidation of NO, H₂ or C₁₀H₂₂ by molecular oxygen. The effect of additional components (H₂, H₂O₂ and CO) in gas stream was also investigated.

The feed consists of helium and concentrations of NO, NO₂, n-C₁₀H₂₂, O₂, H₂O, H₂O₂, H₂, CO in He, in the range 0 - 1000 ppm NO, 0 - 1000 ppm NO₂, 0 - 1 200 ppm n-C₁₀H₂₂, 0 - 12 vol. % O₂, 0 or 12.0 % H₂O, 0 - 7200 ppm H₂, 0 or 7200 ppm CO and 0 or 2000 ppm H₂O₂. The typical composition of gases in the inlet of the reactor with the C₁₀H₂₂-SCR-NO_x reaction was 1000 ppm NO, 300 ppm n-C₁₀H₂₂, 6% O₂, 12 % H₂O and 0 or 2000 ppm H₂. Feed compositions for the individual experiments are given in Chapter 3. The flow rates of gases were controlled by gas mass-flow controllers (Elmet, C gas 02). Water and decane vapor were dosed by saturators, kept by thermostats (GRANT, thermostat GD 120) at constant temperature corresponding to the equilibrium decane or water vapor pressure necessary for obtaining appropriate concentrations in the gas inlet. Vapour of hydrogen peroxide was dosed directly into the reactor by linear dosing

device (Institute of Scientific Instruments, LD 2) equipped with 'home-made' Teflon-coated evaporator. The weight of the catalyst (grains 0.3-0.5 mm) was 26 - 210 mg and the flow rate of $150 \text{ cm}^3 \cdot \text{min}^{-1}$, which corresponded to GHSV of $30,000 - 240,000 \text{ h}^{-1}$. Temperature of the catalyst was kept in the range $323 - 723 \text{ K}$ controlled by an oven equipped by temperature-controller (Eurotherm 2216). The catalysts were calcined in a stream of oxygen at 723 K for 1 h prior to each catalytic test.

2.2.2 Product analysis

NO , NO_2 , N_2 , N_2O , H_2 , CO , CO_2 and $\text{C}_1\text{-C}_{10}$ hydrocarbons were analysed. Concentrations of NO and NO_2 (NO_x) were monitored by a NO/NO_x chemiluminescence analyser (Horiba CLA-355K), enabling determination of NO_x in the presence of high concentration of water vapor. The concentrations of N_2 , N_2O , H_2 , CO , CO_2 and $\text{C}_1\text{-C}_{10}$ hydrocarbons were determined by an on-line connected gas chromatograph (GC Hewlett Packard 6090). For GC analysis two gaseous samples were simultaneously injected using two 10-th port valves. In one branch with thermal conductivity detector (TCD), Haysep column was used for retention and removal of organic compounds and water, and columns of Poraplot Q ($30 \text{ m} \times 0.53 \text{ mm}$, $d_f = 40 \mu\text{m}$) and two Molecular sieve 5A ($30 \text{ m} \times 0.53 \text{ mm}$, $d_f = 25 \mu\text{m}$) were used for separation of H_2 , O_2 , N_2 , CO_2 , CO and N_2O . Poraplot Q column separated CO_2 from H_2 , O_2 , N_2 , CO and N_2O . The 6-th port valve was used to by-pass Molecular sieve 5A columns during the analysis of CO_2 on TCD. After the analysis of CO_2 , mixture of H_2 , O_2 , N_2 , CO and N_2O was separated with column Molecular sieve 5A and monitored on TCD. In the second branch DG-200 column was used for retention and removal of inorganic compounds and water. $\text{C}_1\text{-C}_{10}$ hydrocarbons were separated on a non-polar HP-5 column ($50 \text{ m} \times 0.53 \text{ mm}$, $d_f = 15 \mu\text{m}$) and monitored by flame ionisation detector (FID). Accuracy of measurement for this experimental set up was $< 5\%$ expressed as relative error of measurement ($\delta_{(x)}$). $\delta_{(x)} = 100 \cdot \Delta_{(x)}/X_{(m)}$, where $X_{(m)}$ is measured value and $\Delta_{(x)}$ is absolute error of measurement.

Table 2-3 Characteristic setting of gas chromatograph (GC Hewlett Packard 6090)

	Characteristics
Oven	Constant temperature 313 K for 21.5 min, ramp 40 K.min ⁻¹ up to 473 K and constant temperature for 44 min
Branch with FID detector	<p>Column DG-200, Column HP-5 Al₂O₃ "M" deactivated (50 m x 0.53 mm, d_f = 15 μm)</p> <p>Loop volume 0.250 ml, Load Time 0.5 min, Pressure 10 psi, Total flow 90 ml.min⁻¹, Flow in columns 8.2, Split 1:10</p> <p>Rinsing of DG-200 column from 15 min, flow of He at constant pressure 10 psi</p> <p>Valves at 423 K, Auxiliaries at 453 K, Split at 423 K</p> <p>FID detector: T = 523 K, 40 ml.min⁻¹ H₂, 400ml.min⁻¹ Air, 10 ml.min⁻¹ He (Make up gas flow)</p>
Branch with TCD detector	<p>Column Haysep, Poraplot Q (30 m x 0.53 mm, d_f = 40 μm), 2x Molecular sieve 5A (30 m x 0.53 mm, d_f = 25 μm)</p> <p>Loop volume 1 ml, Load Time 0.5 min, Pressure 20 psi, Splitless, By-pass of Molecular sieve 5A at 5.1-10.0 min</p> <p>Rinsing of Haysep column from 13.5 min, flow of He at constant pressure 15 psi</p> <p>Valves at 423 K, Auxiliaries at 453 K, Split at 423 K</p> <p>TCD detector: T = 523 K, Makeup gas flow: 6 ml.min⁻¹ He, Reference gas flow: 25 ml.min⁻¹ He</p>

Table 2-4 Retention time for the individual inorganic compounds

Compound	Columns	Retention time (min)
CO ₂	Haysep and Poraplot Q	8.1
H ₂	Haysep, Poraplot Q, 2x Molecular sieve 5A	11.1
O ₂	Haysep, Poraplot Q, 2x Molecular sieve 5A	12.8
N ₂	Haysep, Poraplot Q, 2x Molecular sieve 5A	14.0
CO	Haysep, Poraplot Q, 2x Molecular sieve 5A	16.4
N ₂ O	Haysep, Poraplot Q, 2x Molecular sieve 5A	28.2

Table 2-5 Retention time for the individual organic compounds

Compound	Columns	Retention time (min)
CH ₄	DG-200, HP-AI/M	2.1
C ₂ H ₆	DG-200, HP-AI/M	2.8
C ₂ H ₄	DG-200, HP-AI/M	4.2
C ₃ H ₈	DG-200, HP-AI/M	9.5
C ₃ H ₆	DG-200, HP-AI/M	12.4
n-C ₄ H ₁₀	DG-200, HP-AI/M	14.8
n-C ₁₀ H ₂₂	DG-200, HP-AI/M	58

Conversion of the reactants i , i.e. NO, NO₂, C₁₀H₂₂, H₂ was defined as

$$x_i = ((c_i^0 - c_i)/c_i^0) \cdot 100 \text{ (\%)} \quad (2-1)$$

where c_i^0 is the concentration (ppm) of the reactant i before inlet of the reactor and c_i is the concentration of the reactant i after outlet of the reactor.

Yields of N₂ and N₂O related to NO or NO₂ and yields of CO, CO₂ related to C₁₀H₂₂ were defined as

$$y_j = (v_j \cdot c_j / v_i \cdot c_i^0) \cdot 100 \text{ (\%)} \quad (2-2)$$

where c_j is the concentration (ppm) of the product j i.e. N₂, N₂O, CO, CO₂, in the reactor outlet and v_j is the number of C or N atoms in the corresponding molecule, c_i^0 is the concentration (ppm) of the reactant i , i.e. NO or C₁₀H₂₂, in the reactor inlet and v_i is the number of C or N atoms in the corresponding molecule.

The conversion values were calculated from the product compositions obtained at the steady-state conditions of the reaction, corresponding to a constant product composition obtained at about 60-120 min of time on stream (TOS). In selected cases NO_x transformation was followed depending on TOS.

Selectivity of reductant utilization is given by the parameter s that relates the oxygen atoms supplied by NO to all oxygen atoms reacted with decane theoretically to CO₂ and H₂O at SCR-NO_x process.

$$s = (x_{\text{NO}_x} \cdot c_{\text{NO}}^0 \cdot 31) / (100 \cdot x_{\text{decane}} \cdot c_{\text{decane}}^0) \text{ (\%)} \quad (2-3)$$

where x_{NO_x} is the conversion of NO_x to N₂, c_{NO}^0 and c_{decane}^0 is the concentration (ppm) of NO and decane before inlet of the reactor, respectively and x_{decane} is the conversion of decane to CO_x.

Turnover frequencies (TOF), i.e. molecules of NO converted to N₂ or N₂O per Ag atom per second, was calculated from equation

$$\text{TOF} = (F \cdot c_{\text{NO}}^0 \cdot y_{\text{N}_2+\text{N}_2\text{O}} \cdot M(\text{Ag}) \cdot 10^{-6}) / (V_m \cdot w \cdot m) \quad (\text{s}^{-1}) \quad (2-4)$$

where F is the total flow of the reaction mixture (dm³ · s⁻¹), V_m is the gas molar volume (22.4 dm³), c_{NO}^0 is the concentration of NO (ppm) in the inlet of the reactor, $y_{\text{N}_2+\text{N}_2\text{O}}$ is the yield of N₂ and N₂O (%), w is content of Ag in a silver alumina catalyst (wt.%), m is weight of catalyst and $M(\text{Ag})$ is an atomic weight of Ag (g · mol⁻¹).

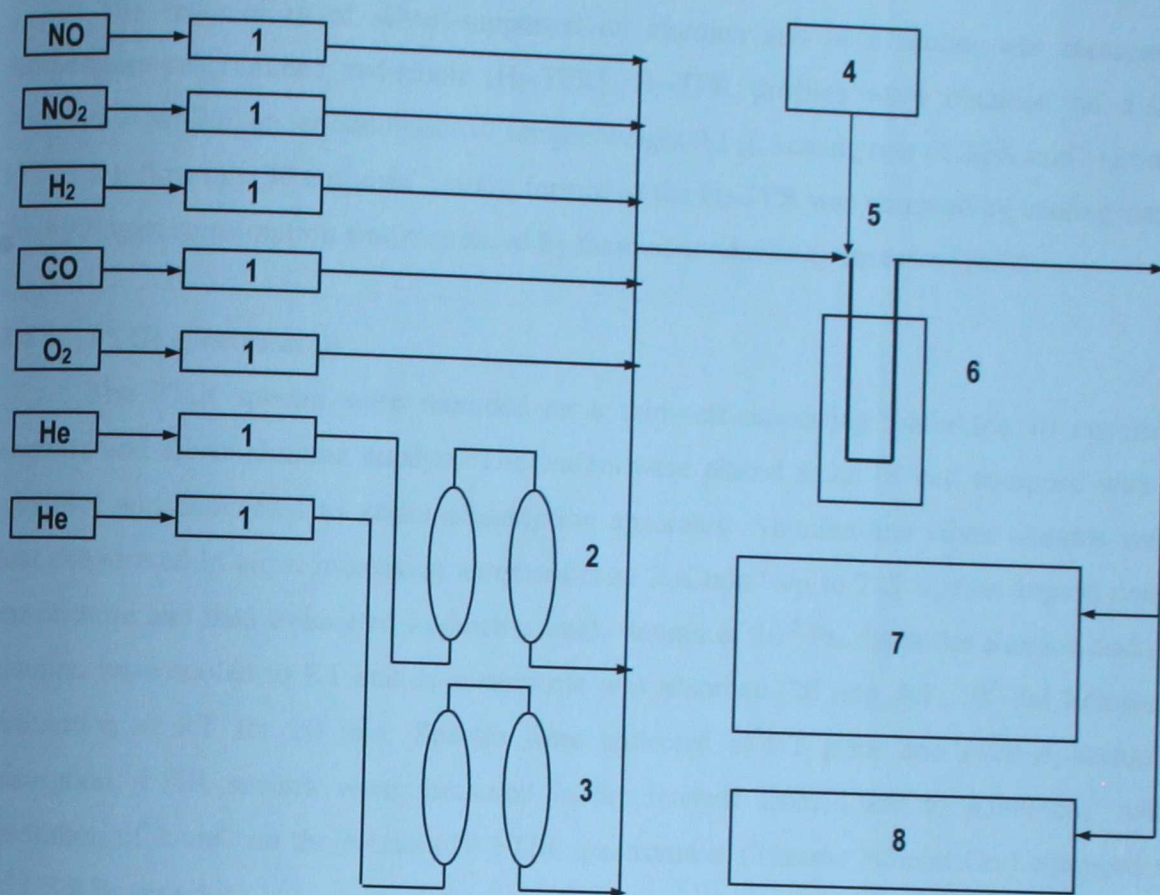


Fig. 2-1. Arrangement of the catalytic tests apparatus.

1. Gas mass flow controllers (Elmet, C gas 02)
2. Water saturators heated by thermostat (GRANT, GD 120)
3. Decane saturators heated by thermostat (GRANT, GD 120)
4. Linear dosing device (Institute of Scientific Instruments, LD 2) equipped with teflon-coated evaporator
5. Fixed-bed through-flow quartz reactor
6. Oven equipped by temperature controller (Eurotherm 2216)
7. Gas chromatograph (Hewlett Packard 6090)
8. NO/NO_x chemiluminescence analyser (Horiba, CLA-355K)

2.3 H₂-TPR

The reducibility of silver supported on alumina and in a zeolite was measured by temperature-programmed reduction (H₂-TPR). H₂-TPR profiles were obtained on a Zeton Altamira AMI-200 under conditions of sample weight 0.1 g, heating rate of 20 K.min⁻¹ (from 308 to 723 K), flow rate 30 cm³.min⁻¹; water formed at the H₂-TPR was removed by cooling trap and the hydrogen consumption was monitored by thermal conductivity detector (TCD).

2.4 FTIR spectroscopy

The FTIR spectra were recorded on a thin self-supporting wafer (ca 10 mg/cm²) of alumina and silver alumina catalyst. The wafers were placed in an IR cell equipped with KBr windows and connected to vacuum/adsorption apparatus. Alumina and silver alumina were at first dehydrated in air at increasing temperature of 3 K.min⁻¹ up to 723 K, than kept at constant temperature and than evacuated to reach a final vacuum of 10⁻⁵ Pa. Then the alumina and silver alumina were cooled to RT and d₃-acetonitrile was adsorbed (20 min, RT, 10³ Pa) followed by evacuation at RT for 20 min. Spectra were collected at RT prior and after d₃-acetonitrile adsorption. FTIR spectra were measured in the interval from 1,000 to 4,000 cm⁻¹ with a resolution of 2 cm⁻¹ on the Nexus 670 FTIR spectrometer (Thermo Nicolet Co.) equipped with DTGS KBr detector.

Table 2-7 Characteristic setting of Nexus 670 FTIR spectrometer (Thermo Nicolet Co.).

	Characteristic
Spectral range	1,000 to 4,000 cm ⁻¹
No. of scans	128
Aperture	69
Gain	2
Beamsplitter	KBr
Detector	DTGS KBr
Windows	KBr

2.6 Diffuse reflectance UV-Vis-NIR spectroscopy

The state of Ag on alumina and in a zeolite was monitored by UV-Vis-NIR spectroscopy. The diffuse reflectance UV-Vis-NIR spectra were collected on a Perkin Elmer UV-Vis-NIR spectrometer Lambda 19 using diffuse reflectance attachment with an integrating sphere. The sphere was coated with BaSO₄ and as a reference BaSO₄ powder was used. The spectra were recorded in the range from 4,000 to 50,000 cm⁻¹ at a speed of 480 nm.s⁻¹, scanning step 1 nm and slit width 5 nm. The F(R_∞) function was calculated from the Schuster-Kubelka-Munk equation

$$F(R_{\infty}) = (1 - R_{\infty})^2 / 2R_{\infty} \quad (2-5)$$

where R_∞ is the diffuse reflectance from a semi-infinite layer. F(R_∞) is proportional to the concentration of absorbing species in solids.

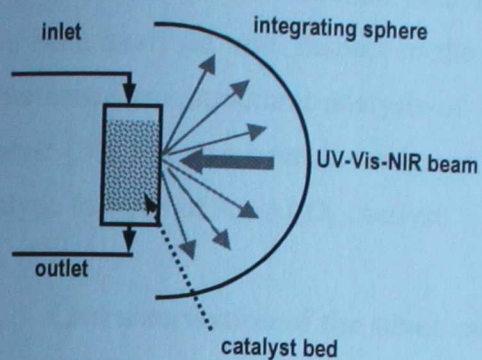
2.4.1 Ex-situ diffuse reflectance UV-Vis-NIR spectroscopy

Granulated silver alumina or silver zeolite samples (300 – 600 μm) were activated in an oxygen stream at 723 K for 1 h in a quartz reactor and cooled to 423 K in an oxygen atmosphere, followed by evacuation at 423 K using a pressure of 7x10⁻² Pa for 15 min. Such treated Ag-samples were transferred under vacuum into the quartz cell (QC, SUPRASIL) of 5 mm thickness and their spectra were recorded.

2.4.2 In-situ diffuse reflectance UV-Vis-NIR spectroscopy

Heated home-made through-flow quartz optical cell (Fig. 2-2) was constructed and used to obtain the spectra under the conditions of the catalytic reactions. The optical cell, placed in the oven with a window for a beam pathway, was attached to the surface of the integrating sphere. *In-situ* UV-Vis-NIR measurements carried out at conditions of the catalytic reaction were run at the reaction temperature of 473 and 523 K and at the identical conditions of reactant compositions and GHSV values as the catalytic tests in the standard micro-reactor set up. Reactant feed was mixed by a mixing station consisting of dosing system for gases, gas mass-flow controllers and saturators for water and decane. The arrangement is similar to that used for the catalytic tests (Fig. 2-1).

(A)



(B)

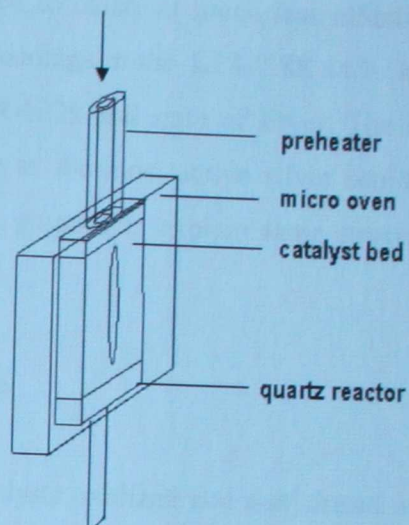


Fig. 2-2. Scheme of experimental arrangement of *in-situ* UV-Vis-NIR spectroscopy (A) and the UV-Vis-NIR heated through-flow optical quartz cell (B).

Table 2-7 Characteristic setting of UV-Vis-NIR spectrophotometer Lambda 19 (Perkin Elmer).

	Characteristic
Start wavelength	2,500 nm
End wavelength	190 nm
Data interval	1.0 nm
Number of cycles	1
Scan speed	480 nm.min ⁻¹
Slit	5 nm
Lamp change	320 nm
Detector change	860 nm

3 Results

Silver alumina catalysts with silver loading around 2 wt.% have been shown as highly active in CH-SCR-NO_x, while higher silver content led to catalysts much less effective [14]. Thus in this study silver alumina catalysts with silver loadings in the 1.28–2.88 wt.% Ag range have been analysed with respect to the activity in SCR-NO_x and state of silver. The catalytic performance and structural analysis of Ag-MFI zeolite as the most active silver zeolite based catalyst [31] has also been investigated especially with purpose to explain same structural and catalytic features of Ag/Al₂O₃ catalyst.

3.1 Characterisation of the silver catalyst structure

3.1.1 UV-Vis spectra of silver alumina

Fig. 3-1 shows UV-Vis spectra of Ag/Al₂O₃ catalysts oxidized and dehydrated at 723 K followed by evacuation at 423 K for 15 min. According to the literature the UV-Vis bands can in general be ascribed as follows: (i) the bands above 40,000 cm⁻¹, including also the absorption bands above 50,000 cm⁻¹ (out of the accessible spectral range here), belong to the electronic transitions of Ag⁺ cations [43], (ii) the bands in the range 27,000 – 40,000 cm⁻¹, can be attributed to small metallic Ag_n^{δ+} clusters (n ≤ 8) [43] (with the increasing number of Ag atoms in the cluster decreases the wavenumber [43]), and (iii) the bands below 27,000 cm⁻¹ can be ascribed to large or oxide-like silver particles (for details of UV-Vis bands attribution see the Discussion).

The investigated Ag/Al₂O₃ catalysts with Ag content ranging from 1.28 to 2.88 wt.% treated in an oxygen stream exhibit the bands at 41,600 and 46,000 cm⁻¹ assigned to single Ag⁺ ions. A small intensity observed as a shoulder at 30,000 – 38,000 cm⁻¹ was found and it increased with metal content of the catalyst. This finding indicates that the shoulder could be ascribed to small metallic Ag_n^{δ+} clusters formed during the procedure of catalyst evacuation. Same increase in the absorbance intensity around and above 50,000 cm⁻¹ might indicate presence of additional band, but this spectral region is out of the measurements of our and all-standard UV-Vis spectrometers.

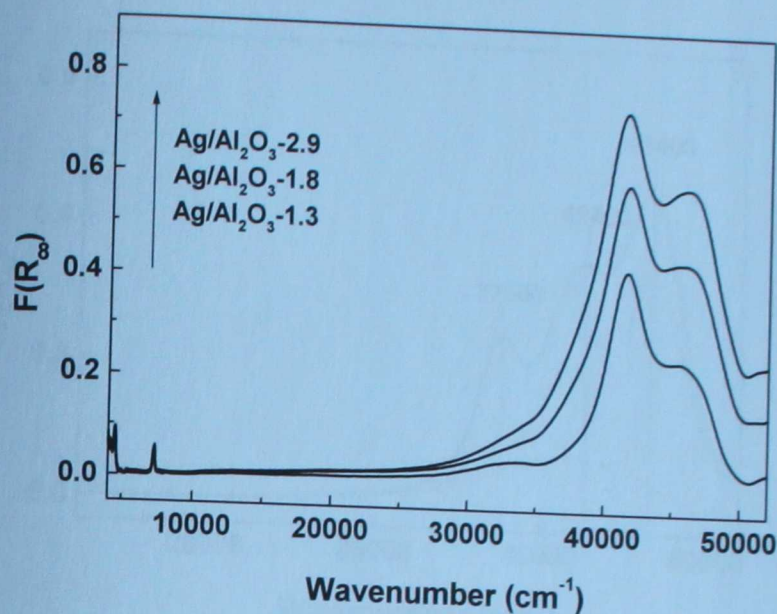


Fig. 3-1. UV-Vis spectra of Ag/Al₂O₃ catalyst calcined in an oxygen at 723 K followed by evacuation at 423 K for 15 min.

3.1.2 UV-Vis spectra of silver MFI

Two bands centred at 42,400 and 46,400 cm⁻¹ are observed in UV-Vis spectral region for all the investigated Ag zeolites (Fig. 3-2). The bands are ascribed to the single Ag⁺ ions. AgNH₄-MFI-4.2 and AgNa-MFI-5.9 catalysts show well-distinguished maxima of the bands. The spectrum of AgNH₄-MFI-1.4 shows only a broad profile due to low concentration of silver and due to weak absorption bands at 28,000 – 44,000 cm⁻¹ of iron impurities (0.1 wt.% Fe). The third strong band with maximum at 37,500 cm⁻¹ appeared in the spectrum of the AgNa-MFI zeolite. The position of the band indicates that it corresponds to small Ag_n^{δ+} intrazeolitic clusters (n ≤ 8). Presence of the Ag_n^{δ+} clusters for AgNa-MFI-5.9 could be explained by lower mobility of Ag⁺ in Na-form of zeolite. Hence Ag_n^{δ+} clusters present in channels of Na⁺ zeolite after catalyst preparation can hardly be dispersed during calcination in a dry O₂ stream. Formation of Ag_n^{δ+} clusters in AgNa-MFI compared to AgNH₄-MFI could be also explained by easier reducibility of Ag⁺ ions in Na-form zeolite compared to H-forms as the presence of H⁺ cations shifts the equilibrium to the Ag⁺ ions.

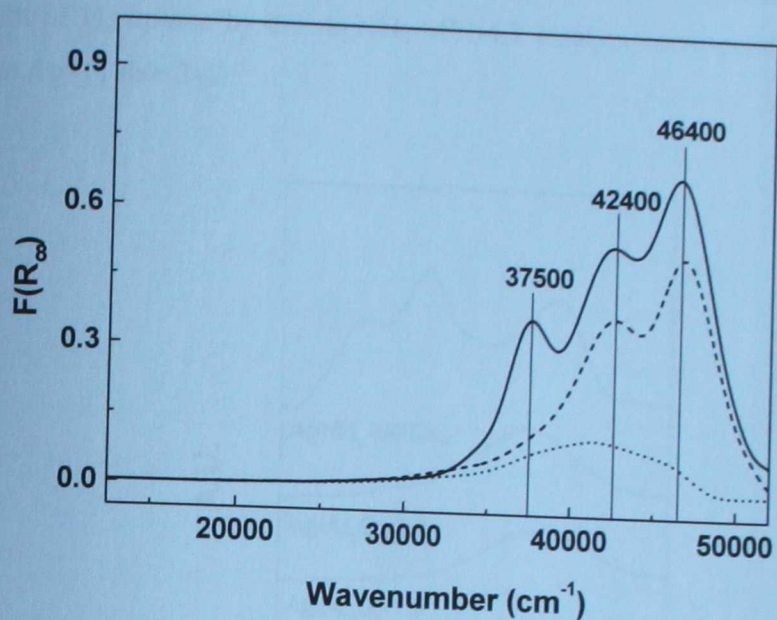


Fig. 3-2. UV-Vis spectra of Ag/zeolite calcined in oxygen at 723 K followed by evacuation at 423 K for 15 min. AgNa-MFI-5.9 (—), AgNH₄-MFI-4.2 (---) and AgNH₄-MFI-1.4 (.....).

3.1.3 H₂-TPR of silver catalysts

All Ag/Al₂O₃ samples contain reducible Ag⁺ ions as follows from H₂-TPR experiments after the *in-situ* pre-treatment in O₂ for 1 h at 723 K (Fig. 3-3, Table 3-1). The position of the temperature maxima of hydrogen consumption over Ag/Al₂O₃ samples is slightly shifted to lower temperatures with increasing Ag loading. This indicates easier formation of metallic silver clusters at higher silver loading. The degree of Ag reduction was calculated according to the stoichiometry that 1 mol Ag⁺ requires 1/2 mol H₂. The values of the blank H₂-TPR run with the alumina support shows hydrogen consumption of 5.2 μmol of H₂.g⁻¹ below 723 K (well below 10% of that for Ag/Al₂O₃), taken into account for the quantitative analysis. As all silver is in the monovalent state in the calcined Ag/Al₂O₃ (Fig. 3-1), the reduction degree indicates that a part of Ag⁺ ions was not reduced under hydrogen flow below 723 K. A continuous hydrogen consumption above 870 K was reported with Ag/Al₂O₃ [18].

The H₂-TPR curve of AgNH₄-MFI-4.2 after treatment in O₂ for 1 h at 773 K (Fig. 3-3) shows three temperature maxima of hydrogen consumption at around 410, 475 and 605 K. It

clearly indicates that Ag^+ ions in the zeolite are much more easily reducible than that in alumina. The amount of H_2 uptake by the $\text{AgNH}_4\text{-MFI-4.2}$ catalyst corresponded to the reduction of all Ag^+ ions to Ag^0 (Table 3-1).

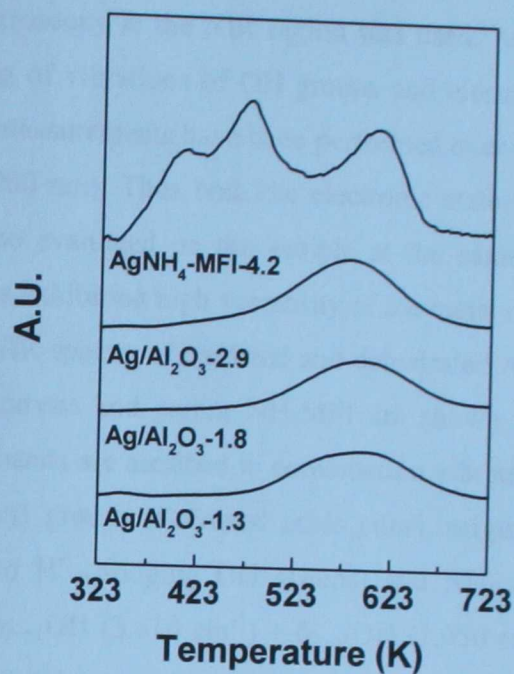


Fig. 3-3. H_2 -TPR profiles of silver catalysts.

Table 3-1. H_2 -TPR data of silver catalysts

Sample	Ag content (wt.%)	H_2 consumption ^a ($\mu\text{mol.g}^{-1}$)	Ag content ($\mu\text{mol.g}^{-1}$)	Reduction degree ^b (%)	Peak maximum T (K)
$\text{Ag}/\text{Al}_2\text{O}_3\text{-1.3}$	1.28	51.2	118.6	86.3	595
$\text{Ag}/\text{Al}_2\text{O}_3\text{-1.8}$	1.76	72.5	163.0	89.0	589
$\text{Ag}/\text{Al}_2\text{O}_3\text{-2.9}$	2.88	71.6	266.8	53.6	576
$\text{AgNH}_4\text{-MFI-4.2}$	4.20	192.2	389.0	98.8	409, 474, 605

^a H_2 consumption up to 723 K

^b $2\text{Ag}^+ + \text{H}_2 \rightarrow 2\text{Ag}^0 + 2\text{H}^+$

3.1.4 Interaction of silver with the support at the silver catalysts

3.1.4.1 NIR spectra of silver MFI

The coordination of Ag^+ ions to bridging oxygen atoms can be observed by changes in OH groups after introduction of the cation into the zeolite. To detect OH groups in silver zeolites diffuse reflectance spectroscopy in the NIR region was used. An advantage of this technique is simultaneous monitoring of vibrations of OH groups and electronics transitions of Ag species. The diffuse reflectance measurements have been performed over the working range from 4,000 to 50,000 cm^{-1} (2,500 to 200 nm). Thus both the electronic state of silver (Fig. 3-2) and the OH groups (Fig. 3-4) can be evaluated on the sample at the same conditions. This is especially important for the systems exhibiting high versatility of the metal redox state.

Two regions of NIR spectra of oxidized and dehydrated AgNa-MFI-5.9 , $\text{AgNH}_4\text{-MFI-4.2}$ and $\text{AgNH}_4\text{-MFI-1.4}$ catalysts and parent NH_4MFI are shown in Fig. 3-4. In the first region (4,000-5,000 cm^{-1}) the bands are ascribed to combination vibrations of hydroxyl groups ($\nu_{0\rightarrow 1} + \delta$). The bridging hydroxyl groups (Brönsted acids sites), originated from NH_4^+ ions by their thermal decomposition to H^+ (bridging OH groups) and NH_3 , are shown by the bands with maxima at 4,660 cm^{-1} ($\nu_{0\rightarrow 1}\text{OH}$ (3,610 cm^{-1}) + $\delta_{0\rightarrow 1}\text{OH}$ (1,050 cm^{-1})) [70]. The intensity of the band of the bridging hydroxyl groups linearly decreases with increasing loading of silver cations for $\text{AgNH}_4\text{-1.4}$ and $\text{AgNH}_4\text{-MFI-4.2}$ samples. With AgNa-MFI-5.9 a negligible intensity of Brönsted site is present. The absorption bands with maximum at 4,530 cm^{-1} ($\nu_{0\rightarrow 1}\text{SiOH}$ (3,745 cm^{-1}) + $\delta_{0\rightarrow 1}\text{SiOH}$ (785 cm^{-1})) [70] demonstrate the terminal Si-OH bands. Their intensities are the same for all the samples. It indicates that terminal Si-OH groups are not exchanged by Ag^+ ions. The absence of the band at 5,280 cm^{-1} confirms complete dehydration of the investigated samples, but for brevity it is not depicted.

In the second region there is a group of partially overlapping bands corresponding to overtone vibrations of hydroxyls ($\nu_{0\rightarrow 2}$). The bands at 7,310 cm^{-1} represent the first overtone vibrations of terminal SiOH groups with fundamental vibration ($\nu_{0\rightarrow 1}\text{SiOH}$ (3,745 cm^{-1})) [70]. The well-defined bands with maxima at 7,070 cm^{-1} are assigned to the first overtone vibrations of bridging hydroxyl groups (fundamental vibrations $\nu_{0\rightarrow 1}\text{OH}$ (3,610 cm^{-1})). The intensity of the bands at 7,070 cm^{-1} decreases after Ag^+ and Na^+ introduction into a zeolite with the same extent as the intensity of the bands at 4,660 cm^{-1} . The low intensity broad band (around 7,200 cm^{-1}) occurring between the vibrations of terminal and bridging hydroxyl groups are assigned to first

overtone vibrations of Al-OH species (fundamental vibrations $\nu_{0-1}\text{OH}$ ($3,650 - 3,660 \text{ cm}^{-1}$)). This low intensity band indicates only low number of defects in the zeolite.

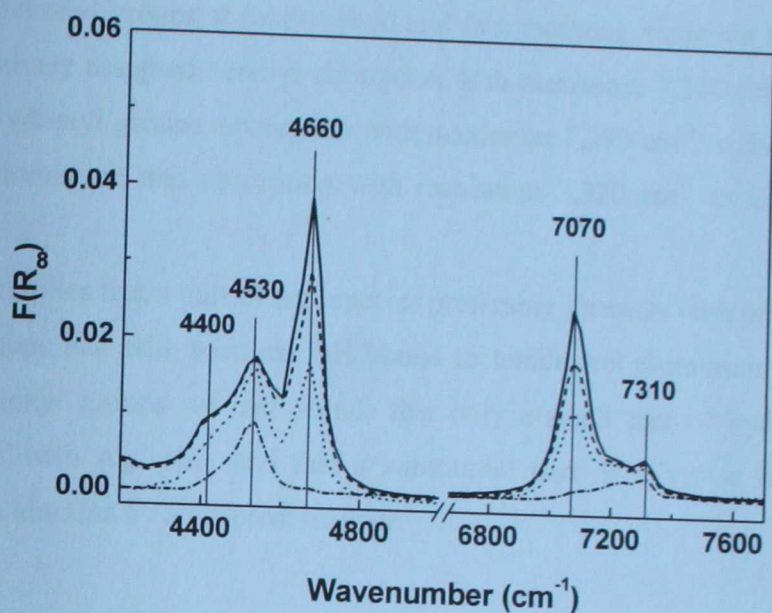


Fig. 3-4. NIR diffuse reflectance spectra of Ag-zeolites calcined in oxygen at 723 K followed by evacuation at 423 K for 15 min. H-MFI (—), AgNH_4 -1.4 (---), AgNH_4 -MFI-4.2 (·····) and AgNa -MFI-5.9 (— · — · —).

3.1.4.2 NIR spectra of silver alumina

The comparison of the spectra of zeolites and alumina allows attribution of the absorption bands of alumina in the NIR region to hydroxyl groups (Fig. 3-5). The absorption bands at $7,000 - 7,400 \text{ cm}^{-1}$ represent first overtone of the hydroxyl-stretching mode and at $4,300 - 4,700 \text{ cm}^{-1}$ combination stretching and deformation mode of hydroxyl groups. The overlapping bands of parent alumina exhibit maxima at $4,450, 4,500$ and $4,560 \text{ cm}^{-1}$ and at $7,200, 7,290$ and $7,320 \text{ cm}^{-1}$ in the first and second region, respectively. $\text{Ag}/\text{Al}_2\text{O}_3$ -1.3 exhibited a decrease in the intensity of the bands at $7,200$ and $7,320 \text{ cm}^{-1}$. Higher silver loading did not lead to any further change in the intensity of the hydroxyl bands.

Busca et al. [71] described OH structures on alumina by FTIR spectra; two types of terminal OH bound to tetrahedral aluminium ($\nu = 3,800 \text{ cm}^{-1}$ and $\nu = 3,770 \text{ cm}^{-1}$), terminal OH bound to octahedral aluminium ($\nu = 3,740 \text{ cm}^{-1}$), bridged OH ($\nu = 3,690 \text{ cm}^{-1}$) and tri-bridged OH ($\nu = 3,590 \text{ cm}^{-1}$) were indicated. With superposition conservation of the absorption bands of the individual hydroxyl groups at fundamental and first overtone mode the bands at the NIR region can be tentatively assigned hereby: absorption with maximum $7,200 \text{ cm}^{-1}$ to the bridged and/or tri-bridged hydroxyl groups, absorption with maximum $7,290 \text{ cm}^{-1}$ to the terminal OH bound to octahedral aluminium and absorption with maximum $7,320 \text{ cm}^{-1}$ to OH bound to tetrahedral aluminium.

This implies that a part of Ag^+ species preferably interacts with bridged and/or tri-bridged hydroxyl groups and with terminal OH bound to tetrahedral aluminium. From the intensity of residual hydroxyl groups we can deduce that only a small part of hydroxyl groups could be exchangeable with Ag^+ ions and that a substantial part of silver in higher loading samples interacts with alumina by a different manner.

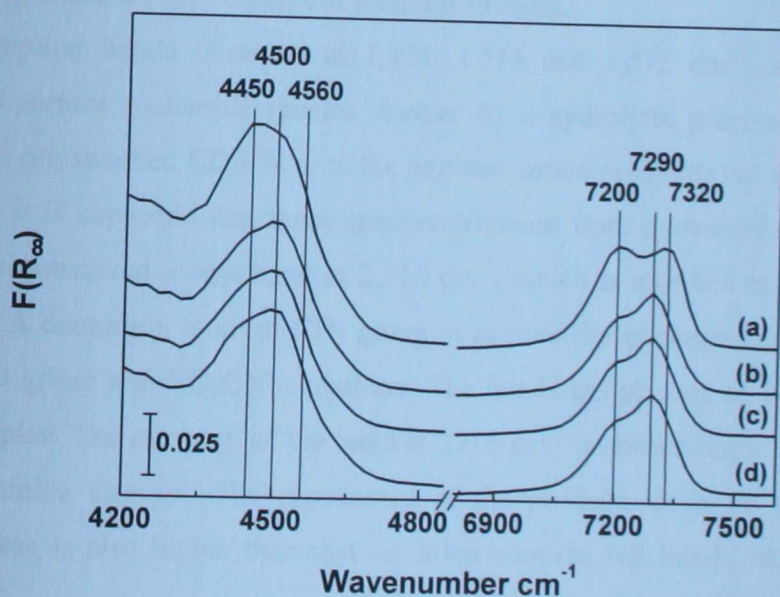


Fig. 3-5. NIR diffuse reflectance spectra of Al_2O_3 and $\text{Ag}/\text{Al}_2\text{O}_3$ catalysts calcined in an oxygen stream at 723 K followed by evacuation at 423 K for 15 min. (a) Al_2O_3 , (b) $\text{Ag}/\text{Al}_2\text{O}_3$ -1.3, (c) $\text{Ag}/\text{Al}_2\text{O}_3$ -1.8, (d) $\text{Ag}/\text{Al}_2\text{O}_3$ -2.9.

3.1.4.2 FTIR spectra of d_3 -acetonitrile

To describe the interaction of silver with Lewis sites and/or basic sites of alumina adsorption of d_3 -acetonitrile was used as a probe. Figure 3-6 shows difference FTIR spectra of Al_2O_3 and $Ag/Al_2O_3-1.8$ after d_3 -acetonitrile adsorption (20 min, RT, 10^3 Pa) and evacuation at RT. The bands at 2,255 and 2,110 cm^{-1} exhibit the same positions as the bands for liquid CD_3CN [71] and thus correspond to the $\nu(CN)$ and $\nu_s(CD_3)$ modes of physisorbed CD_3CN on alumina [73, 74]. The second derivative mode of the spectrum in the region of 2,270 – 2,370 cm^{-1} (absorbance around 2,320 cm^{-1}) and its decomposition to the Gaussian bands yields two bands with maxima with 2,313 and 2,327 cm^{-1} (Fig. 3-7). The bands correspond to the $\nu(CN)$ mode of CD_3CN interacting, through the N lone-pair, with strong (2,327 cm^{-1}) and weak (2,313 cm^{-1}) Lewis sites [73]. The intensities of the bands are substantially higher for Al_2O_3 than those for $Ag/Al_2O_3-1.8$. It evidences that silver interacts with both types of Lewis acid sites. Figure 3-7 and Table 3-2 show a higher decrease in the band intensity of strong Lewis sites. Only rough estimate of the number of interacting Lewis sites on the alumina support is possible. As silver species on alumina could also play a role of weak Lewis sites quantitative analysis cannot be done. The absence of the $\nu(CN)$ bands shifted upward by 10-35 cm^{-1} with respect to the liquid phase shows the absence of Brønsted acid centers of medium strength.

Absorption bands observed at 1,425, 1,515 and 1,575 cm^{-1} (see Fig. 3-6) could be attributed to surface acetamide species, formed by a hydrolytic process and the component at 2,180 cm^{-1} to physisorbed CD_3CN or to the polymerisation product(s) of CD_2CN^- carbanion [73]. In Ref. [73] it is supposed that those species originate from acetonitrile interaction with basic sites. We also observed a new band at 2,715 cm^{-1} , which is ascribed to stretching band of OD groups [75]. A deuterium atom of CD_3 group in acetonitrile is eliminated with formation of the observed OD group and CD_2CN^- carbanion. The bands are present on both alumina and silver alumina samples. The intensity of the band at 2715 cm^{-1} is substantially higher on alumina than on silver alumina catalyst. The appearance of the products of basic catalysed reactions on alumina surface is also higher than that on silver alumina (cf. bands intensities at 1575, 1515 1425 cm^{-1}).

It can be concluded that the introduction of Ag^+ ions leads to a decrease of both Lewis acid site and basic sites on alumina.

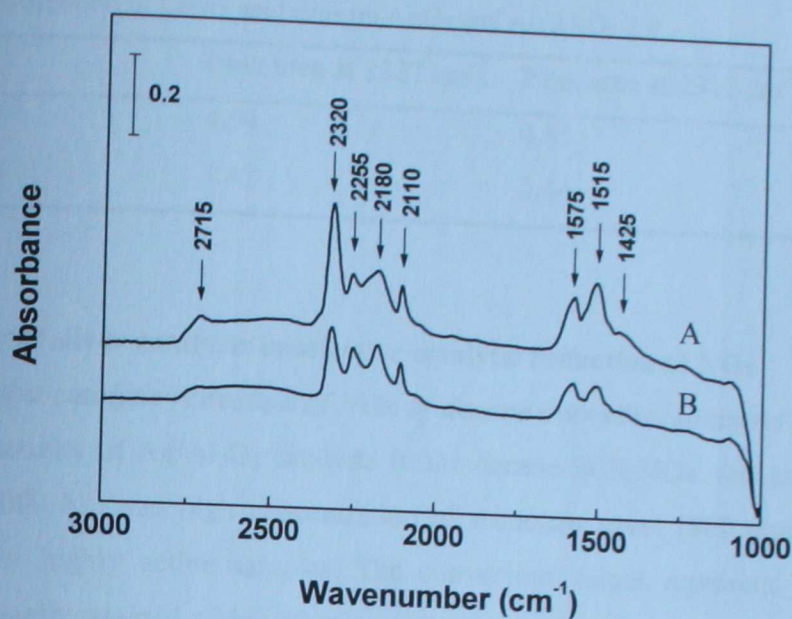


Fig. 3-6. Differential FTIR absorbance spectra of CD_3CN onto Al_2O_3 (A) and $\text{Ag}/\text{Al}_2\text{O}_3\text{-1.8}$ (B). The spectra were collected at RT on Al_2O_3 and $\text{Ag}/\text{Al}_2\text{O}_3\text{-1.8}$ (both calcined in air at 723 K) prior and after CD_3CN adsorption for 20 min at RT and 10^3 Pa followed by evacuation at RT for 20 min.

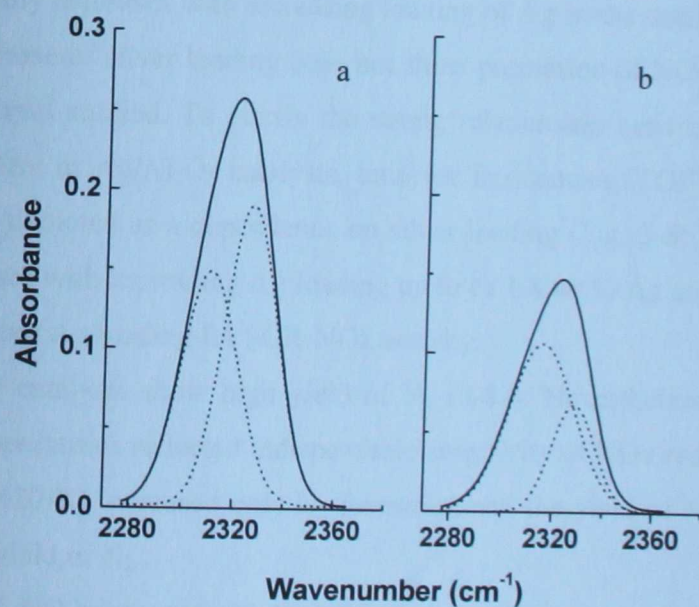


Fig. 3-7. Decomposition of the spectra of CD_3CN coordinated to Lewis sites to Gaussian curves in range $2,270 - 2,370 \text{ cm}^{-1}$, (Al_2O_3 (a) and $\text{Ag}/\text{Al}_2\text{O}_3$ (b)).

Table 3-2. Distribution of Lewis acid sites on Al_2O_3 and $\text{Ag}/\text{Al}_2\text{O}_3$ -1.8

	Peak area at 2327 cm^{-1}	Peak area at 2313 cm^{-1}
Al_2O_3	4.04	4.85
$\text{Ag}/\text{Al}_2\text{O}_3$ -1.8	1.47	3.44

3.2 Activity of silver catalysts in selective catalytic reduction of NO_x

3.2.1 Selective catalytic reduction of NO_x by decane over silver alumina catalyst

The activity of $\text{Ag}/\text{Al}_2\text{O}_3$ catalysts in the decane-SCR- NO_x was tested at high value of GHSV ($240,000\text{ h}^{-1}$) and high concentration of reductant agent (600 ppm) to avoid complete conversion for highly active samples. The conversion values represent those at steady-state conditions, usually attained within 90 min.

Figs. 3-8a and 3-9a show general trends of conversions of both NO_x and decane, which increase with temperature. At low conversion $\text{NO}-\text{N}_2$ values the dependence of conversions on temperature follows Arrhenius plot approx. up to the temperature of 623 K. Above 623 K the increase in NO_x to N_2 conversion with temperature decline for $\text{Ag}/\text{Al}_2\text{O}_3$ -1.8 and $\text{Ag}/\text{Al}_2\text{O}_3$ -2.9, but not for $\text{Ag}/\text{Al}_2\text{O}_3$ -1.3. The silver loading has a large effect on the NO_x to N_2 conversion, which substantially increases with increasing loading of Ag in the catalysts from 1.3 to 1.8 wt.% Ag. Further increase of silver loading does not show promotion of NO_x conversion in the whole temperature interval studied. To clarify the strong relationship between NO_x to N_2 conversion and the Ag content in $\text{Ag}/\text{Al}_2\text{O}_3$ catalysts, turnover frequencies (TOF) for the SCR-NO at 573 and 673 K were depicted as a dependence on silver loading (Fig. 3-8b). The TOF for NO to N_2 reduction increases with increasing Ag loading up to ca 1.8 wt.% Ag and then decreases. That is, there is an optimum Ag loading for SCR- NO_x activity.

All silver catalysts show high yield of N_2 (3-8a). Nevertheless, values of N_2O and N_2 yields at low temperatures reflected indispensable selectivity of NO_x reduction to N_2O . At higher temperatures ($> 620\text{ K}$) increased only N_2 formation and the yield of N_2O become insignificant compared to the yield of N_2 .

A part of NO was oxidized to NO_2 at the complex decane-SCR- NO_x reaction. The conversion of NO to NO_2 increased with temperature up to 573 K. At 723 K conversion of NO to NO_2 become negligible for $\text{Ag}/\text{Al}_2\text{O}_3$ -1.3, while it is significant for $\text{Ag}/\text{Al}_2\text{O}_3$ -1.8.

Decane at $C_{10}H_{22}$ -SCR-NO_x was converted mostly to carbon oxides (Fig. 3-9a) and hydrocarbon-like products (Fig. 3-9b). Fig 3-9a shows that conversion of $C_{10}H_{22}$ to CO and CO₂ increases with temperature in the temperature interval of 523 - 723 K for Ag/Al₂O₃-1.8 and Ag/Al₂O₃-2.9, while with Ag/Al₂O₃-1.3 is rather low up to 673 K. This decane conversion corresponds to the NO_x conversions. Yields of CO₂ and CO shows that CO production is a drawback of all Ag/Al₂O₃ catalyst studied. The quantitative analysis of decane and CO and CO₂ showed that decane is converted predominantly to CO_x and only <10% of decane to hydrocarbon-like products. Fig. 3-9b depicts chromatograms of hydrocarbon-like products at $C_{10}H_{22}$ -SCR-NO at 623 K. A spectrum of products was detected. Among them were low chain hydrocarbons (CH₄, C₂H₆, C₂H₄, C₃H₈, C₃H₆) other peaks might correspond to other hydrocarbons and their oxo/nitro-derivates. The GC signal intensity of the hydrocarbon-like products is highest over Ag/Al₂O₃-1.8, lower over Ag/Al₂O₃-2.9 and negligible over Ag/Al₂O₃-1.3 at 623 K it corresponds roughly to the conversion values of NO_x conversion. The complexity of product composition disables analysis of all the products by GC equipped only with FID. The gaseous hydrocarbon-like products were analysed at the Laboratory of Industrial Chemistry AAU Turku, Finland within the EU cooperative research project. They detected by GC-MS minute concentrations of various hydrocarbons, oxygenates, amines and other N-containing hydrocarbons products over Ag/Al₂O₃-1.8 at C_8H_{10} -SCR-NO_x. These products are involved in gas-phase reactions initiated on the catalyst surface and proceeding in the free gas volume of the reactor behind the catalyst bed. The contribution of gas phase reactions at SCR-NO_x over Ag/Al₂O₃ was also studied at Laboratory of Industrial Chemistry AAU [14], and this subject is not a matter of this study.

Fig. 3-9c shows the decane utilization that relates the oxygen atoms supplied by NO to all oxygen atoms reacted with the decane to CO₂ and H₂O at the complex SCR-NO_x process over Ag/Al₂O₃ catalysts. The NO_x conversions are negligible at 473 K, and thus selectivity values cannot be either estimated. It should be noted that a comparison of selectivity of various catalyst is correct if the conversion values over individual samples are similar. This condition cannot be fulfilled due to the high complexity of SCR-NO_x process over Ag/Al₂O₃. However, the selectivity utilization of decane at SCR-NO_x appears to be a parameter that describes non-selective consumption of decane by oxygen occurred at SCR-NO_x. The values of selectivity

utilization show that $\text{Ag}/\text{Al}_2\text{O}_3$ catalysts exhibit the highest selectivity between 523 and 723 K and the selectivity decrease at higher temperature.

3-8a

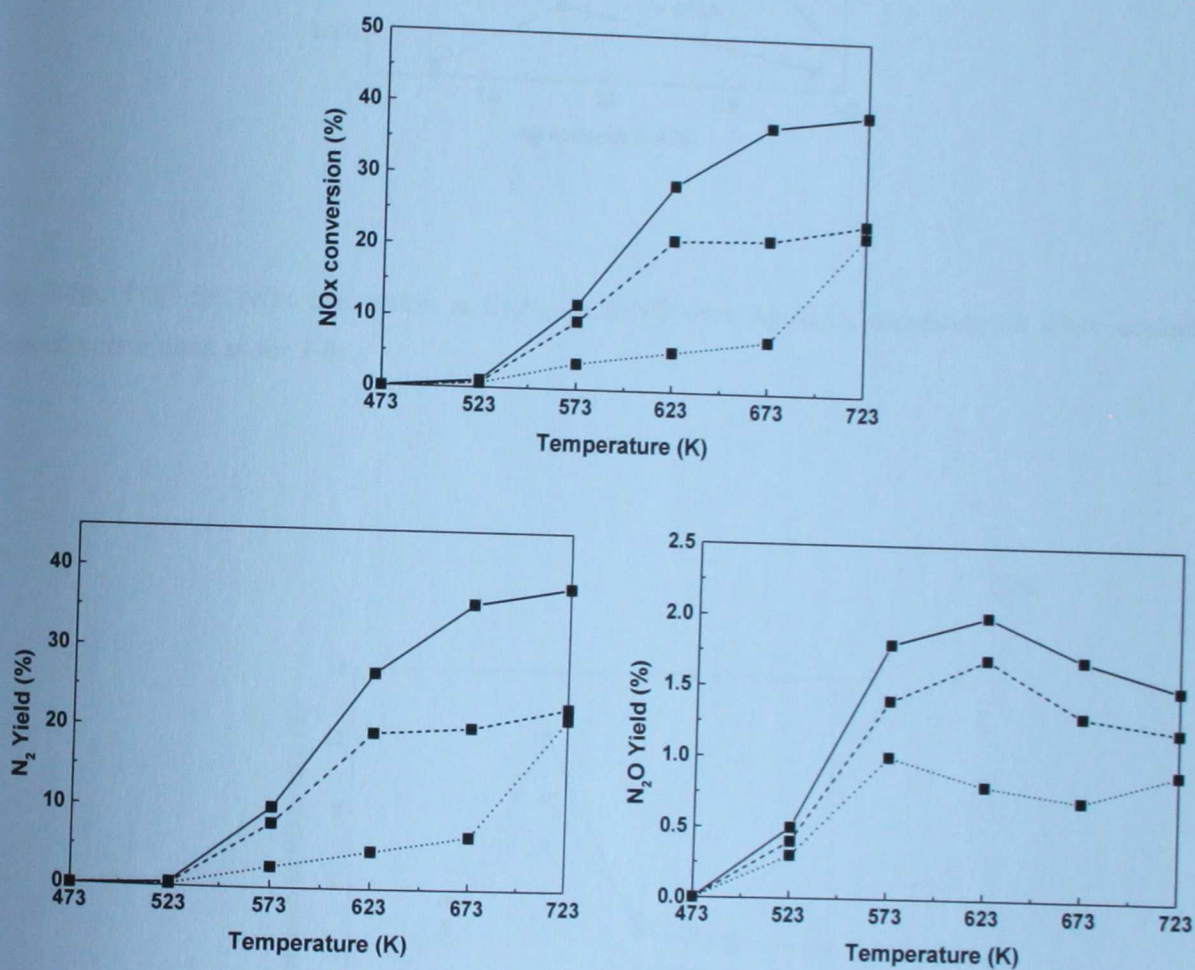


Fig. 3-8a. Conversion of NOx to N₂ and N₂O and yield of N₂ and N₂O at C₁₀H₂₂-SCR-NO over Ag/Al₂O₃ depending on temperature. Reaction conditions: 1,000 ppm NO, 600 ppm C₁₀H₂₂, 6% O₂, 12% H₂O, GHSV = 240,000 h⁻¹.

Ag/Al₂O₃-1.3 (.....), Ag/Al₂O₃-1.8 (—) and Ag/Al₂O₃-2.9 (---).

3-8b

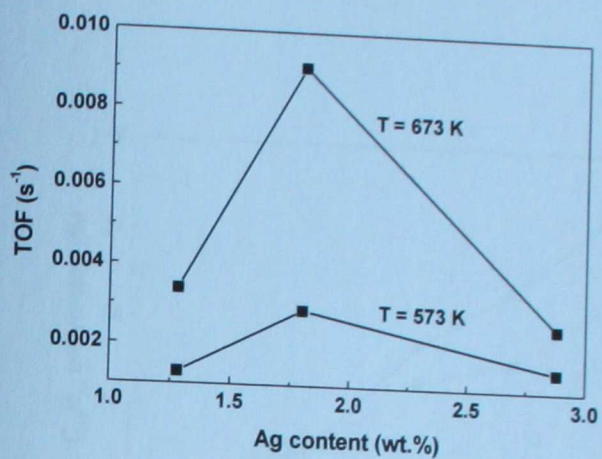


Fig. 3-8b. TOF for NO_x conversion at C₁₀H₂₂-SCR-NO over Ag/Al₂O₃ depending on silver content. Reaction conditions as for 3-8a.

3-8c

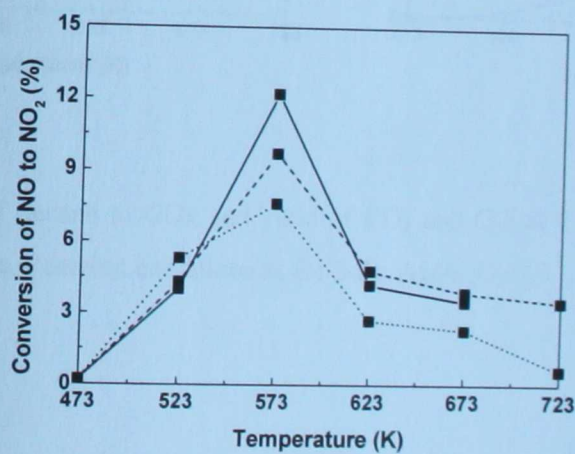


Fig. 3-8c. Conversion of NO to NO₂ at C₁₀H₂₂-SCR-NO over Ag/Al₂O₃ depending on temperature. Reaction conditions as for 3-8a. Ag/Al₂O₃-1.3 (·····), Ag/Al₂O₃-1.8 (—) and Ag/Al₂O₃-2.9 (---).

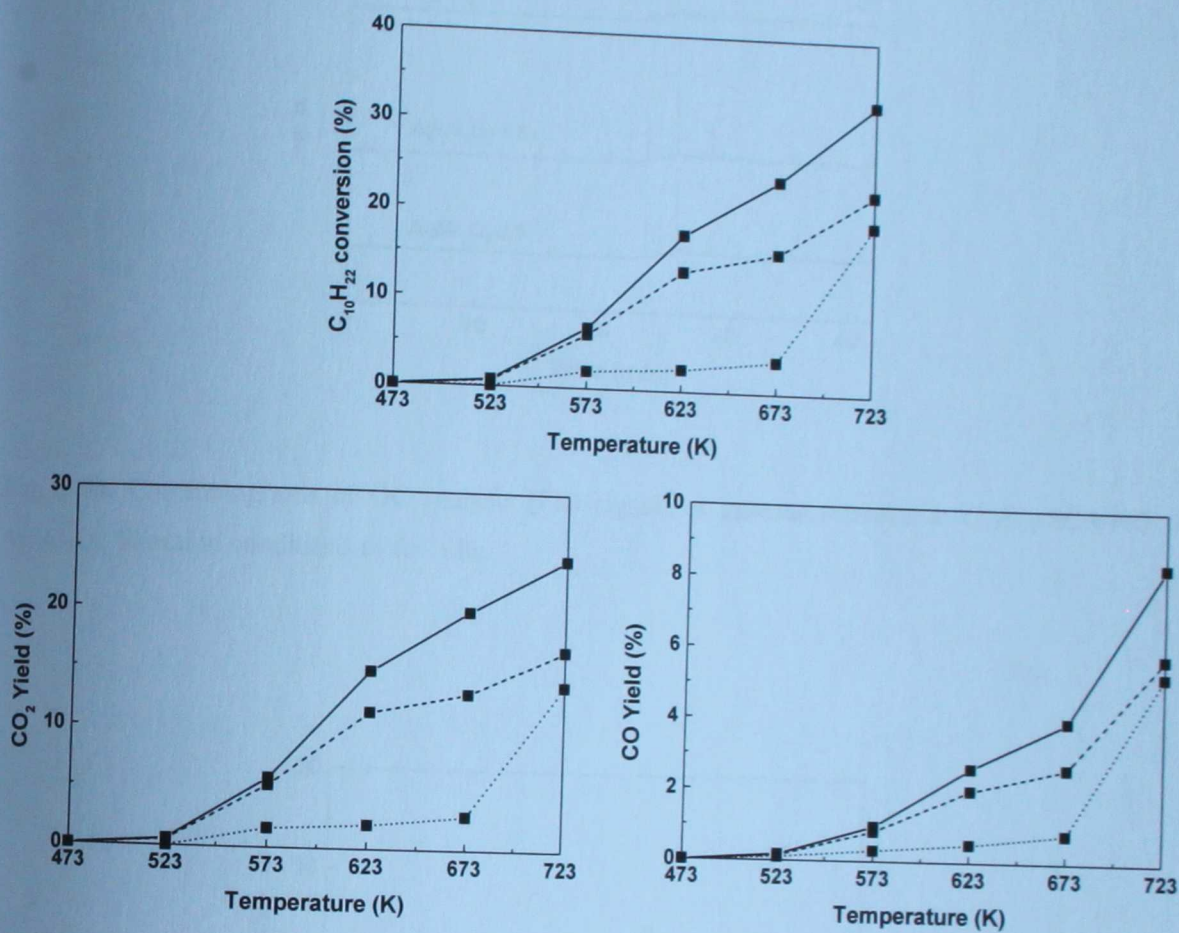


Fig. 3-9a. Conversion of decane to CO_x and yield of CO_2 and CO at $C_{10}H_{22}$ -SCR-NO over Ag/Al_2O_3 depending on temperature. Reaction conditions as for 3-8a. Ag/Al_2O_3 -1.3 (.....), Ag/Al_2O_3 -1.8 (—) and Ag/Al_2O_3 -2.9 (---).

3-9b

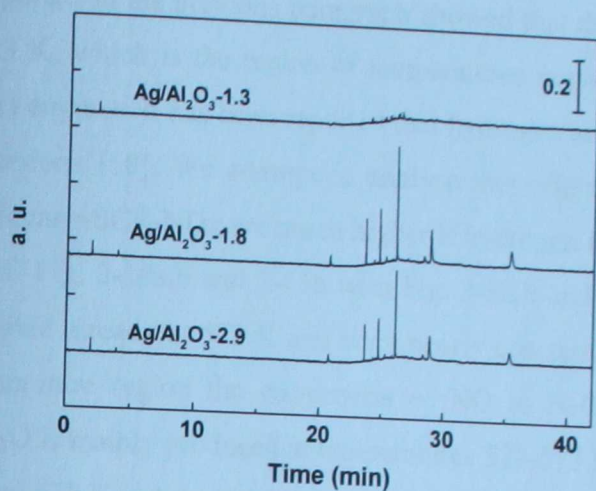


Fig. 3-9b. Chromatograms of GC analysis (FID signal) of gaseous products at $C_{10}H_{22}$ -SCR-NO over Ag/Al_2O_3 . Reaction conditions as for 3-8a.

3-9c

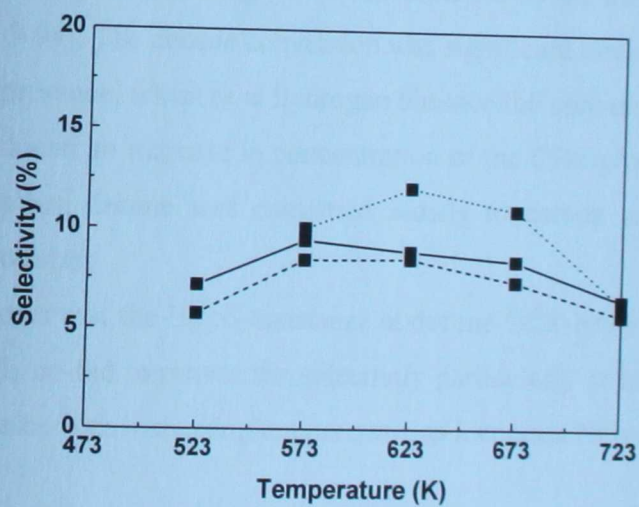


Fig. 3-9c. Selectivity of decane utilization at $C_{10}H_{22}$ -SCR-NO over Ag/Al_2O_3 depending on temperature. Ag/Al_2O_3 -1.3 (.....), Ag/Al_2O_3 -1.8 (—) and Ag/Al_2O_3 -2.9 (---). Reaction conditions as for 3-8a.

3.2.2 Selective catalytic reduction of NO_x over silver alumina catalyst by decane and hydrogen

The results reported in the previous paragraph showed that the conversion of NO_x is low at temperatures < 623 K, which is the region of temperatures important for NO_x abatement in exhaust gases of diesel engines. It has been reported that hydrogen added to the feed substantially increases NO_x conversions [58]. We attempt to analyse this effect. It is clearly seen that the conversion values at decane-SCR-NO_x are much higher if hydrogen is added as a co-reactant into the reactant stream (cf. Fig. 3-10a,b and 3-11a with Fig. 3-8a,b and 3-9a). High values of NO_x conversions were reached already at 573 K and were nearly constant up to 723 K for Ag/Al₂O₃-1.8. In the low temperature region the conversion of NO to N₂O was slightly increased at hydrogen presence. N₂O is mainly produced at temperatures 523-573 K. Turnover frequencies for the SCR-NO at 573 and 673 K indicate high increase in efficiency of NO_x reduction at hydrogen presence in the reactant mixture (cf. Fig. 3-10b with 3-8b). Values of TOF show that ca 2 wt.% is an optimum Ag loading for C₁₀H₂₂-SCR-NO_x co-assisted by hydrogen.

Presence of hydrogen in the reactant stream yielded also high activity in oxidation of NO to NO₂ at SCR-NO_x particularly at low temperatures (473-523 K). Conversion of NO to NO₂ had a decreasing tendency at higher temperature (Fig. 3-10c).

The promotion effect of hydrogen was accompanied by the increase of decane conversion (cf. Fig. 3-11a with 3-9a). The decane conversion was significant already at temperatures of 473 - 523 K at hydrogen presence, whereas at hydrogen absence the conversion is negligible. Addition of hydrogen also induced an increase in concentration of the CH_x-products over all the catalysts (Fig. 11b); nevertheless, decane was converted mostly to carbon oxides and only < 10% to hydrocarbon-like products.

Fig 3-11c shows that the H₂ co-assistance at decane-SCR-NO_x modifies the selectivity of decane utilization. H₂ co-fed improves the selectivity particularly at low temperature region and the selectivity decreases with increasing temperature, as increases NO_x conversion.

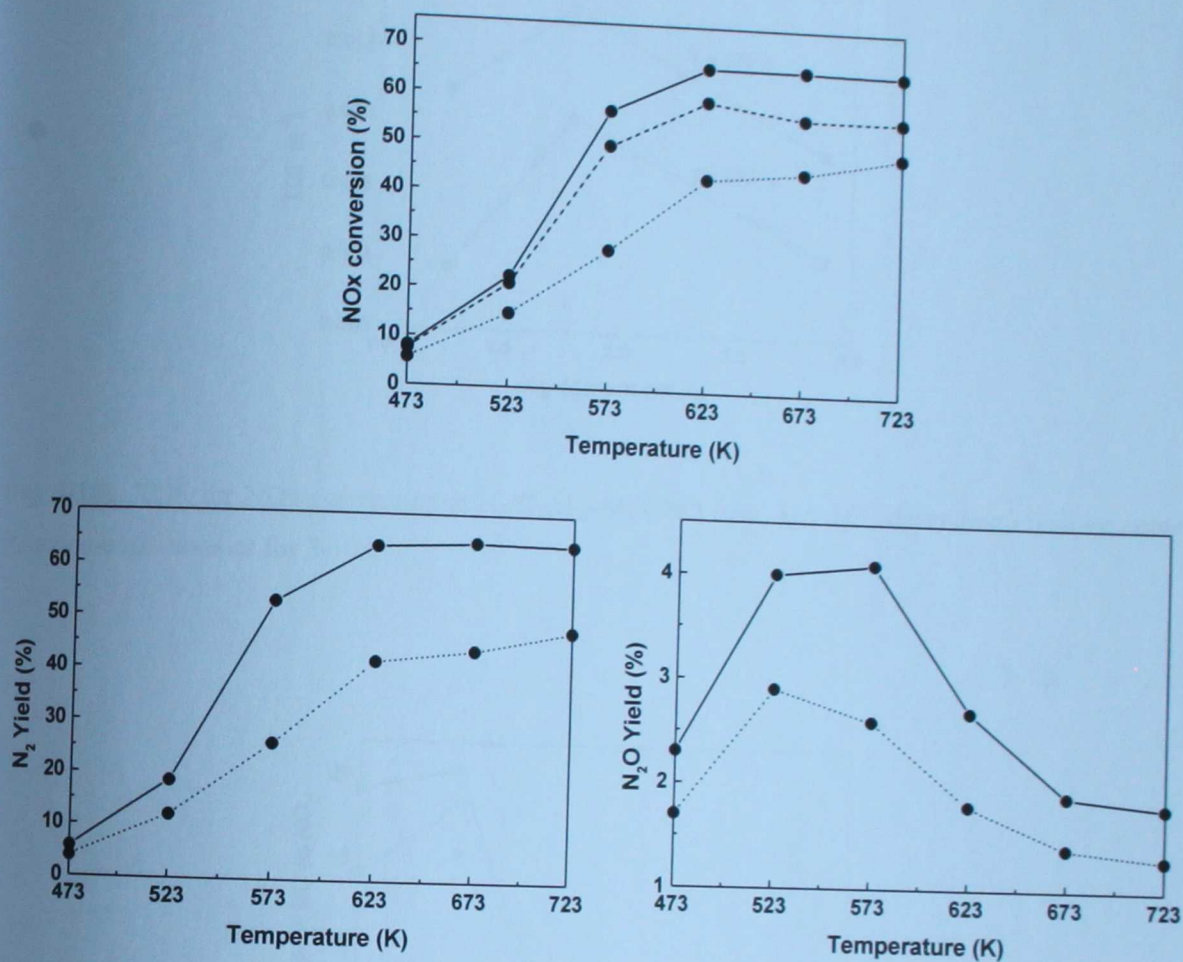


Fig. 3-10a. Conversion of NO_x to N₂ and N₂O and yield of N₂ and N₂O at C₁₀H₂₂-SCR-NO co-assisted by hydrogen over Ag/Al₂O₃ depending on temperature. Reaction conditions: 1,000 ppm NO, 600 ppm C₁₀H₂₂, 2,000 ppm H₂, 6% O₂, 12% H₂O, GHSV = 240,000 h⁻¹. Ag/Al₂O₃-1.3 (·····), Ag/Al₂O₃-1.8 (—) and Ag/Al₂O₃-2.9 (---).

3-10b

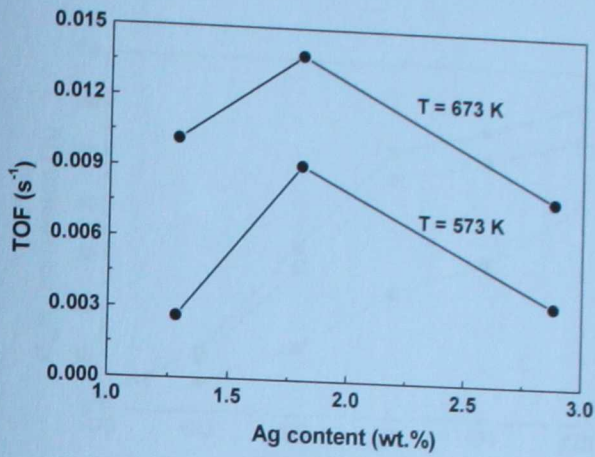


Fig. 3-10b. TOF for NO_x conversion at H₂/C₁₀H₂₂-SCR-NO over Ag/Al₂O₃ depending on silver content. Reaction conditions as for 3-10a.

3-10c

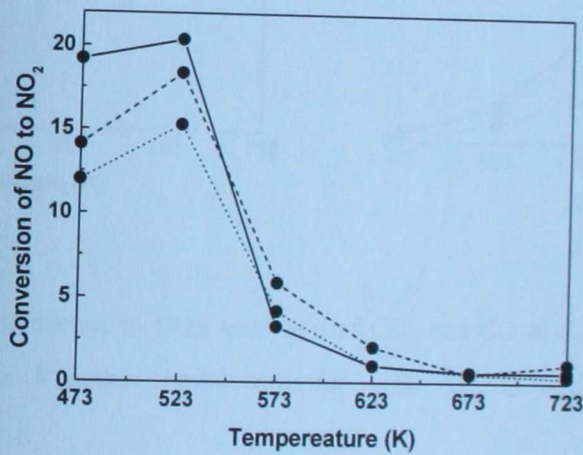


Fig. 3-10c. Conversion of NO to NO₂ at C₁₀H₂₂-SCR-NO over Ag/Al₂O₃ depending on temperature. Reaction conditions as for 3-10a. Ag/Al₂O₃-1.3 (·····), Ag/Al₂O₃-1.8 (—) and Ag/Al₂O₃-2.9 (---).

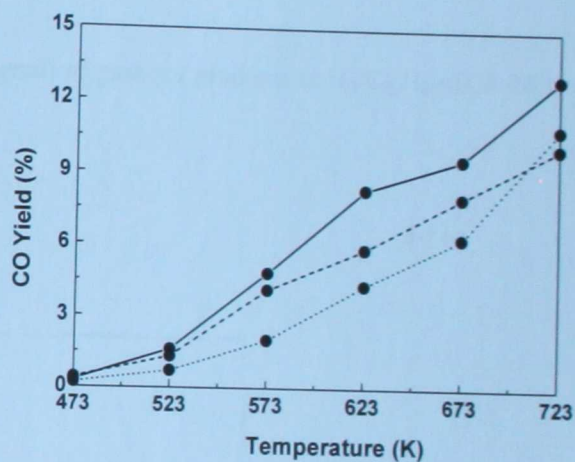
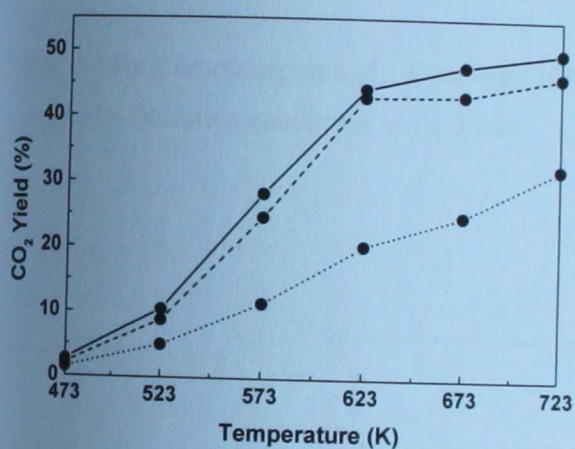
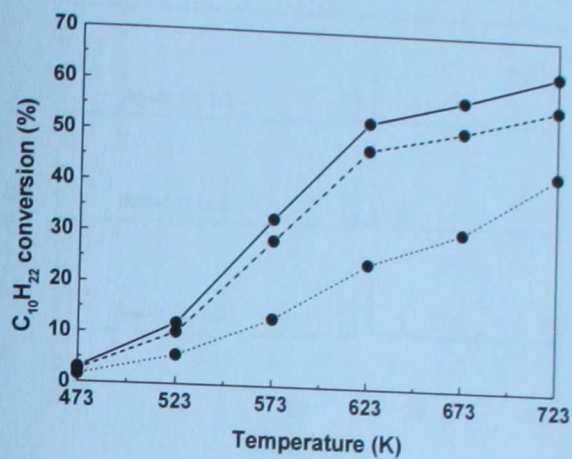


Fig. 3-11a. Conversion of decane to CO_x and yield of CO₂ and CO at C₁₀H₂₂-SCR-NO over Ag/Al₂O₃ depending on temperature. Reaction conditions as for 3-10a. Ag/Al₂O₃-1.3 (.....), Ag/Al₂O₃-1.8 (—) and Ag/Al₂O₃-2.9 (---).

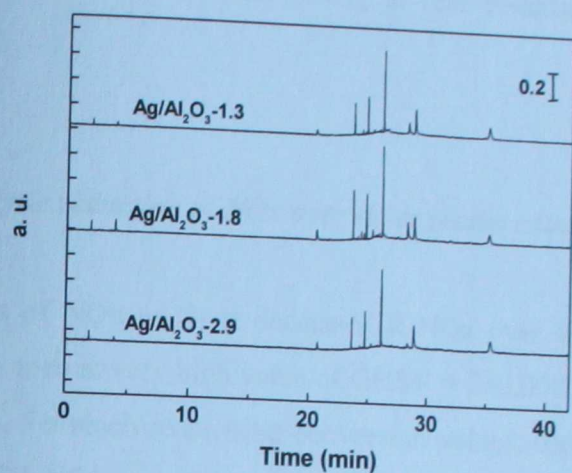


Fig. 3-11b. Chromatograms of GC analysis (FID signal) of gaseous products at $H_2/C_{10}H_{22}$ -SCR-NO over Ag/Al_2O_3 . Reaction conditions as for 3-10a.

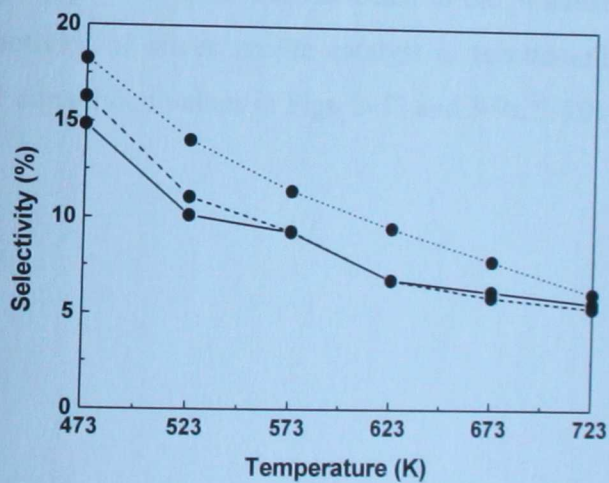


Fig. 3-11c. Selectivity of decane utilization of $C_{10}H_{22}$ -SCR-NO over Ag/Al_2O_3 depending on temperature. Reaction conditions as for 3-10a. Ag/Al_2O_3 -1.3 (·····), Ag/Al_2O_3 -1.8 (—) and Ag/Al_2O_3 -2.9 (---).

It can be concluded that among Ag/Al₂O₃ catalysts the Ag/Al₂O₃-1.8 exhibits the highest NO_x conversion, moreover, long-term performance in SCR-NO_x (Fig 3-16) and thus it was selected for further analysis of the state of Ag at real conditions of the decane-SCR-NO_x reaction.

3.2.3 *Selective catalytic reduction of NO_x over silver zeolite catalyst by decane and co-assisted by hydrogen*

The conversions of NO_x to N₂ at decane-SCR-NO_x over silver zeolite catalyst AgNH₄-MFI-4.2 were close to zero at very high value of GHSV = 240,000 h⁻¹ at temperature region 473 – 673 K (not plotted). To reach reasonable conversion values, the activity of the silver zeolite catalysts at decane-SCR-NO_x and H₂/decane-SCR-NO_x were tested at lower values of GHSV (30,000 h⁻¹), (Fig. 3-12). Conversion of NO_x increased with increasing temperature up to 673 K and declined at higher temperatures due to complete conversion of decane. Addition of hydrogen caused a slight increase in both conversion of NO_x and decane. It is to be pointed out that the activity of Ag-MFI decreased in time due to coke formation [77] and steady-state conversions in this study were achieved within several hours. NO was reduced predominantly to N₂ as only trace concentrations of N₂O (up to 15 ppm) were detected in the products (not depicted). It is clearly seen that catalytic activity of silver zeolite catalyst is substantially lower than that of silver alumina catalysts (cf. conversion values in Figs. 3-12 and 3-9a, 3-10a and GHSV values).

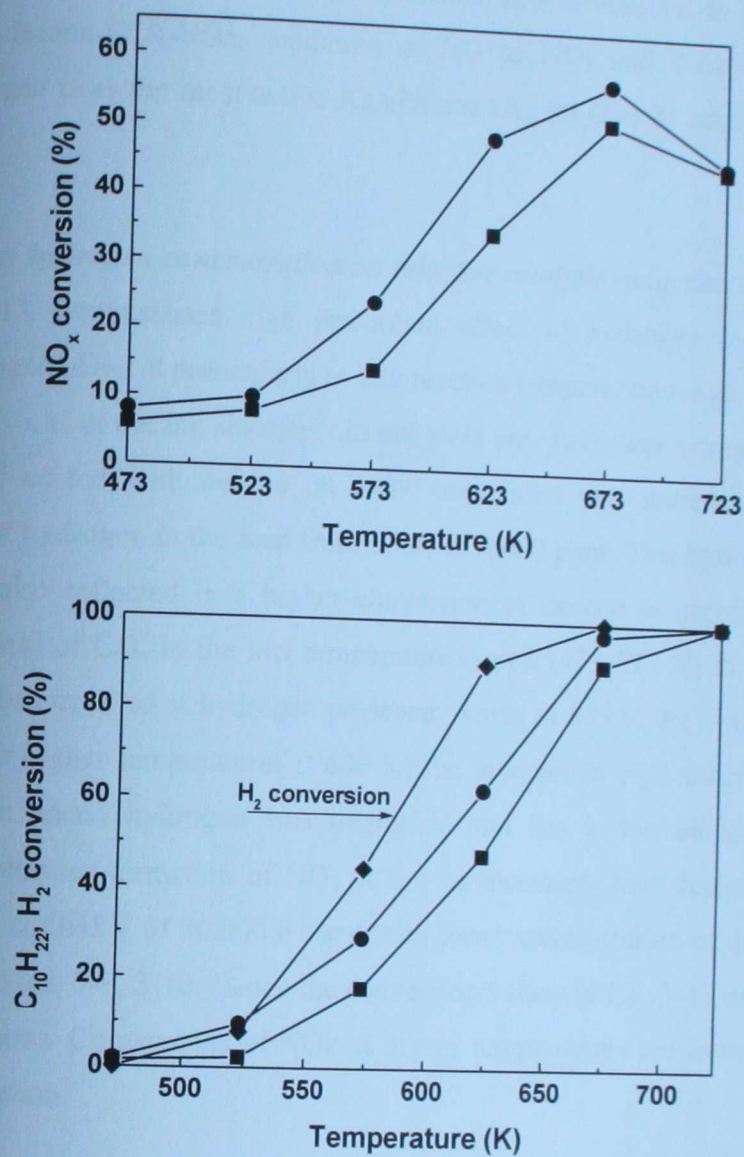


Fig. 3-12. Conversion of NO_x to N₂ and decane to CO_x at C₁₀H₂₂-SCR-NO and H₂/C₁₀H₂₂-SCR-NO over AgNH₄-MFI-4.2 depending on temperature. Feed: 1,000 ppm NO, 450 ppm C₁₀H₂₂, 6% O₂, 12% H₂O and 0 ppm H₂ (■) or 2,000 ppm H₂ (●). GHSV = 30,000 h⁻¹. Hydrogen conversion (◆).

3.3 Effect of hydrogen on selective catalytic reduction of NO_x over silver alumina catalyst

To obtain an insight into hydrogen function as a co-reactant to hydrocarbons, effect of hydrogen on decane-SCR-NO_x, oxidation of NO to NO₂ and decane to CO and CO₂ by molecular oxygen over the most active Ag/alumina (Ag/Al₂O₃-1.8) catalyst was investigated in detail.

3.3.1 Effect of hydrogen concentration on selective catalytic reduction of NO_x

Fig. 3-13 demonstrates high promotion effect of hydrogen on the C₁₀H₂₂-SCR-NO reaction over Ag/Al₂O₃-1.8 particularly at low reaction temperature range, i. e. below 623 K. But hydrogen alone, i. e. at decane absence, did not yield any molecular nitrogen. The positive effect of hydrogen if co-fed with decane on NO_x conversion was increased with the increasing concentration of hydrogen in the feed from 1,000 to 4,000 ppm. This hydrogen-effect on C₁₀H₂₂-SCR-NO was also reflected in a higher conversion of decane to carbon oxides, but without changing the yield of CO. In the low temperature region (473-573 K) the conversion of NO to N₂O was slightly increased at hydrogen presence, where at 573 K the N₂O yield increased from ca 3 to 10%. At higher temperatures (>600 K) the increase in N₂O formation compared to the reaction without added hydrogen was negligible and has a decreasing tendency. Hydrogen addition also enhances formation of NO₂ at low temperatures (not depicted). The experiments were performed at GHSV of 30,000 h⁻¹ and with lower concentration of decane (300 ppm) than that depicted in Figs. 3-9, 3-10. Hence the conversion values in Fig. 3-13 are substantially higher at low temperatures. Conversions of NO_x at higher temperatures are lower due to limitation of decane concentration.

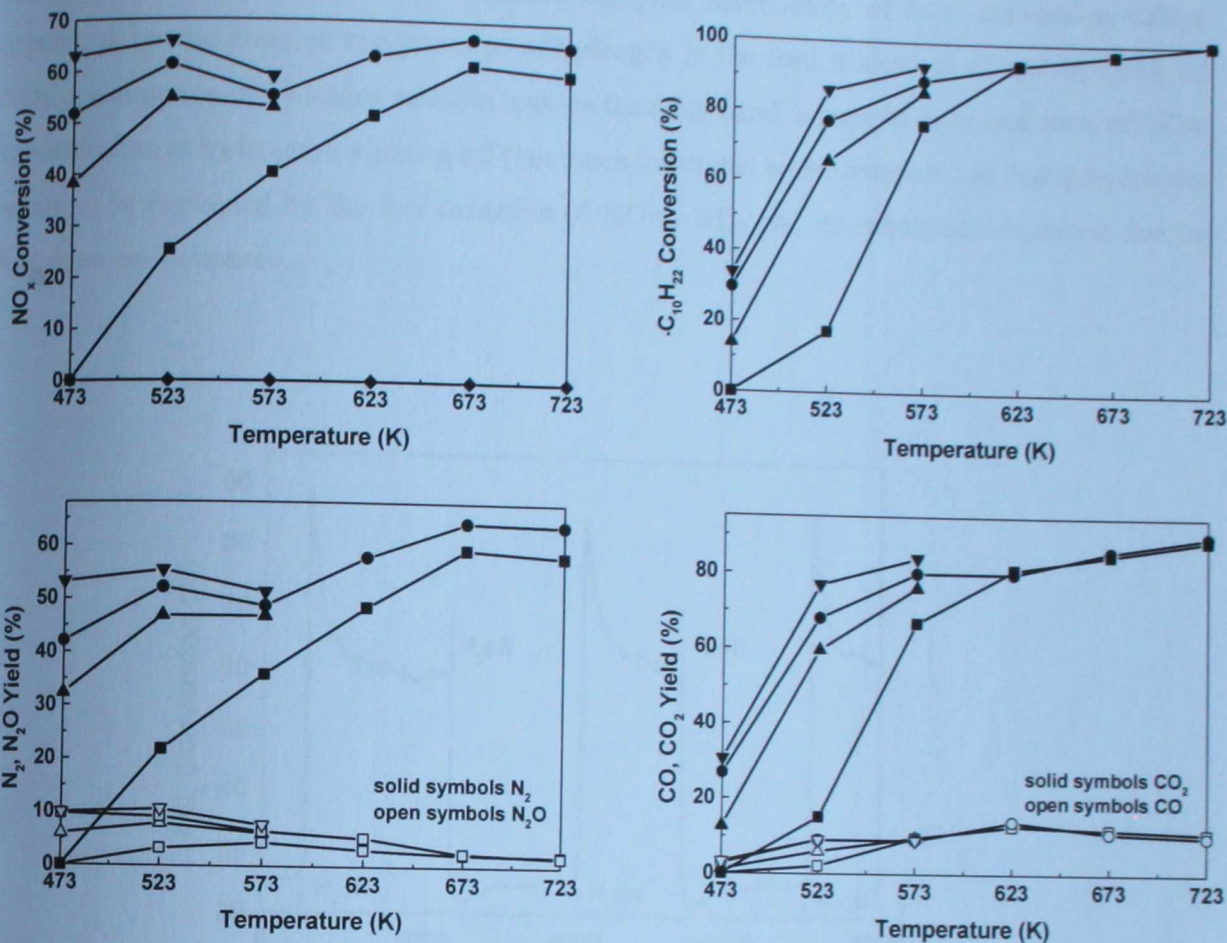


Fig. 3-13. Effect of hydrogen on C₁₀H₂₂-SCR-NO over Ag/Al₂O₃-1.8. Feed: 1,000 ppm NO, 400 ppm C₁₀H₂₂, 6% O₂, 12% H₂O and 0 ppm H₂ (■, □), 1,000 ppm H₂ (●, ○), 2,000 ppm H₂ (▲, △), 4,000 ppm H₂ (▼, ▽) and 2,000 ppm H₂, 0 ppm C₁₀H₂₂ (◆), GHSV = 30,000 h⁻¹.

3.3.2 Reversibility of the hydrogen effect on selective catalytic reduction of NO_x

A time response of the NO_x consumption to the addition and removal of hydrogen into the reactant stream at C₁₀H₂₂-SCR-NO_x is shown in Fig. 3-14. The NO consumption sharply increased (within seconds, being limited by the response of the NO/NO_x analyser to concentration changes) showing a sharp peak in the NO_x conversion followed by stabilization of NO_x concentration. Switching off of hydrogen caused an opposite response in NO_x concentration, again with a temporary higher NO_x concentration than that stabilized within

several minutes. These experiments showed complete reversibility of NO_x conversion values depending on the absence and presence of hydrogen in the feed. Existence of a sharp peak of NO_x consumption at hydrogen addition and, on the other hand, a peak of increased level of NO_x concentration at hydrogen switching off (but much lower and wider compared to that at hydrogen addition) is explained by the fast oxidation of NO to NO₂ and its enhanced adsorption due to hydrogen co-assistance.

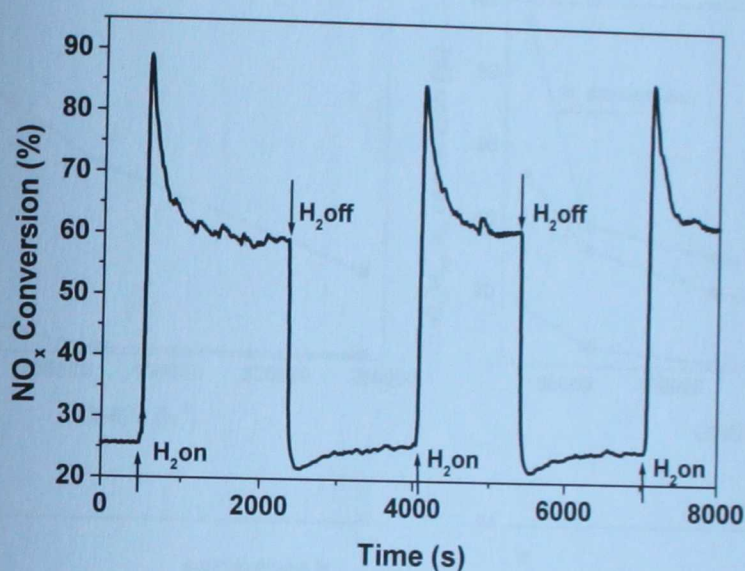


Fig. 3-14. Effect of hydrogen switching on and off in C₁₀H₂₂-SCR-NO over Ag/Al₂O₃-1.8. Feed: 1,000 ppm NO, 300 ppm decane, 6% O₂ and 0 or 2,000 ppm H₂, 12% H₂O. GHSV = 30,000 h⁻¹. T = 523 K.

3.3.3 Effect of hydrogen on selective catalytic reduction of NO_x as a function of GHSV

The effect of hydrogen on C₁₀H₂₂-SCR-NO at 523 K as a function of reciprocal contact time (GHSV) is also remarkable (Fig. 3-15). While without hydrogen the conversion of NO_x in C₁₀H₂₂-SCR-NO at GHSV > 60,000 h⁻¹ was close to zero, under hydrogen presence the increase of GHSV from 30,000 to 60,000 h⁻¹ resulted in a decrease in NO_x conversion from 100% only to 80%. At extremely high GHSV values of 120,000 and 240,000 h⁻¹ the NO_x conversions were still ca 50 and 30%, respectively. Nitrogen was a major product of NO reduction in both the absence

and presence of hydrogen in the whole range of GHSV values investigated. NO_2 was also found in the products and the yield of N_2O was only slightly increased under the presence of hydrogen, i.e. from 0 to 2% and from 2 to 6% at GHSV values of 240,000 and 30,000 h^{-1} , respectively. Understandably, both the hydrogen and decane conversions considerably decreased with increasing GHSV values. As for decane, it was mostly converted to CO_2 . The yield of CO was only slightly higher at hydrogen presence compared to the $\text{C}_{10}\text{H}_{22}$ -SCR- NO_x reaction.

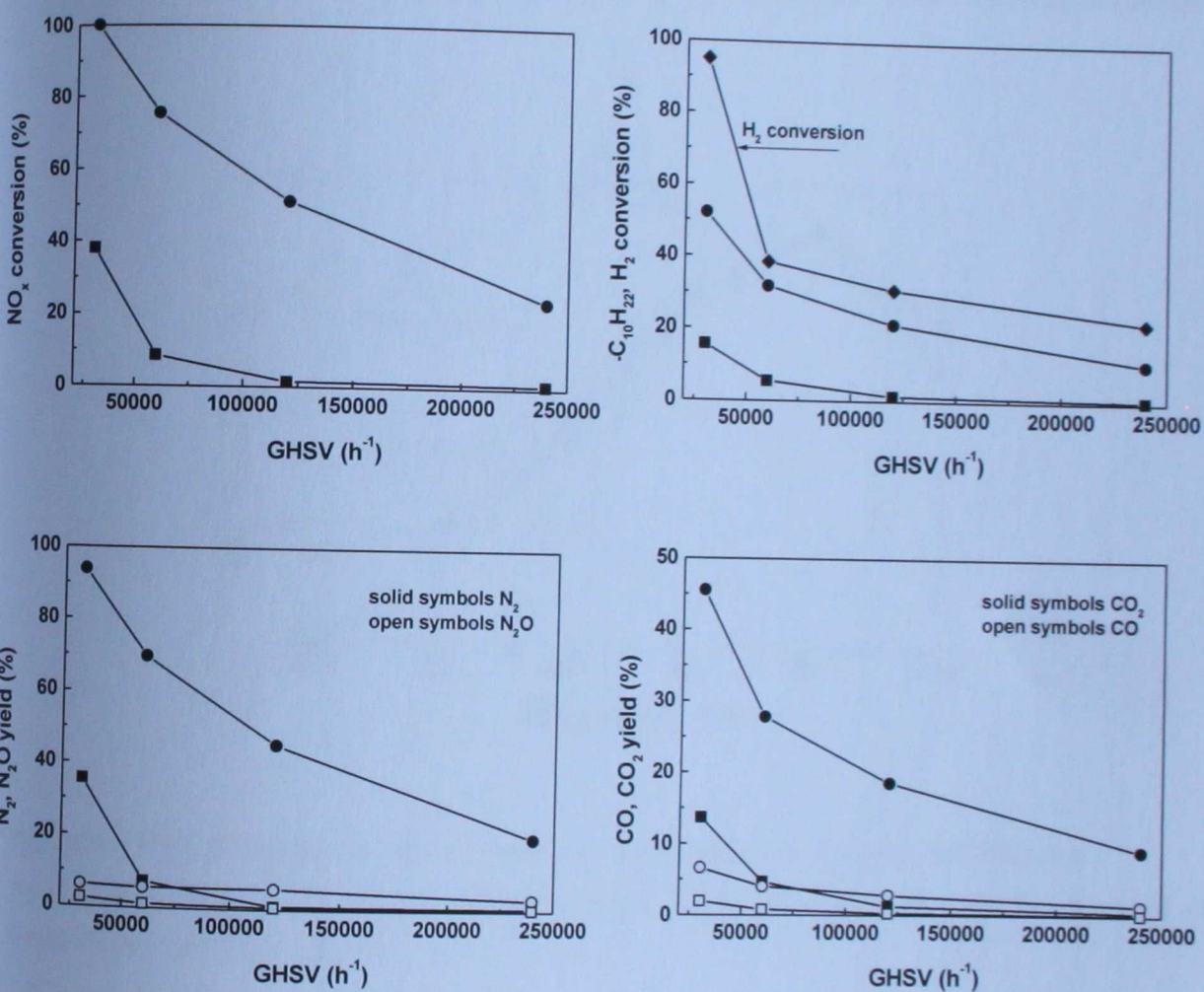


Fig. 3-15. Effect of hydrogen on $\text{C}_{10}\text{H}_{22}$ -SCR- NO at 523 K over $\text{Ag}/\text{Al}_2\text{O}_3$ -1.8 as a function of GHSV.

Feed: 1,000 ppm NO , 600 ppm $\text{C}_{10}\text{H}_{22}$, 6% O_2 , 12% H_2O and 0 ppm H_2 (■, □), 2,000 ppm H_2 (●, ○).

Hydrogen conversion (◆).

3.3.4 Effect of water vapour on selective catalytic reduction of NOx by decane and hydrogen

The effect of water vapour on $H_2/C_{10}H_{22}$ -SCR-NO over Ag/Al_2O_3 was also investigated. If water vapor was not fed at the $H_2/C_{10}H_{22}$ -SCR-NO_x reaction, slow but substantial deactivation of the catalyst took place (Fig. 3-16). After 300 min, the NO conversion decreased to the values similar to those obtained in the reaction carried out without hydrogen as a co-reactant. Thus, a concentration of water vapor of 12% in the stream (like that present in the real exhausts of diesel engines) is valuable, as it prevents catalyst deactivation. This implies that water vapor suppresses the adsorption of various hydrocarbons and their derivatives and thus "cleans" the catalyst surface.

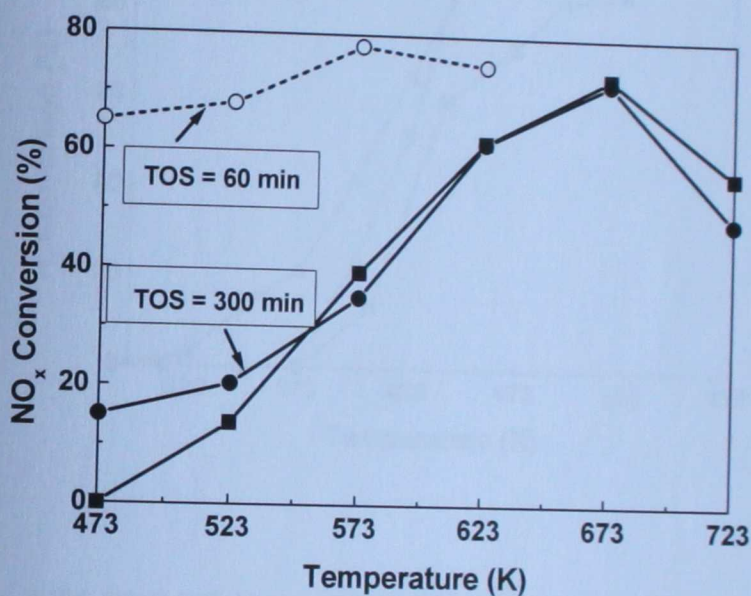


Fig. 3-16. Effect of hydrogen and deactivation in the water absence in $H_2/C_{10}H_{22}$ -SCR-NO over Ag/Al_2O_3 -1.8. Feed: 1,000 ppm NO, 300 ppm decane, 6% O_2 , 0% H_2O , 2,000 ppm H_2 (● or ○) or 1,000 ppm H_2 (■). GHSV = 30,000 h^{-1} .

3.5 Oxidation of hydrogen, and effect of hydrogen on oxidation of NO and decane

Fig. 3-17 shows that the oxidation of hydrogen with molecular oxygen over Ag/Al_2O_3 -1.8 started below 373 K and was complete at ca 470 K. If water vapor was added (12%) it only slightly decreased hydrogen conversion at low temperature region, but complete conversion of

hydrogen was reached at the same temperature of 470 K. As the decrease of hydrogen conversion is found at temperature below 450 K it can be caused by water molecules adsorption on active sites. If decane and water vapour were added into the (H_2+O_2+He) stream, oxidation of hydrogen was shifted to higher temperatures (depending on the feed composition), and complete hydrogen oxidation was obtained for a given reactant concentrations at about 570 K. It follows that the rate of hydrogen oxidation is primarily affected by the presence of hydrocarbons.

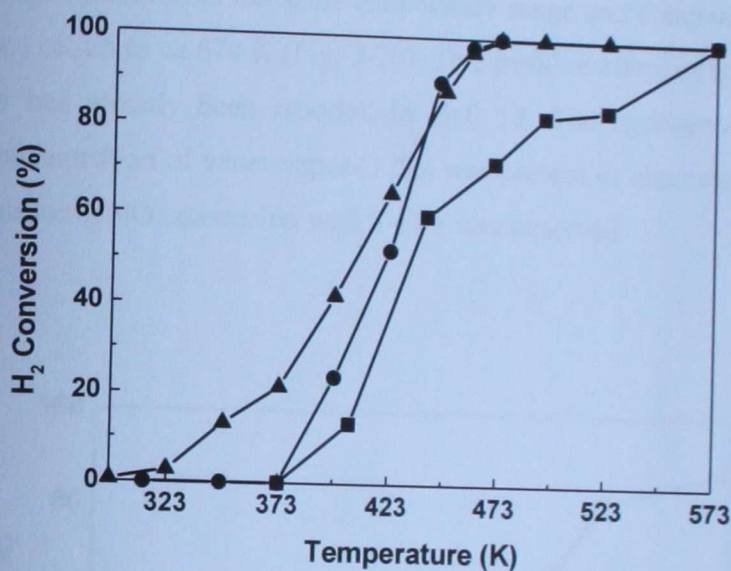


Fig. 3-17. Effect of water vapor and decane on hydrogen oxidation over $Ag/Al_2O_3-1.8$. Feed: 2,000 ppm H_2 and 6% O_2 (▲), 2,000 ppm H_2 , 6% O_2 and 12% H_2O (●), 2,000 ppm H_2 , 6% O_2 , 12% H_2O and 600 ppm decane (■). GHSV = 30,000 h^{-1} .

The contribution of hydrogen to decane oxidation by molecular oxygen is shown in Fig. 3-18. At low temperature region decane conversion to CO_2 was enhanced by hydrogen added, but the yield of CO was not changed, like at the SCR- NO_x reaction. In the absence of water vapour in the ($\text{decane} + \text{O}_2 + \text{H}_2$) stream a considerable catalyst deactivation in T-O-S occurred (Fig. 3-19), analogously to the catalyst deactivation at $\text{H}_2/\text{decane-SCR-NO}$ carried out in the absence of water vapour in the reactant feed. This again indicates that water vapor suppresses adsorption of reaction intermediates and oligomerization processes leading to catalyst coking and deactivation.

Oxidation of NO to NO_2 by molecular oxygen over $\text{Ag}/\text{Al}_2\text{O}_3$ catalyst was strongly enhanced by hydrogen addition in the same temperature range and comparable conditions as the SCR- NO_x reaction, i.e. up to ca 670 K (Fig. 3-20). This positive effect of hydrogen on the rate of NO- NO_2 reaction has already been reported in Ref. 58. The hydrogen-effect was observed regardless high concentration of water vapor (12%) was present or absent in the reactant feed. In both cases no decrease in NO conversion with T-O-S was observed.

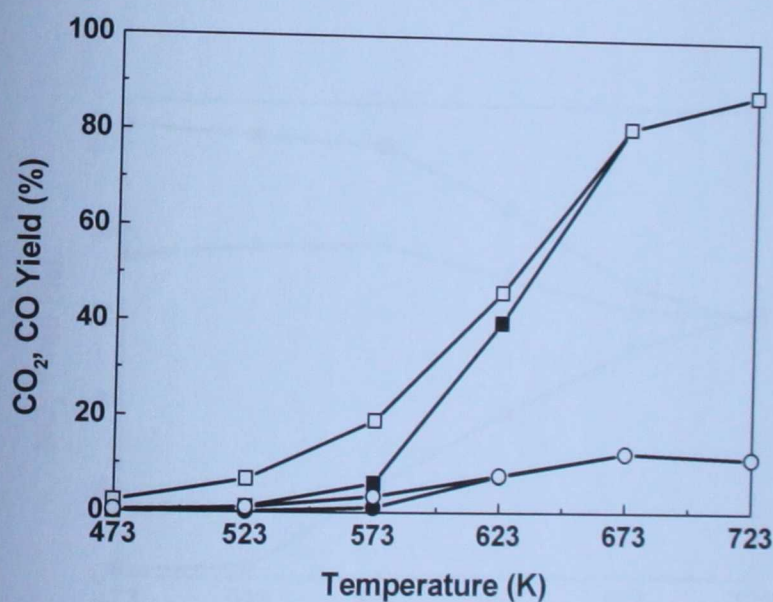


Fig. 3-18. Effect of hydrogen on the oxidation of $\text{C}_{10}\text{H}_{22}$ to CO (\bullet, \circ) and CO_2 (\blacksquare, \square) over $\text{Ag}/\text{Al}_2\text{O}_3$ -1.8, 3% O_2 , 300 ppm $\text{n-C}_{10}\text{H}_{22}$ and 0 ppm H_2 (solid symbols) or 2,000 ppm H_2 (open symbols). GHSV = 10,000 h^{-1} .

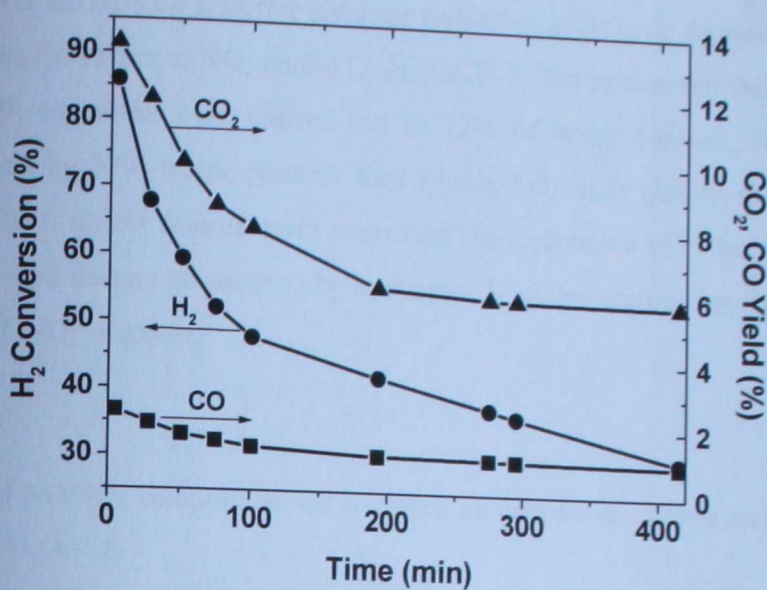


Fig. 3-19. Deactivation of the catalyst at hydrogen + decane oxidation on Ag/Al₂O₃-1.8 in the absence of water vapor. Conversion of hydrogen (●), and yield of CO (■) and CO₂ (▲). Feed: 300 ppm decane, 2,000 ppm H₂ and 6% O₂. GHSV = 30,000 h⁻¹. T = 523 K.

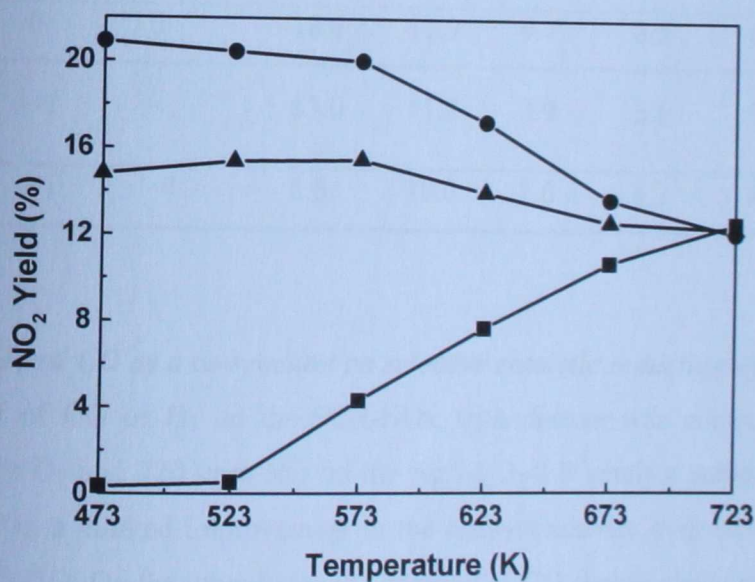


Fig. 3-20. Effect of hydrogen on the oxidation of NO to NO₂ over Ag/Al₂O₃-1.8. Feed: 1,000 ppm NO, 6% O₂ and 0 ppm H₂ (■), 1,000 ppm H₂ (▲), 2,000 ppm H₂ (●). GHSV = 30,000 h⁻¹.

3.3.6 Effect of NO vs. NO₂ on selective catalytic reduction of NO_x by decane and hydrogen

To elucidate the effect of NO₂ on the C₁₀H₂₂-SCR-NO_x reaction and the reaction co-assist by hydrogen (both reactions were carried out in 12% of water vapour), NO was partly or completely replaced by NO₂ in the reactant feed (Table 3-3). It is clearly seen that the higher concentrations of NO₂ at low temperatures decreased the conversion of NO_x to N₂ for SCR-NO using both decane and decane co-assisted by hydrogen. It is also shown that hydrogen enhanced the rate of the SCR-NO₂ reaction.

Table 3-3. Effect of NO/NO₂ composition and hydrogen on conversion of NO_x and C₁₀H₂₂ at C₁₀H₂₂-SCR-NO_x over Ag/Al₂O₃-1.8.

Feed: 1,000 ppm NO_x, 500 ppm C₁₀H₂₂, 6% O₂, 12% H₂O and 0 and 2,000 ppm H₂.

GHSV = 60,000 h⁻¹.

NO _x fed composition	473 K		523 K					
	0 ppm H ₂		2,000 ppm H ₂		0 ppm H ₂		2,000 ppm H ₂	
	NO _x (%)	C ₁₀ H ₂₂ (%)	NO _x (%)	C ₁₀ H ₂₂ (%)	NO _x (%)	C ₁₀ H ₂₂ (%)	NO _x (%)	C ₁₀ H ₂₂ (%)
1,000 ppm NO	0	0	18.4	11.9	9.7	8.5	64.8	47.0
500 ppm NO + 500 ppm NO ₂	~1	~1	13.0	11.5	3.9	5.6	54.4	42.3
1,000 ppm NO ₂	~1	~1	8.6	10.0	1.6	4.2	44.3	41.7

3.3.7 Effect of H₂ vs. CO as a co-reactant on selective catalytic reduction of NO_x by decane

The effect of CO or H₂ on the SCR-NO_x with decane was compared with the feed containing of 4.3% O₂ and 720 ppm NO on the Ag/Al₂O₃-1.8 catalyst sample. The addition of hydrogen resulted in a marked improvement in the catalyst activity over the temperature range 473 - 673 K (Fig. 3-21). On the other hand, the addition of CO (being also a reductant) to decane had practically no effect on the SCR-NO_x activity of the catalyst.

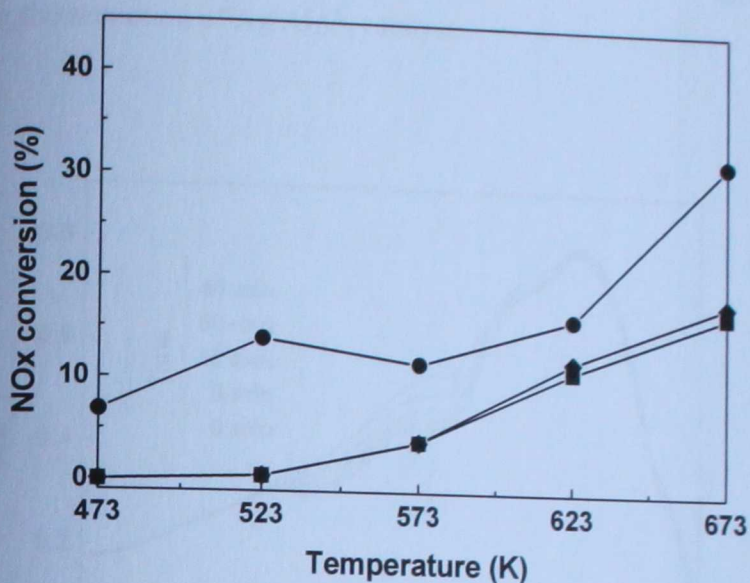


Fig. 3-21. NO_x conversion as a function of temperature for the C₁₀H₂₂-SCR-NO_x by decane over Ag/Al₂O₃-1.8 that with CO or H₂ added. With decane (■), 0.72% CO added (◆) and with 0.72% H₂ added (●). Conditions: 720 ppm NO, 4.3% O₂, 435 ppm C₁₀H₂₂, 4.3% H₂O. GHSV = 240,000 h⁻¹.

3.4 State of silver at silver alumina catalyst at the conditions of the catalytic process

UV-Vis spectra were used to monitor the state of silver in the 1.8-Ag/Al₂O₃ catalyst under real the condition of the reactions.

3.4.1 Reduction of Ag/alumina by hydrogen

Reduction of silver in Ag/Al₂O₃ occurred already under very mild conditions at RT. At this experiment the UV-Vis spectra were measured after calcination of the sample in an oxygen stream at 723 K, cooled down to RT, and after replacement of oxygen by a helium stream and hydrogen (Fig. 3-22a,b). Due to some low extent of hydration the spectra of Ag/Al₂O₃ exhibited a change in intensities of the bands of Ag⁺ ions. The low intensity bands at ca 28,000 and 34,000 cm⁻¹, which increased in intensity after introduction of hydrogen into the system, indicate development of small Ag_n^{δ+} clusters. As the position of the both bands did not significantly

change with time, the nuclearity of $Ag_n^{\delta+}$ clusters can be expected to was not changed but increase their concentration. It indicates that define nuclearity of $Ag_n^{\delta+}$ clusters might be preserved during the reduction of Ag/Al_2O_3 catalyst.

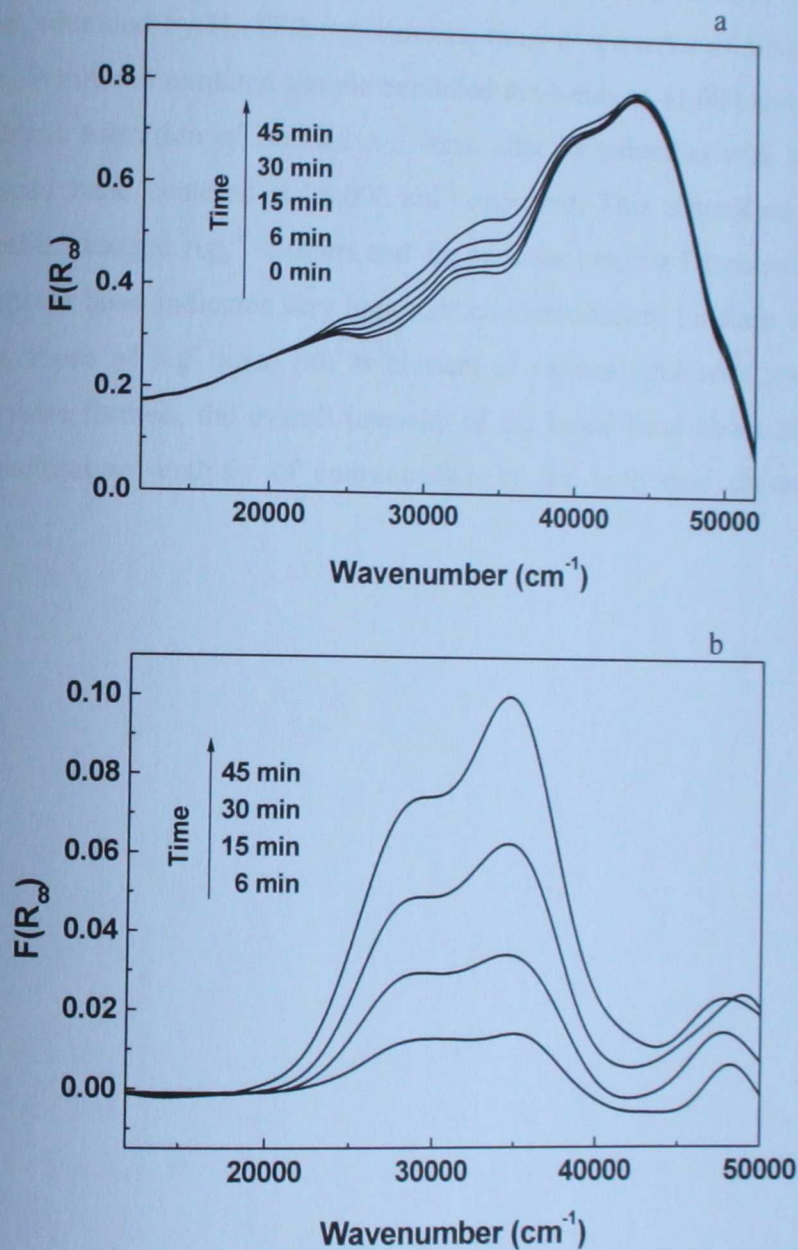


Fig. 3-22a,b. Ag clusters formation at 2,000 ppm H_2 in He over Ag/Al_2O_3 -1.8 at RT.
a) Evolution of the *in-situ* diffuse reflectance UV-Vis-NIR spectra of Ag/Al_2O_3 at hydrogen
b) Difference spectrum between that under reaction conditions and the spectrum in flow of O_2 .

To obtain a rough estimation of the intensity of the spectral bands corresponding to $\text{Ag}_n^{\delta+}$ clusters the UV-Vis spectra were measured at the experimental conditions simulating H_2 -TPR experiment. Thus the amount of Ag^+ reduced to Ag^0 was known from the amount of H_2 consumption. Fig. 3-23 depicts *in-situ* UV-Vis spectra of Ag/alumina calcined in an oxygen stream at 723 K for 1 h and reduced at 520 K in hydrogen. According to the hydrogen consumption, obtained by H_2 -TPR experiments, roughly a quarter of silver was reduced at this temperature. While the oxidized sample exhibited the bands at 41,600 and 46,600 cm^{-1} assigned to the electronic transition of isolated Ag^+ ions, after its reduction with hydrogen at 520 K an intensive broad band centered at 26,000 cm^{-1} appeared. This absorption reflects formation of various metallic charged $\text{Ag}_n^{\delta+}$ clusters and Ag particles (see the Discussion). The high intensity of the absorption band indicates very high extinction coefficient for these metallic silver species compared to those of Ag^+ ions. But as clusters of various nuclearity and particles of various dimensions were formed, the overall intensity of the broad band about 26,000 cm^{-1} , cannot be used for quantitative analysis of concentration of the individual clusters or metallic silver particles.

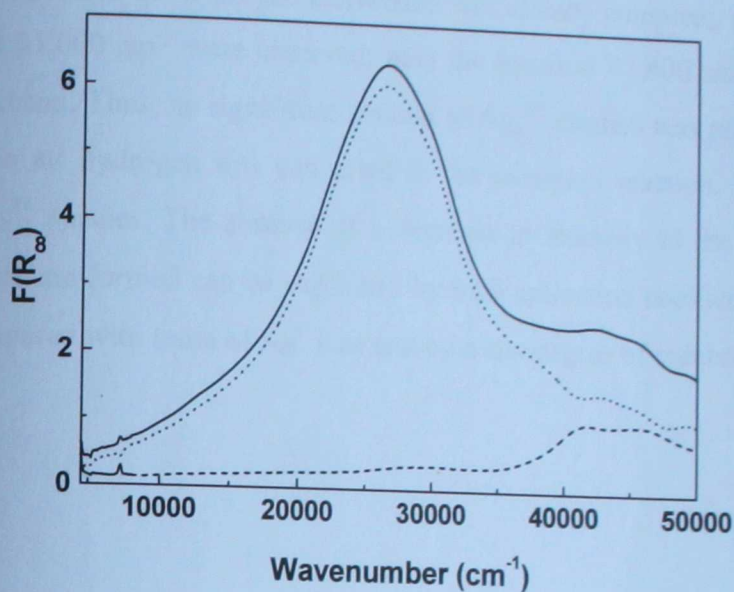


Fig. 3-23. *In-situ* UV-Vis-NIR spectra of reduced $\text{Ag}/\text{Al}_2\text{O}_3\text{-1.8}$ in H_2 flow at 523 K, when $\frac{1}{4}$ of Ag^+ content was reduced to metal. Spectrum of oxidized (---) and reduced (—) $\text{Ag}/\text{Al}_2\text{O}_3$. Difference spectrum (.....).

3.4.2 Oxidation of H_2 and CO by oxygen

Fig. 3-24a shows *in-situ* UV-Vis-NIR spectra of $\text{Ag}/\text{Al}_2\text{O}_3\text{-1.8}$ in a stream of oxygen and at oxidation of hydrogen by oxygen at 473. The complete conversion of H_2 is just attained at 473 K (cf. Fig. 3-17). If only oxygen was present in the feed the bands at 41,600 and 46,600 cm^{-1} assigned to electronic transitions of isolated Ag^+ ions were found. When hydrogen was added into the feed an intensive broad band centered at ca 31,000 cm^{-1} appeared immediately, indicating formation of small charged $\text{Ag}_n^{\delta+}$ clusters. The intensity of the band around 31,000 cm^{-1} increased fast, and more than 80% of the intensity was attained after ca 25 s; a delay-time in which hydrogen reached the catalyst bed was ca 3 s (see Fig. 3-24b). After a fast increase of the absorbance intensity with maximum at 31,000 cm^{-1} , the intensity increase was much slower, but without changing the shape of the complex band. Surprisingly, when considerable absorption at

31,000 cm^{-1} was developed, the bands of Ag^+ ions at 41,600 and 46,600 cm^{-1} did not change their intensities (see the abstracted spectrum). It is to be pointed out that at hydrogen oxidation at 50 K higher, i.e. at 523 K, when the hydrogen conversion was already complete, no Ag clusters with absorption around 31,000 cm^{-1} were observed; only the bands at 41,600 and 46,600 cm^{-1} were present in the spectrum. Thus, no significant amount of $\text{Ag}_n^{\delta+}$ clusters was present in the catalyst at conditions when all hydrogen was converted in the oxidation reaction. This indicates easy reoxidation of $\text{Ag}_n^{\delta+}$ species. The absence of a decrease in intensity of the bands of Ag^+ ions when $\text{Ag}_n^{\delta+}$ clusters are formed can be explained by high extinction coefficient for the metallic $\text{Ag}_n^{\delta+}$ clusters compared with those of Ag^+ ions and by a low degree of reduction of these ions.

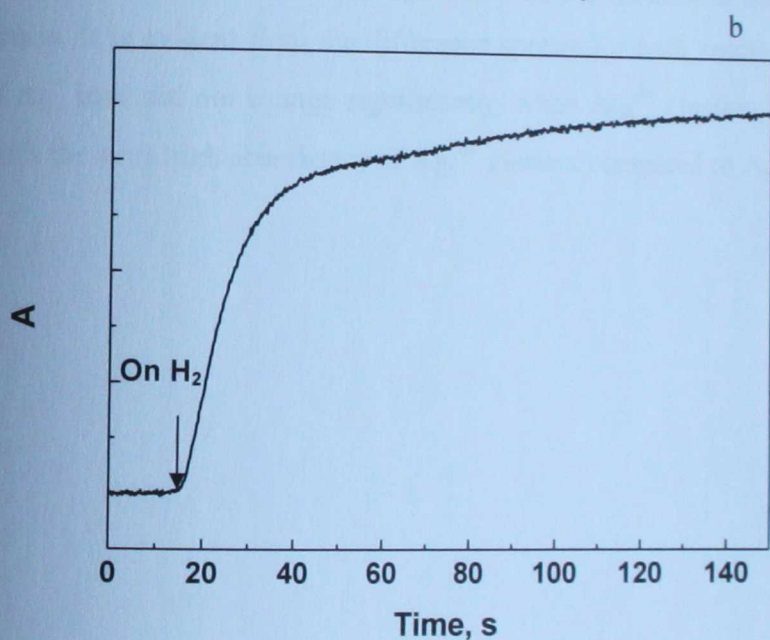
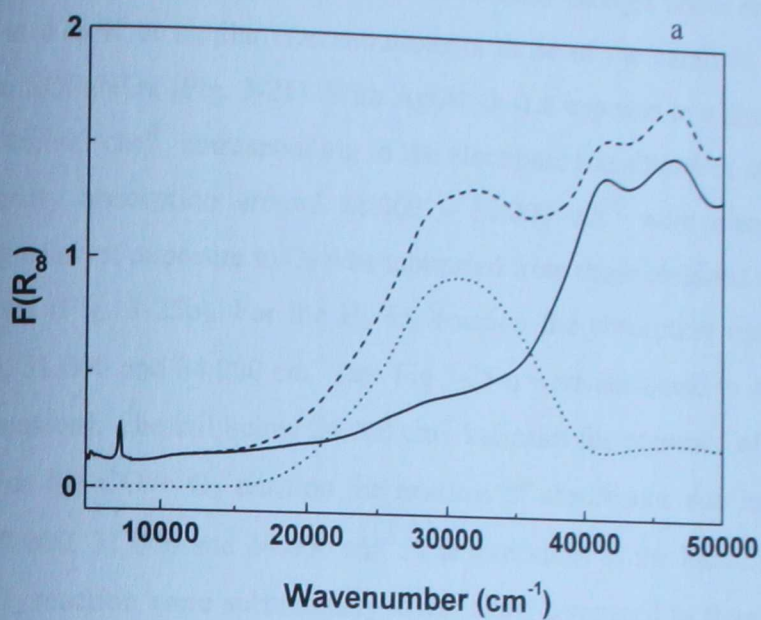


Fig. 3-24a. *In-situ* diffuse reflectance UV-Vis-NIR spectra of $\text{Ag}/\text{Al}_2\text{O}_3\text{-1.8}$ in a stream of O_2 (—) and under reaction conditions: 2,000 ppm H_2 and 6% O_2 (---). Difference spectrum between that under reaction conditions and the spectrum in flow of O_2 (.....). $T = 473$ K.

Fig. 3-24b. Rate of growth of silver clusters, expressed as absorbance intensity at $31,000\text{ cm}^{-1}$, after hydrogen (2,000 ppm) addition. *In-situ* diffuse reflectance UV-Vis-NIR spectra of $\text{Ag}/\text{Al}_2\text{O}_3\text{-1.8}$.

Fig. 3-25a shows UV-Vis spectra of silver alumina catalyst under streams of O_2 , $H_2 + O_2$ and $CO + O_2$ at 473 K at similar concentrations to those of the catalytic test analysing of the effect of CO on SCR- NO_x (Fig. 3-21). With $Ag/Al_2O_3-1.8$ exposed to a stream of oxygen, bands at 41,600 and 46,600 cm^{-1} , corresponding to the electronic transitions of isolated Ag^+ ions, and very low intensity absorption around 28,000 – 30,000 cm^{-1} were observed. The spectrum obtained during catalyst exposure to O_2 was subtracted from those obtained during the H_2+O_2 and $CO+O_2$ reactions (Fig. 3-25b). For the H_2+O_2 reaction the absorption maxima observed at ca 24,000, 29,000, 31,000 and 34,000 cm^{-1} (see Fig 3-25a) were attributed to $Ag_n^{\delta+}$ clusters, for $n \leq 8$ [see the Discussion]. The tail below 24,000 cm^{-1} indicates the presence of some larger metallic Ag particles. For the $CO + O_2$ reaction the maxima of absorbance due to $Ag_n^{\delta+}$ clusters were located at ca 29,000, 31,000 and 34,000 cm^{-1} . The intensities of the bands due to $Ag_n^{\delta+}$ clusters for the $CO + O_2$ reaction were substantially lower when compared to those obtained during the $H_2 + O_2$ reaction. It is evident from the difference spectra for both reactions that the intensity of the bands of Ag^+ ions did not change significantly, when $Ag_n^{\delta+}$ clusters were formed. This is in agreement with the very high absorbance of $Ag_n^{\delta+}$ clusters compared to Ag^+ ions.

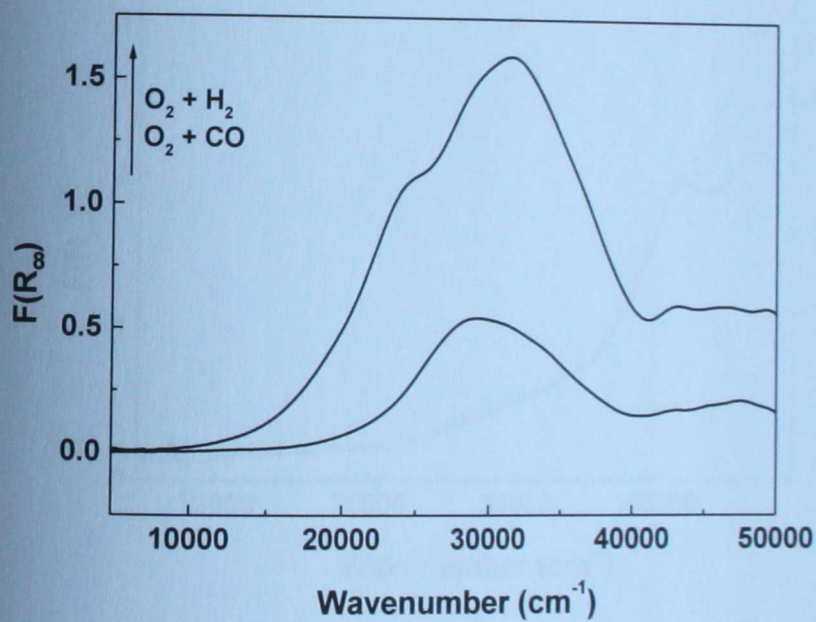
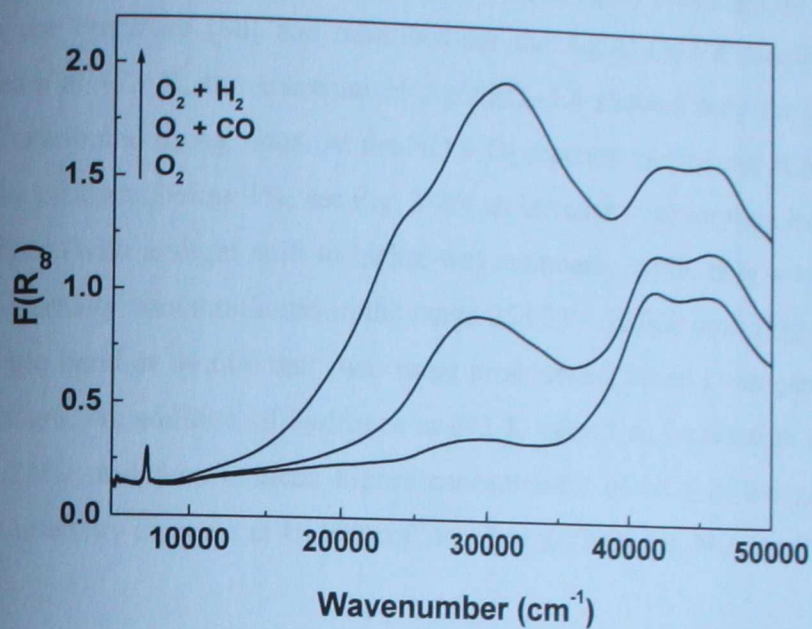


Fig. 3-25a. *In-situ* diffuse reflectance UV-Vis-NIR spectra of Ag/Al₂O₃-1.8 at hydrogen or CO oxidation over Ag/Al₂O₃-1.8 at 473 K. Feed: 7 200 ppm H₂ or 7 200 ppm CO, 4.3% O₂, rest He.

Fig. 3-25b. Difference spectra to that of Ag/Al₂O₃-1.8 in flow of O₂.

3.4.3 Oxidation of NO to NO₂ by molecular oxygen and the effect of hydrogen presence

Oxidation of NO by molecular oxygen to NO₂ is highly promoted by hydrogen addition as reported in the literature [58] and described for the Ag/Al₂O₃-1.8 sample (Fig. 3-20). In an oxygen stream at 473 K, the spectrum of Ag/Al₂O₃-1.8 showed only the bands at 41,600 and 46,600 cm⁻¹ attributed to Ag⁺ ions. At the NO + O₂ reaction carried out at 523 K (with the yield of NO₂ in the products below 1%, see Fig. 3-20) an increase in absorption intensity at 46,600 cm⁻¹ was observed (with a slight shift to higher wavenumbers), while only a very small increase in absorbance intensity was monitored in the range 25,000 – 30,000 cm⁻¹ (Fig. 3-26). The intensity increase of the band at 46,600 cm⁻¹ was more pronounced, when hydrogen was added into the reaction mixture. As addition of hydrogen at 473 K caused an increase in conversion of NO to NO₂ up to 21%, and thus induced higher concentration of NO₂ in the gaseous products, we ascribed the intensity increase at 46,600 cm⁻¹ to adsorbed NO₂, i.e. NO₂⁻ and/or NO₃⁻ species.

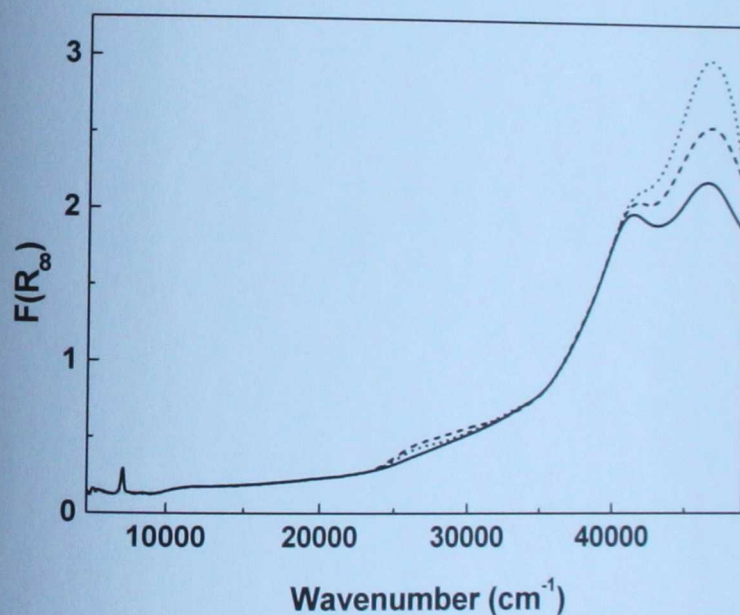


Fig. 3-26. Effect of hydrogen on the oxidation of NO to NO₂ over Ag/Al₂O₃-1.8 at 523 K. *In-situ* diffuse reflectance UV-Vis spectra of Ag/Al₂O₃-1.8 in flow of O₂ (—) and under reaction conditions: 1,000 ppm NO, 6% O₂, without H₂ (---) and with 2,000 ppm H₂ (·····).

3.4.4 Adsorption of NO_x species on silver alumina catalyst

Pre-treated Ag/Al₂O₃-1.8 in oxygen flow at 523 K was contacted with a gas stream of 1,000 ppm NO₂ (Fig. 3-27a,b). First, a band centered around 26,600 cm⁻¹ grew in the first 20 min. Subsequently, this band eroded while a new band around 33,400 cm⁻¹ appeared. The spectra displayed an isosbestic point around 30,300 cm⁻¹, evidencing that the species responsible for the band around 26,600 cm⁻¹ is converted into the species that absorbs around 33,400 cm⁻¹. The intensity of the bands at 26,600 and 33,400 cm⁻¹ grow only up to F(R_∞) = 0.1. Thus extinction of these bands can be estimated to be several times lower than those of silver clusters. An intensive band after NO₂ adsorption was found above 40,000 cm⁻¹ due to NO₂⁻ and NO₃⁻ adsorbed species.

An intensive broad band appeared after subsequent addition of hydrogen to the stream. This band reflects formation of silver clusters and metallic silver particles. The intensity of this bands show that the presence of NO₂ substantially suppresses reduction of Ag⁺ ions (cf. reduction of Ag/Al₂O₃-1.8 at the presence and the absence of NO₂ in the stream).

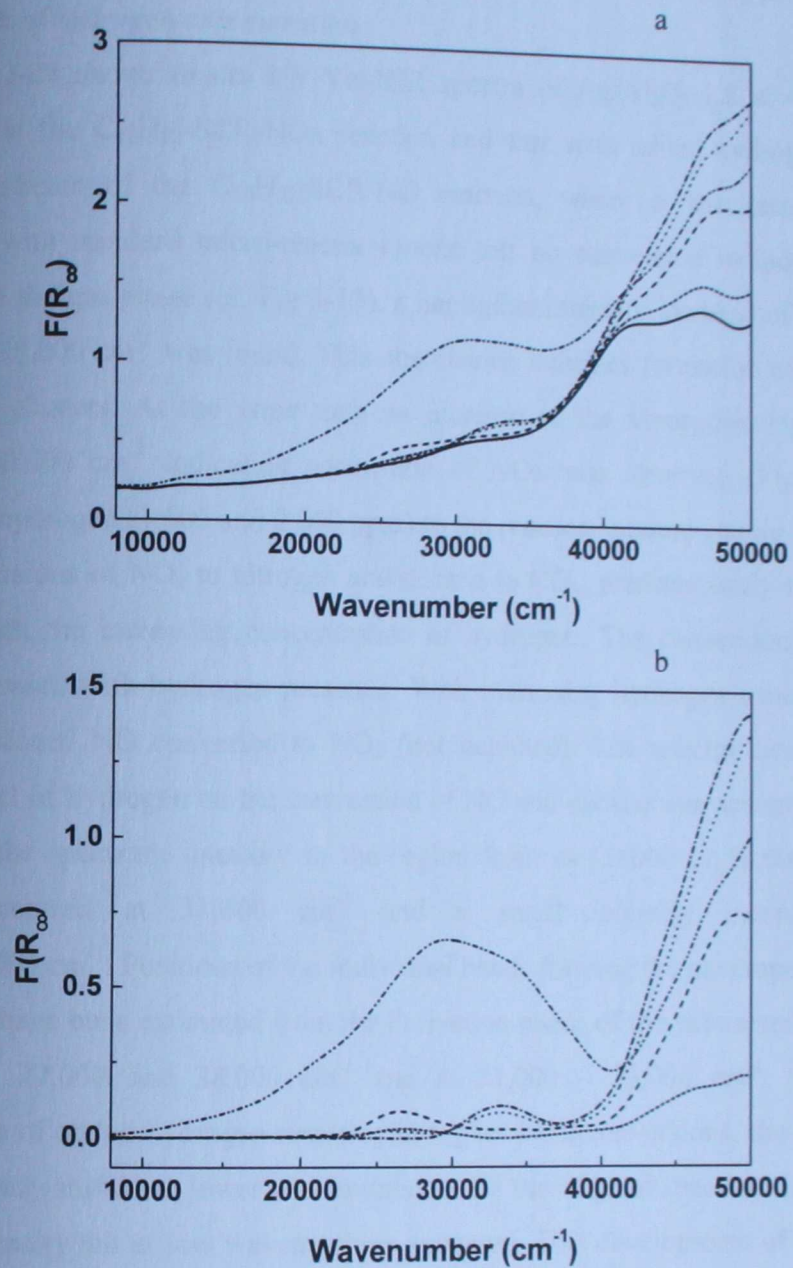


Fig. 3-27a. *In-situ* diffuse reflectance UV-Vis spectra of Ag/Al₂O₃-1.8 in flow of O₂ (—) and in a stream of 1,000 ppm NO₂ (rest of He) in 5 min (----), 15 min (---), 30 min (.....), 60 min (-----) and after subsequent addition of 2,000 ppm H₂ to the stream of NO₂ for 20 min (-----). T = 473 K.

Fig. 3-27b. Difference spectra to that of Ag/Al₂O₃-1.8 in flow of O₂.

3.4.5 Selective catalytic reduction of NO_x depending on H₂/C₁₀H₂₂/O₂ compositions

3.4.5.1 Effect of hydrogen concentration

Fig. 3-28 shows *in-situ* UV-Vis-NIR spectra of Ag/Al₂O₃-1.8 at 473 K in an oxygen stream and at the C₁₀H₂₂-SCR-NO_x reaction and that with added hydrogen as a co-reactant. Under the stream of the C₁₀H₂₂-SCR-NO reaction, where at the same conditions of the experiment with standard micro-reactor kinetic test no conversion to molecular nitrogen was monitored in the gas phase (cf. Fig 3-13), a negligible intensity increase of the absorbance at ca 27,000 and 38,000 cm⁻¹ was found. This absorbance indicates formation of very low amount of small Ag_n^{δ+} clusters. At the same time an increase of the absorption intensity ranging from 44,000 to 50,000 cm⁻¹ indicating adsorption of NO_x was observed (Fig. 3-28a and 3-28b). Addition of hydrogen (1,000 and 2,000 ppm) to the reaction mixture caused a substantial increase in the conversions of NO_x to nitrogen and decane to CO_x, predominantly to CO₂, which values increased with the increasing concentration of hydrogen. The conversion of NO to N₂O was slightly increased with hydrogen presence. With increasing hydrogen concentration increases a part of unreduced NO converted to NO₂ (not depicted). The spectra clearly indicate that the positive effect of hydrogen on the conversion of NO and decane was accompanied by a dramatic increase of the spectrum intensity in the region from ca 20,000 to 38,000 cm⁻¹ with a broad maximum centred at 31,000 cm⁻¹ and a small intensity increase in the region 44,000 - 50,000 cm⁻¹. Positions of the individual bands forming the envelope of the broad band at 31,000 cm⁻¹ have been estimated from the derivation mode of the subtracted spectra (Fig. 3-28b) to be at ca 27,000 and 38,000 cm⁻¹ and at 31,000 - 33,000 cm⁻¹. With the increasing concentration of added hydrogen resulting in higher NO_x conversions, the overall absorption is not significantly shifted to lower wavenumbers, and the original spectrum increases in intensity; only low intensity tail at low wavenumbers appeared. This development of the spectrum feature indicates that with increasing concentration of hydrogen small charged Ag_n^{δ+} clusters, likely of a similar dimension, are increased in concentration and larger metallic agglomerates are formed only at rather low extent.

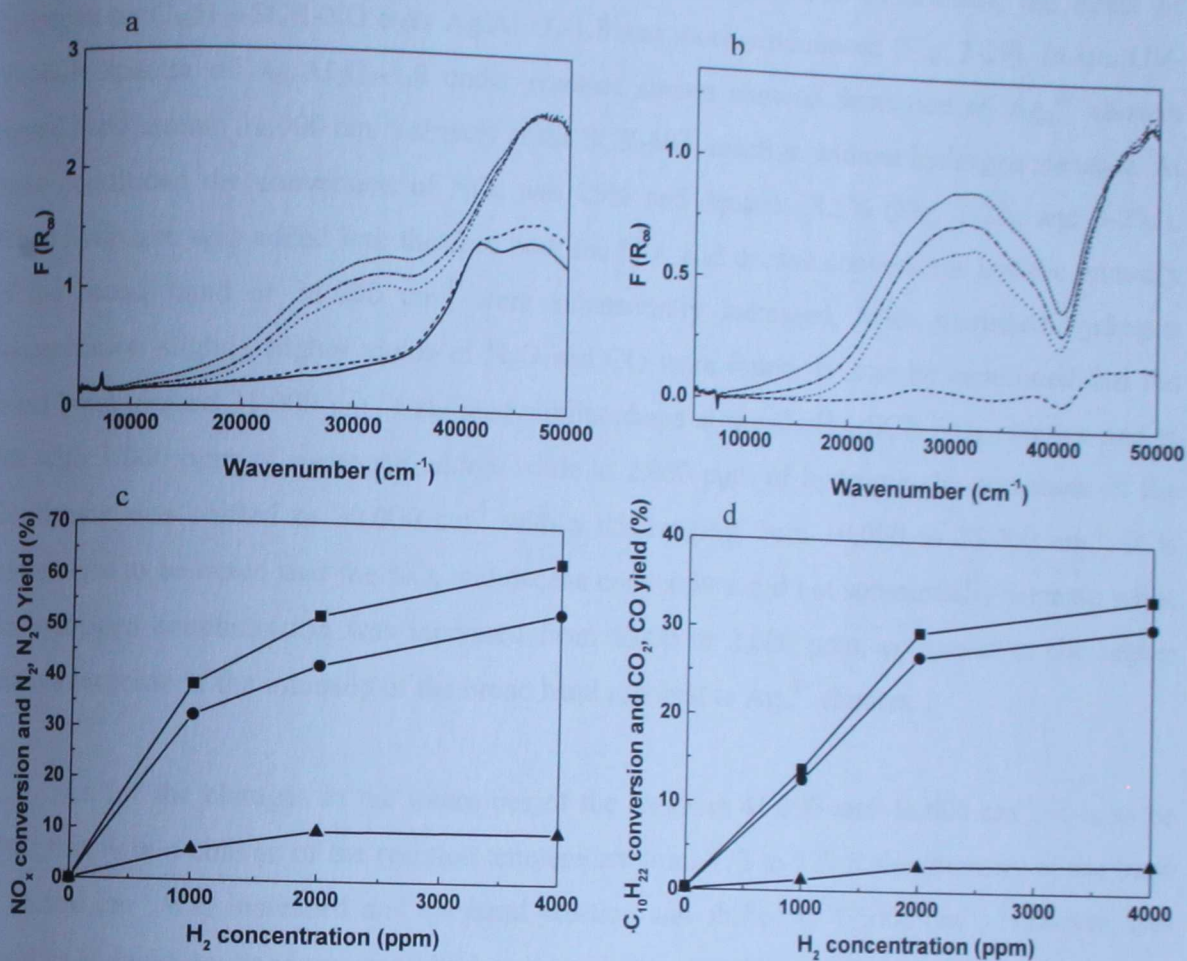


Fig. 3-28. Effect of hydrogen on decane-SCR-NO over Ag/Al₂O₃-1.8 at 473 K. GHSV = 30,000 h⁻¹. Feed: 1,000 ppm NO, 300 ppm C₁₀H₂₂, 6% O₂, 12% H₂O and 0 – 4,000 ppm H₂.

a) *In-situ* diffuse reflectance UV-Vis-NIR spectra of Ag/Al₂O₃-1.8 in flow of O₂ (—) and under reaction conditions: without H₂ (---) and with 1,000 ppm H₂ (.....), 2,000 ppm H₂ (-·-·-) or 4,000 ppm H₂ (- - - -).

b) Difference spectrum between that under reaction conditions and the spectrum in flow of O₂.

c) and d) Catalytic activity as a function of hydrogen concentration. NO_x or C₁₀H₂₂ conversion (■), N₂ or CO₂ yield (●) and N₂O or CO yield (▲).

At higher temperature (523 K) compared to the previous experiment, the effect of hydrogen on $C_{10}H_{22}$ -SCR-NO over $Ag/Al_2O_3-1.8$ was more pronounced (Fig. 3-29). *In-situ* UV-Vis-NIR spectra of $Ag/Al_2O_3-1.8$ under reactant stream showed formation of $Ag_n^{\delta+}$ clusters (broad band around $31,000\text{ cm}^{-1}$) already at the SCR- NO_x reaction without hydrogen presence. At these conditions the conversion of NO_x was 25% and decane 18.5% (Fig. 3-29c and 3-29d). When hydrogen was added into the feed both the NO_x and decane conversions and the intensity of the broad band at $31,000\text{ cm}^{-1}$ were substantially increased. With increased hydrogen concentration slightly higher yields of N_2O and CO were found. It is to be mentioned that the broad band around $31,000\text{ cm}^{-1}$ exhibited similar shape at the $C_{10}H_{22}$ -SCR- NO_x reaction and at that with 1,000 ppm of hydrogen added, while at 2,000 ppm of hydrogen the maximum of the absorbance was shifted to $30,000\text{ cm}^{-1}$ with a tail ranging from 10,000 to $25,000\text{ cm}^{-1}$. It is worthwhile to be noted that the NO_x and decane conversions did not substantially increase when the hydrogen concentration was increased from 1,000 to 2,000 ppm, compared to the higher relative increase in the intensity of the broad band ascribed to $Ag_n^{\delta+}$ clusters.

As for the changes in the intensities of the bands at $41,600$ and $46,600\text{ cm}^{-1}$, it is to be noted that with a change of the reaction temperature from 473 to 523 K the intensity of the band at $46,600\text{ cm}^{-1}$ was increased and the band position was shifted to $47,000\text{ cm}^{-1}$. However, that could be induced by an increase of the broad band above $50,000\text{ cm}^{-1}$ belonging to the spectrum of Ag^+ ions. A substantial changes in the intensity of the broad band at $47,000\text{ cm}^{-1}$ at the $C_{10}H_{22}$ -SCR- NO_x reaction at 523 K (Fig. 3-29) and at $H_2/C_{10}H_{22}$ -SCR- NO_x at 473 K (Fig. 3-28) might be a result of a balance of the effects of higher rate of oxidation of NO to NO_2 , and thus formation of adsorbed NO_x^- species, and at the same time the increased rate of NO_2 (adsorbed NO_x^-) reduction by hydrocarbons. However, the changes in the intensities of the absorbance in the range $45,000 - 50,000\text{ cm}^{-1}$ could not be analysed with respect to adsorbed species as several components might contribute to the absorbance in this region.

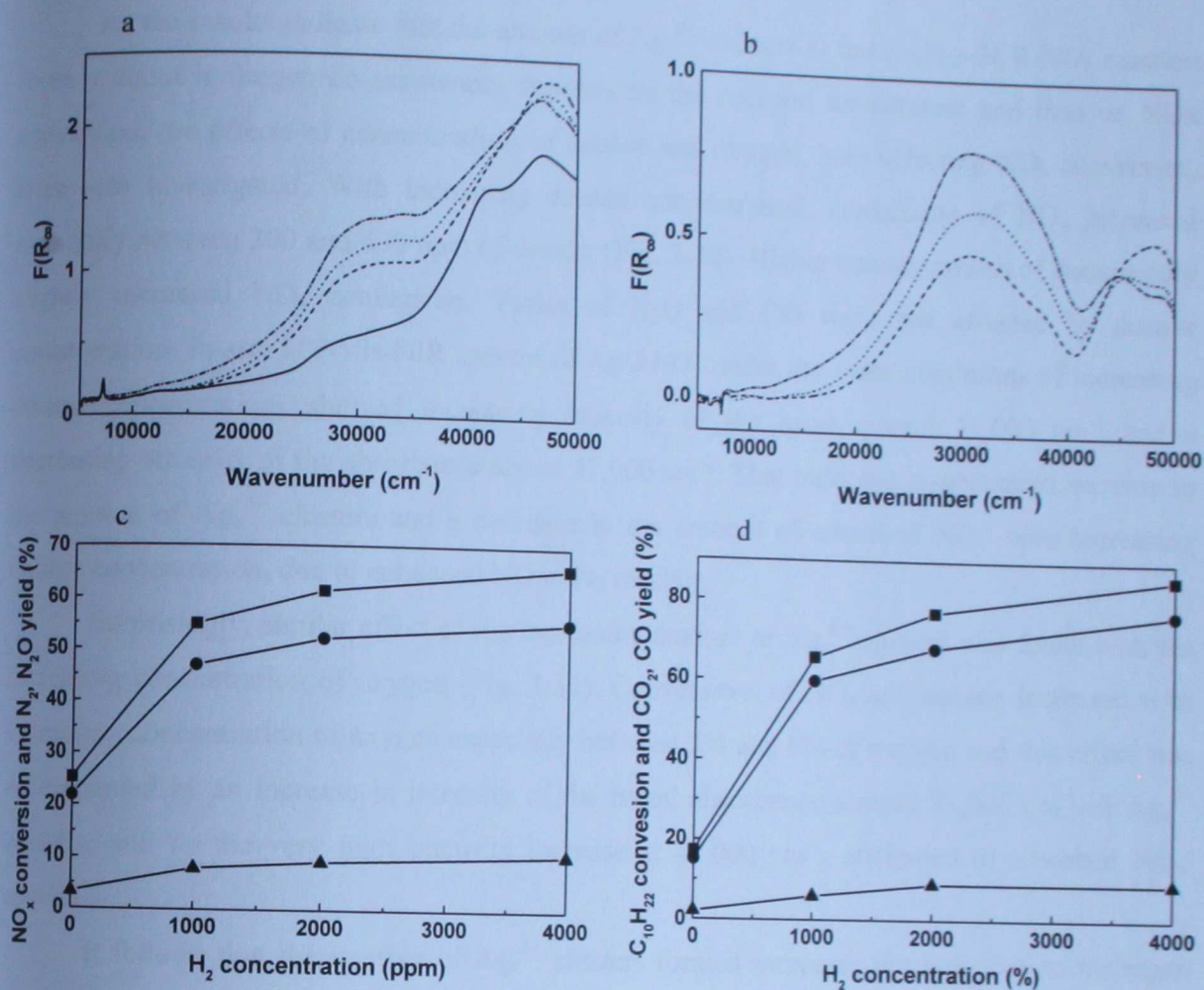


Fig. 3-29. Effect of hydrogen on decane-SCR-NO over Ag/Al₂O₃-1.8 at 523 K. GHSV = 30,000 h⁻¹. Feed: 1,000 ppm NO, 400 ppm C₁₀H₂₂, 6% O₂, 12% H₂O and 0–4,000 ppm H₂.

- a) *In-situ* diffuse reflectance UV-Vis-NIR spectra of Ag/Al₂O₃-1.8 in flow of O₂ (—) and under reaction conditions: without H₂ (---), with 1,000 ppm H₂ (·····) and with 2,000 ppm H₂ (-·-·-).
- b) Difference spectrum between that under reaction conditions and the spectrum in flow of O₂.
- c) and d) Catalytic activity as function of hydrogen concentration. NO_x or C₁₀H₂₂ conversion (■), N₂ or CO₂ yield (●) and N₂O or CO yield (▲).

3.4.5.2 Effect of decane and oxygen concentration

As the results indicate that the amount of $\text{Ag}_n^{\delta+}$ clusters at the $\text{C}_{10}\text{H}_{22}$ -SCR- NO_x reaction (even without hydrogen co-assistance) depends on the reaction temperature and thus on NO_x conversion, the effects of concentrations of decane and oxygen, both affecting NO_x conversion, were also investigated. With increasing decane concentration, conversion of NO_x increased especially between 300 and 600 ppm of decane (Fig. 3-30). Higher concentrations of decane only slightly increased NO_x conversion. Yields of N_2O and CO were not affected by decane concentration. *In-situ* UV-Vis-NIR spectra of $\text{Ag}/\text{Al}_2\text{O}_3$ under the same conditions of increasing decane concentrations showed increasing intensity of the band around $31,000\text{ cm}^{-1}$ and a decreasing intensity of the absorbance above $47,000\text{ cm}^{-1}$. That indicates a substantial increase in the amount of $\text{Ag}_n^{\delta+}$ clusters and a decrease in the amount of adsorbed NO_x^- with increasing decane concentration, due to enhanced NO to N_2 reaction.

Surprisingly, similar effect of the increasing amount of $\text{Ag}_n^{\delta+}$ clusters was found with the increasing concentration of oxygen (Fig. 3-31). Conversions of NO_x and decane increased with increasing concentration of oxygen especially between 3% and 6% of oxygen and this effect was accompanied by an increase in intensity of the broad absorbance around $31,000\text{ cm}^{-1}$ of $\text{Ag}_n^{\delta+}$ clusters, and by the very high intensity increase at $47,000\text{ cm}^{-1}$, attributed to adsorbed NO_x^- species.

It follows that the number of $\text{Ag}_n^{\delta+}$ clusters formed increases not only due to hydrogen presence, as reported in literature, but with increasing NO_x conversion to N_2 , regardless this is achieved by H_2 , O_2 or decane. This finding is decisive for the SCR- NO_x reaction over silver alumina and will be analysed in detail in the Discussion part.

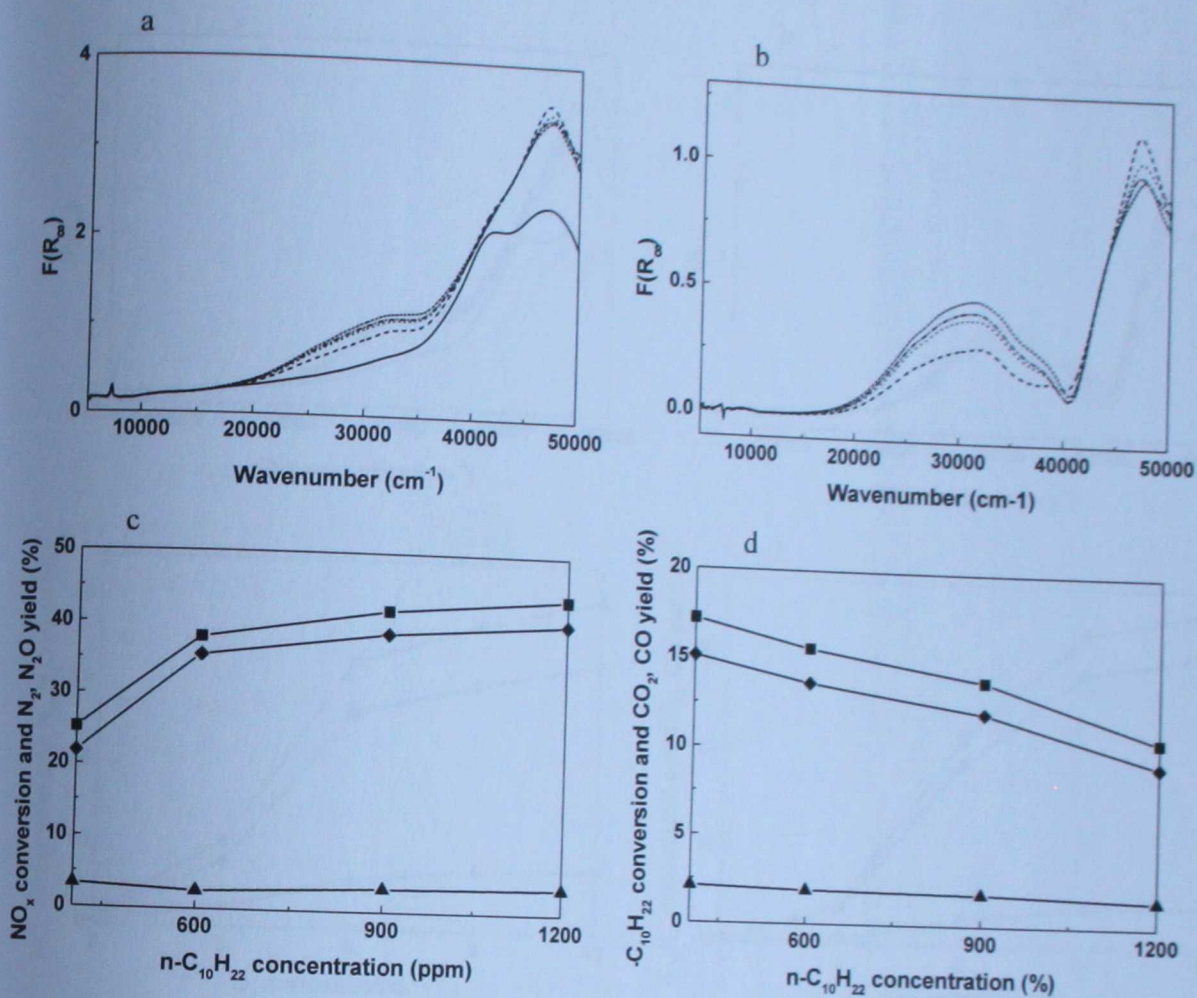


Fig. 3-30. Effect of decane concentration on decane-SCR-NO at 523 K over Ag/Al₂O₃-1.8. GHSV = 30,000 h⁻¹. Feed: 1,000 ppm NO, 6% O₂, 12% H₂O and 300 – 1200 ppm C₁₀H₂₂.

a) *In-situ* diffuse reflectance UV-Vis-NIR spectra of Ag/Al₂O₃-1.8 in flow of O₂ (—) and under reaction conditions: with 300 ppm decane (---), 600 ppm decane (.....), 900 ppm decane (-.-.-) and with 1200 ppm decane (- - - -).

b) Difference spectrum between that under reaction conditions and the spectrum in flow of O₂.

c) and d) Catalytic activity as function of decane concentration. NO_x or C₁₀H₂₂ conversion (■), N₂ or CO₂ yield (●) and N₂O or CO yield (▲).

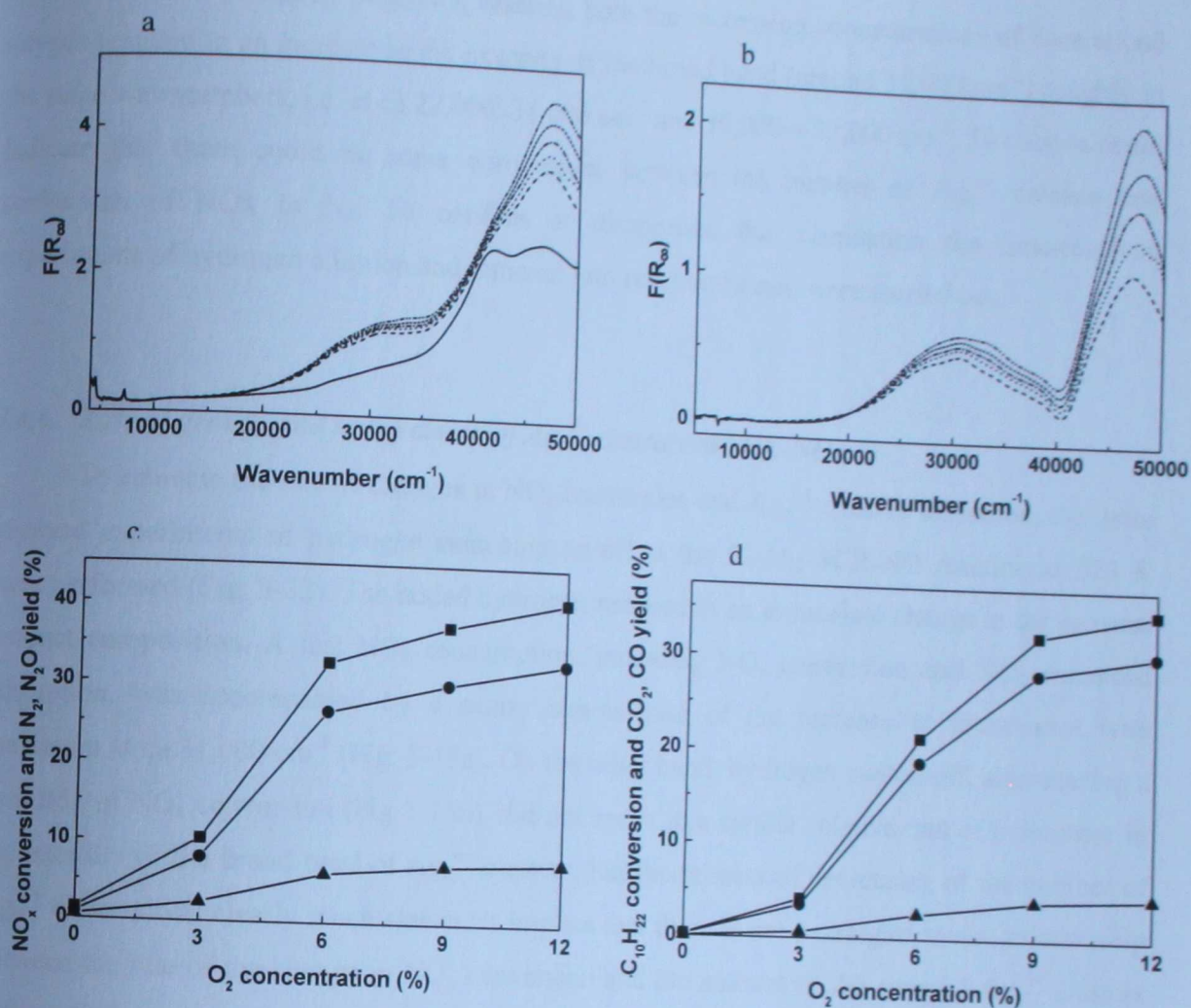


Fig. 3-31. Effect of oxygen concentration on decane-SCR-NO at 523 K over Ag/Al₂O₃-1.8. GHSV = 30,000 h⁻¹. Feed: 1,000 ppm NO, 300 ppm C₁₀H₂₂, 12% H₂O and 0–12% O₂.
 a) *In-situ* diffuse reflectance UV-Vis-NIR spectra of Ag/Al₂O₃-1.8 in flow of O₂ (—) and under reaction conditions: without O₂ (---) and with 3% O₂ (·····), 6% O₂ (-·-·-), 9% O₂ (- - - -) and 12% O₂ (- · - · - · - · - · -).
 b) Difference spectrum between that under reaction conditions and the spectrum in flow of O₂
 c) and d) Catalytic activity as function of oxygen concentration. NO_x or C₁₀H₂₂ conversion (■), N₂ or CO₂ yield (●) and N₂O or CO yield (▲).

Thus, in the $C_{10}H_{22}$ -SCR- NO_x reaction both the increasing concentrations of decane and oxygen resulted in an increase in the intensity of the broad band (around $31,000\text{ cm}^{-1}$) roughly at the same wavenumbers, i.e. at ca $27,000$, $38,000\text{ cm}^{-1}$ and $30,000 - 32,000\text{ cm}^{-1}$. The above result indicate that there could be some correlations between the number of $Ag_n^{\delta+}$ clusters and conversion of NO_x to N_2 . To confirm or disapprove that correlation the time-resolved experiments of hydrogen addition and removal into reactant stream were carried out.

3.4.6. Rate of growth and redispersion of $Ag_n^{\delta+}$ clusters at SCR- NO_x

To estimate the rate of changes in NO_x conversion and $Ag_n^{\delta+}$ clusters formation, the time-resolved experiments of hydrogen switching on/off at the $C_{10}H_{22}$ -SCR- NO reaction at 523 K were performed (Fig. 3-32). The added hydrogen resulted in an immediate change in the gaseous product composition. A fast NO_x consumption, including NO_x conversion and NO_2 enhanced adsorption, was accompanied by a nearly similar rate of the increase in absorbance with maximum at ca $31,000\text{ cm}^{-1}$ (Fig. 3-15a). On the other hand, hydrogen switch off, also causing a fast drop of NO_x conversion (Fig 3-15b), did not result in a similar relative rate of a decrease in the intensity of the broad band of $Ag_n^{\delta+}$ clusters, but the process of decreasing of the number of $Ag_n^{\delta+}$ clusters was clearly much slower. It implies that there is not a straightforward relationship between the rate of the change in NO_x conversion and the amount of the charged $Ag_n^{\delta+}$ clusters present at the reaction conditions.

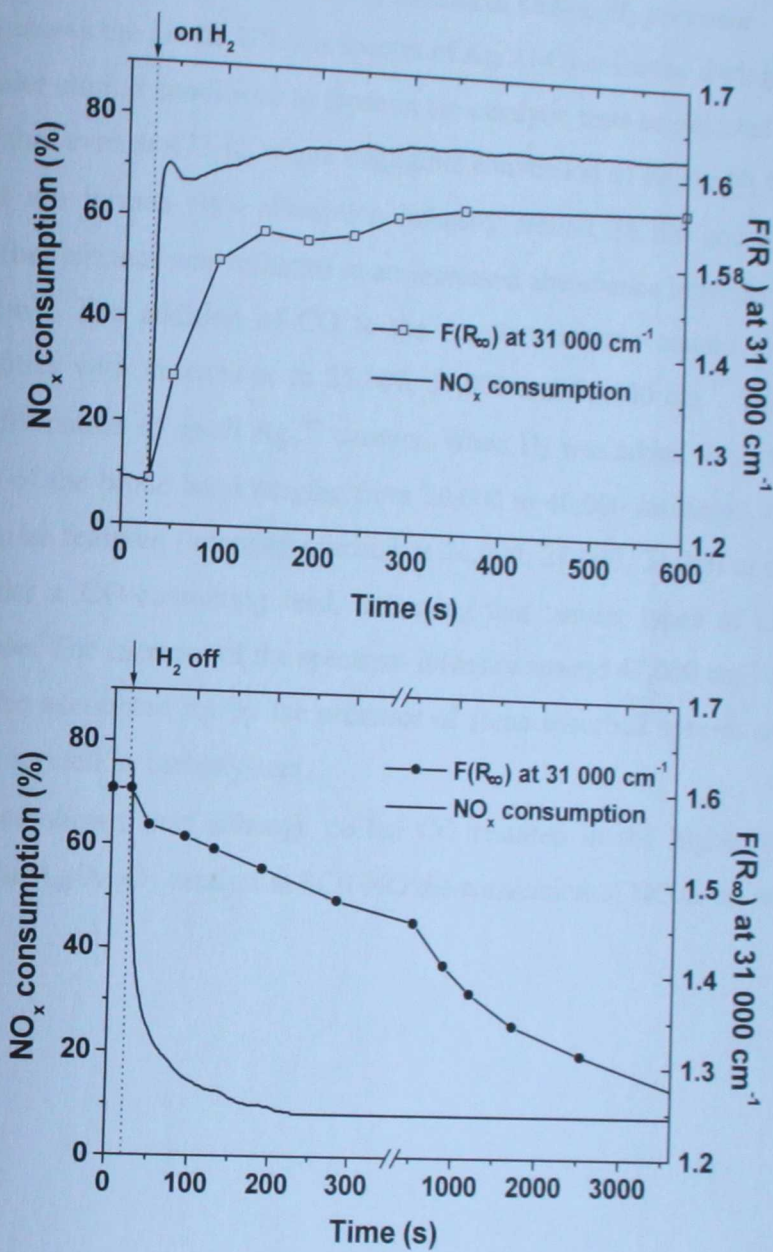


Fig. 3-32. Effect of hydrogen switching on and off in decane-SCR-NO over Ag/Al₂O₃-1.8 monitored by NO/NO_x analyser and *in-situ* UV-Vis spectroscopy. Reactant stream: 1,000 ppm NO, 600 ppm decane, 6% O₂, 12% H₂O, and 0 or 2,000 ppm H₂. T = 523 K, GHSV = 60,000 h⁻¹.

- a) Changes in NO_x consumption and evolution of the intensity of *in-situ* diffuse reflectance UV-Vis spectra of Ag/Al₂O₃-1.8 at 31,000 cm⁻¹ after hydrogen switch on as function of time
- b) Changes in NO_x consumption and evolution of the intensity of *in-situ* diffuse reflectance UV-Vis spectra of Ag/Al₂O₃-1.8 at 31,000 cm⁻¹ after hydrogen switch off as function of time

3.4.7 Selective catalytic reduction of NO_x by decane at CO vs. H₂ presence

Fig. 3-33 shows the *in-situ* UV-Vis spectra of Ag/Al₂O₃ collected during the decane-SCR-NO_x reaction under similar conditions to those in the catalytic tests as depicted in Fig. 3-21. The spectra revealed that even at 473 K, where negligible conversion of NO to N₂ takes place, traces of Ag_n^{δ+} clusters are formed (low absorption intensity around 28,000 and 38,000 cm⁻¹). The presence of adsorbed nitrates was reflected in an increased absorbance intensity with a maximum around 47,000 cm⁻¹. The addition of CO to the reaction mixture caused an increase in the absorption intensities with maxima at ca 25,000, 34,000 and 38,000 cm⁻¹. These bands can be attributed to the formation of small Ag_n^{δ+} clusters. When H₂ was added into the feed instead of CO, the intensity of the broad band ranging from 20,000 to 40,000 increased substantially. This band showed similar features (intensity maxima at 24,000, 28,000, 34,000 and 38,000 cm⁻¹) to that obtained under a CO-containing feed, indicating that similar types of silver clusters are formed in each case. The increase of the spectrum intensity around 47,000 cm⁻¹ after hydrogen or CO addition can be accounted for by the presence of some adsorbed species on Ag or Al ions, e.g., some nitrates as well as carboxylates.

Thus it was shown that although co-fed CO resulted in the higher number of Ag_n^{δ+} clusters (n≤8) in the Ag/Al₂O₃ catalyst at SCR-NO the conversion of NO to N₂ was not enhanced.

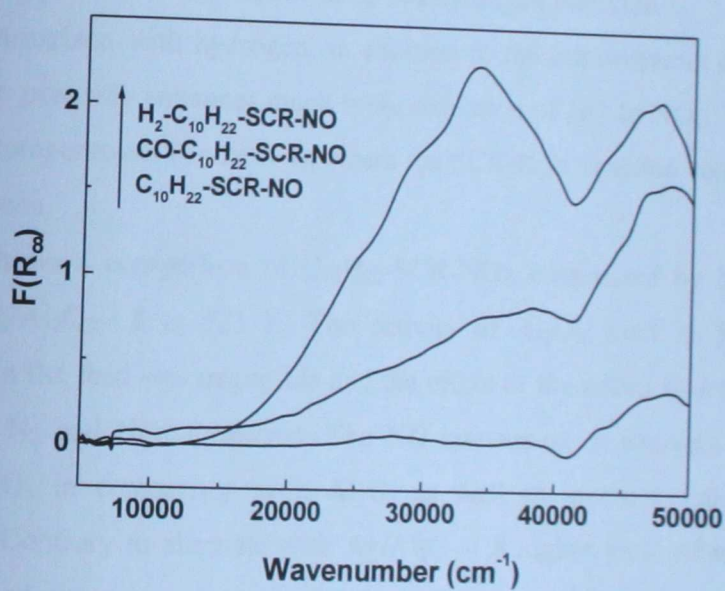
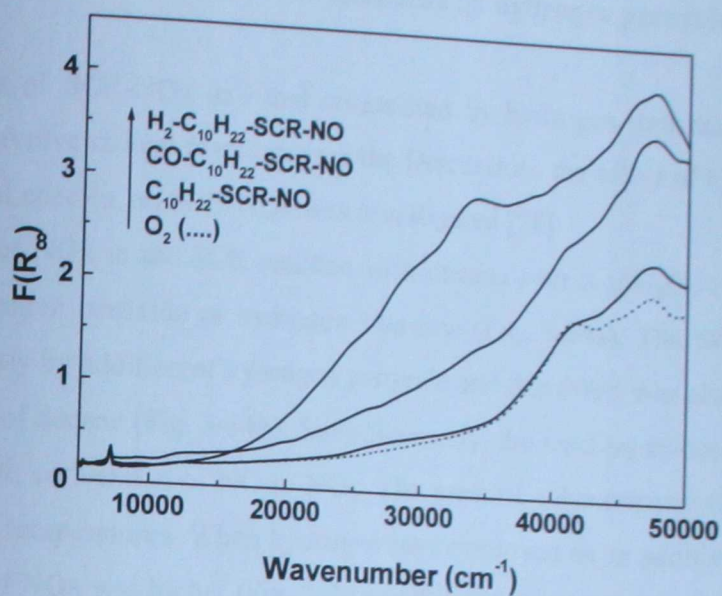


Fig. 3-33a. *In-situ* diffuse reflectance UV-Vis-NIR spectra of Ag/Al₂O₃-1.8 during exposure to different reactant gas mixes. SCR feed: 720 ppm NO; 435 ppm n-C₁₀H₂₂; 4.3% O₂; 4.3% H₂O; (7,200 ppm CO or H₂).

Fig. 3-33b. Difference spectra to that of Ag/Al₂O₃ in flow of O₂.

3.5 Selective catalytic reduction of NO_x enhanced by hydrogen peroxide over silver alumina catalyst

As the results of SCR-NO_x and that co-assisted by hydrogen indicate that the reaction mechanism might involve radical reactions (see the Discussion) the effect of hydrogen peroxide, as a source of radical species, on SCR-NO_x was investigated [78].

Conversion of NO_x in the SCR reaction with decane over Ag/Al₂O₃-1.8 at 473 - 523 K without co-fed hydrogen peroxide or hydrogen was low (Fig. 3-34a). The NO conversion was increased considerably by addition of hydrogen peroxide and this effect was also accompanied by a higher conversion of decane (Fig. 3-34b). Simultaneously, the reaction co-assisted by hydrogen peroxide yielded high conversion of NO to NO₂. The greatest enhancement of NO_x conversion was achieved at low temperatures. When hydrogen was employed as an additive over Ag/Al₂O₃-1.8, the conversion of NO_x was higher (Fig. 3-34 and Tab. 3-4) and the conversion of NO to NO₂ was much lower compared to the reaction with co-fed hydrogen peroxide.

Thus, in comparison with hydrogen, in addition to the improvement of the reduction of NO to N₂, hydrogen peroxide enhances much more oxidation of NO to NO₂. This effect is more pronounced at low temperatures (Table 3-4), where the SCR-NO_x reaction contributes less to the overall transformations.

Table 3-5 shows a comparison of C₁₀H₂₂-SCR-NO_x co-assisted by hydrogen peroxide over Al₂O₃ and Ag/Al₂O₃-1.8 at 523 K. The activity of Al₂O₃ itself in SCR-NO_x without hydrogen peroxide in the feed was negligible and the effect of the added hydrogen peroxide was remarkable in both N₂ and NO₂ formation. The NO conversion to nitrogen was significantly higher over Ag/Al₂O₃ in comparison with Al₂O₃ as well as in the reaction co-assisted by hydrogen peroxide. Contrary to alumina, with Ag/Al₂O₃-1.8 higher yield of molecular nitrogen than NO₂ was obtained under co-assistance of H₂O₂ to decane.

The positive effect of hydrogen on CH-SCR-NO_x has been observed only with silver on alumina or Ag-zeolite catalysts [48,49]. Analogously to hydrogen, with Cu-MFI and Fe-MFI catalysts the increase in NO_x conversion under hydrogen peroxide presence was not observed [78].

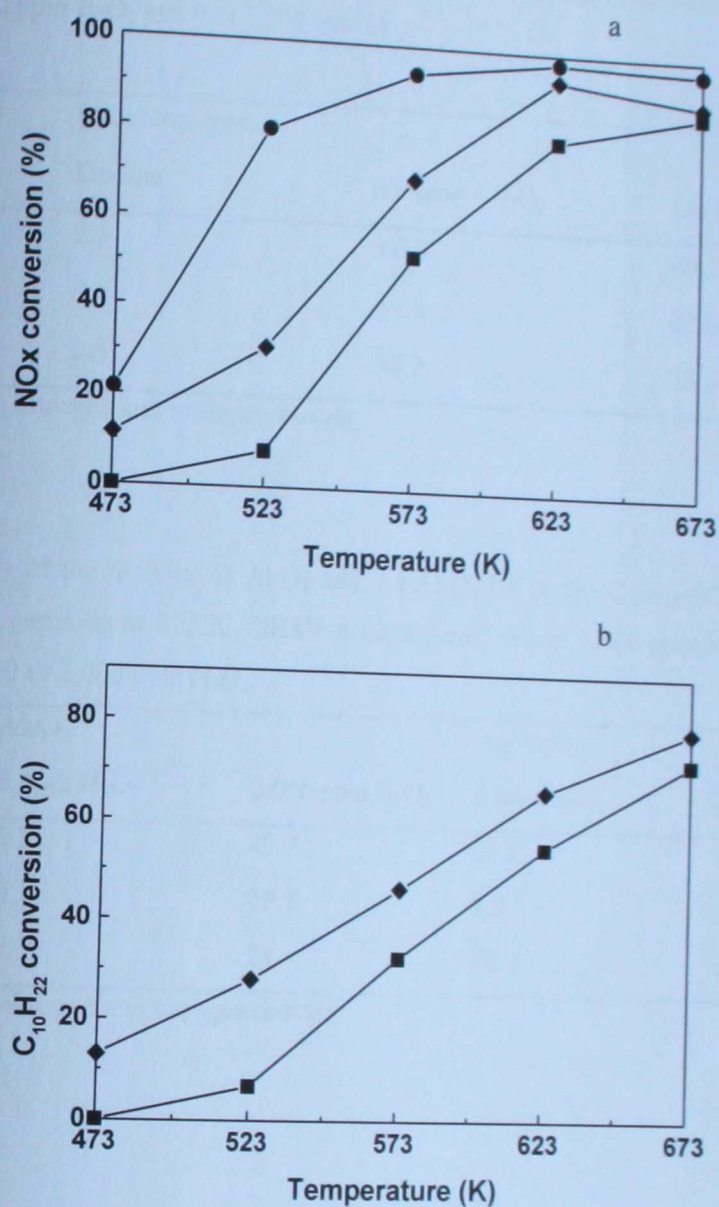


Fig. 3-34a,b. Effect of hydrogen peroxide and hydrogen on conversion of NO_x to N₂ (a) and C₁₀H₂₂ to CO_x (b) in C₁₀H₂₂-SCR-NO over Ag/Al₂O₃-1.8 depending on temperature. Feed: 1,000 ppm NO, 600 ppm C₁₀H₂₂, 6% O₂, 12% H₂O and 0 ppm H₂O₂ (■), 2,000 ppm H₂O₂ (◆) or 2,000 ppm H₂ (●). GHSV = 60,000 cm⁻¹.

Tab. 3-4 Comparison of the effect of hydrogen and hydrogen peroxide on the $C_{10}H_{22}$ -SCR-NO reaction over Ag/Al₂O₃-1.8 at 473 K. GHSV = 60,000 cm⁻¹. Feed: 1,000 ppm NO, 600 ppm C₁₀H₂₂, 6% O₂, 12% H₂O, 0 or 2,000 ppm H₂O₂ and 0 or 2,000 ppm H₂.

	Reducing agent		
	Decane	Decane + H ₂ O ₂	Decane + H ₂
xNO*	2.5	60.0	49.5
Yield of N ₂	0	11.8	21.0
Yield of NO ₂	2.5	48.2	28.5

* conversion of NO to nitrogen and nitrogen dioxide

Tab. 3-5 Comparison of the activity of Al₂O₃ and Ag/Al₂O₃-1.8 in the $C_{10}H_{22}$ -SCR-NO reaction, co-assisted by hydrogen peroxide at 523 K. GHSV = 60,000 cm⁻¹. Feed: 1,000 ppm NO, 600 ppm C₁₀H₂₂, 6% O₂, 12% H₂O and 0 or 2,000 ppm H₂O₂.

	Al ₂ O ₃		Ag/Al ₂ O ₃	
	0 ppm H ₂ O ₂	2,000 ppm H ₂ O ₂	0 ppm H ₂ O ₂	2,000 ppm H ₂ O ₂
xNO*	0.2	43.7	28.2	58.6
Yield of N ₂	0.1	15.7	8.0	32.1
Yield of NO ₂	0.1	28	20.2	26.6

* conversion of NO to nitrogen and nitrogen dioxide

4 Discussion

4.1 Structure of the silver catalyst

4.1.1 State of silver in alumina and MFI zeolite

The peculiar structure of the silver species on alumina has not been analysed so far in detail particularly at the conditions of the SCR-NO_x reactions. It is known that impregnation of alumina supports with a silver salt solution leads to a wide distribution of silver species depending on loading and atmosphere over silver alumina. According to the literature [14,20,34,45,46,48], silver species in alumina, highly flexible in the valence state, have been suggested to adopt structure of Ag⁺ ions atomically dispersed, small silver oxide or silver aluminate species, metallic charged Ag_n^{δ+} clusters of various nuclearity and charge, and larger metallic silver particles (see Chapters 1.4.5 and 1.4.6).

The electronic spectra of silver in solutions, inert gas-solid matrices and in zeolites show that Ag⁺ ions and small Ag clusters exhibit characteristic absorption bands in the UV-Vis region. It is widely accepted that the components of the UV bands above 40,000 cm⁻¹ correspond to 4d¹⁰ → 4d⁹5s¹ electronic transitions of Ag⁺ ions in various matrices [42] and the bands between 30,000 – 40,000 cm⁻¹ are ascribed to the 4d¹⁰5s¹ → 4d⁹5s¹5p¹ and 4d¹⁰5s¹ → 4d⁹5s¹6p¹ transitions in Ag_n^{δ+} clusters with n ≤ 8 [43,79]. There is no doubt that the observed UV absorption bands at 41,600 and 46,600 cm⁻¹ in Ag/Al₂O₃ samples studied (Fig 3-1) correspond to the isolated Ag⁺ ions. However, all the Ag⁺ ions could not be quantitatively reflected in these bands. Beside the 4d¹⁰ → 4d⁹5s¹ Ag⁺ transitions below 49,000 cm⁻¹ reported for various solids, the spectrum of Ag⁺ ions can be also reflected in the region above 50,000 cm⁻¹, and moreover, the absorption in this region can be dominant [42]. This was observed for Ag⁺ ion aqueous solutions [42] and recently also for some Ag⁺ ions in Ag-MFI zeolite [31,80]. Thus some types of Ag⁺ ions or a part of their spectrum can be "invisible" for UV-Vis spectroscopy recorded in a standard region of the UV-Vis spectrometers up to 50,000 cm⁻¹. The possibility of the presence of the spectral component above 50,000 cm⁻¹ in our Ag/Al₂O₃ samples is indicated in some experiments by an increase of the absorbance intensity around 50,000 cm⁻¹ (see, e.g., Fig. 3-1).

UV-Vis spectra of all oxidised Ag/Al₂O₃ catalysts in this study have similar pattern and show without any doubt that the silver is predominantly in a form of Ag⁺ ions. A shoulder at 35,000 – 38,000 cm⁻¹ found with increasing metal content of the catalyst, indicating small silver clusters, have very low intensity and thus represents very small part of silver.

The bands at 42,400 and 46,400 cm^{-1} observed in the spectra of oxidized Ag-MFI zeolites in H^+ form show that silver is in a form of Ag^+ ions. On the other hand, strong band with maximum at 37,500 cm^{-1} in the spectrum of AgNa-MFI zeolite revealed a presence of small silver $\text{Ag}_n^{\delta+}$ ($n \leq 8$) clusters [31,65]. The difference between the state of Ag in AgNa- and AgH-MFI zeolite treated under the same conditions can be accounted for a lower tendency of AgH-zeolite to reduction due to presence of H^+ ions and also higher mobility of Ag^+ ions. The nature and size of the metal-type $\text{Ag}_n^{\delta+}$ clusters, ascribed to bands below 40,000 cm^{-1} in the spectra of Ag/ Al_2O_3 , is still under discussion (see Table 4-1). The EXAFS experiments enabled direct identification of cluster size in zeolites only up to four Ag atoms (see Refs. 49,65). The surrounding local field of silver in zeolites is different from that affecting Ag clusters on the alumina support. Moreover, in the case of zeolites, strong guest-host interaction between the Ag species and the framework can also be accompanied by spatial restrictions, as shown, e.g., in Ref. 79. Pestryakov and Davydov [43] attributed the bands found with Ag/ Al_2O_3 at 34,000 – 36,000 cm^{-1} and 25,000 – 27,000 cm^{-1} to small Ag_n clusters ($n = 2-7$) with s-s* and n-s* electron transitions, respectively. As they observed a strong donor-acceptor interaction between the Ag^+ ions and the alumina carrier when using adsorbed CO, they suggested induction of an effective charge on silver clusters with formation of $\text{Ag}_n^{\delta+}$ species.

It could be concluded that silver in oxidized Ag/ Al_2O_3 and Ag-MFI zeolites studied is in the form of Ag^+ ions. However, in the Na-form of the zeolite also small $\text{Ag}_n^{\delta+}$ ($n \leq 8$) clusters are formed. As the positions of absorption bands at UV-Vis spectra of the silver clusters of different nuclearity are not yet determined (Tab 4-1) and, moreover, might be different depending on the type of support, the assignment of the bands to the individual $\text{Ag}_n^{\delta+}$ clusters is not clear.

4.1.2 Reducibility of silver catalysts

The shifts of the broad temperature maxima of H_2 consumption and the deficit at hydrogen consumption at H_2 -TPR with respect to complete reduction of Ag^+ with increasing silver loading in Ag/ Al_2O_3 indicate various nature of the silver species (Fig 3-3). Bogdanchikova et al. [45] also suggested that the nature of the silver in Ag/ Al_2O_3 catalysts could markedly change with silver loading. They supposed that small oxide species and/or layer of silver oxide

are present in low loaded Ag/Al₂O₃, while a substantial part of silver aluminate beside silver oxide species is formed in highly loaded Ag/Al₂O₃.

This assumption is supported by the *in-situ* UV-Vis spectra of Ag/Al₂O₃-1.8 during its H₂-TPR (Fig. 3-23). The maxima of UV-Vis broad bands reflecting the formation of metallic charged Ag_n^{δ+} clusters are shifted to lower wavenumbers after temperature-programmed reduction performed up to 473 or 523 K. This indicates reduction of Ag⁺ ion species step by step with the increased temperature to charged metallic Ag clusters and further to larger Ag particles. Bulk silver oxides have strong broad absorption from NIR to UV region at UV-Vis-NIR spectra [81]. However, our spectra (Fig. 3-2) do not show presence of that absorption.

It could be concluded that in Ag/Al₂O₃ well dispersed Ag⁺ ions and small Ag oxide-like clusters are reduced to metallic Ag_n^{δ+} charged clusters and step by step to metallic silver particles. With difficulty are reduced Ag-aluminate species. Therefore it can be suggested that the oxidized Ag/Al₂O₃ contains predominantly atomically dispersed Ag⁺ ions and very small silver oxide clusters as well as a part of silver in the form of silver aluminate.

The hydrogen consumption at H₂-TPR clearly shows completely different character of Ag⁺ bonding in the zeolite compared to alumina. The three maxima of H₂-TPR profile of Ag-MFI-4.2 catalyst might indicate the presence of Ag⁺ ions of different reducibility bound to different lattice sites. On the other hand, the observed three peaks could be explained as Ag⁺ ions are reduced to charged metallic Ag_n^{δ+} clusters in the first and/or second peak and these Ag_n^{δ+} clusters are reduced to metal Ag particles in the second and/or third peak. Shibata et al. [65] supported this assumption by XRD patterns of Ag-MFI treated at various temperatures in H₂. They reported absence of diffraction lines of the metallic Ag crystallites after the H₂ treatment below 573 K. It seems that this result does not support the possibility that Ag⁺ ions are coordinated to different lattice sites, where they might exhibit different reducibility, but it is to be pointed out that XRD might detect only crystalline metallic silver. Thus, we suggest that Ag⁺ ions are reduced to charged silver clusters at the first and second peak and then the charged silver clusters are reduced to metallic silver. What is the most important is the fact that Ag⁺ ions in MFI zeolite, as ion exchanged and replacing bridging OH groups (see Fig. 3-4), are "ideally" atomically dispersed and reduced at much lower temperature compared to Ag species in alumina. This implies higher ionicity of bonding, and decreased charges on Ag⁺ ions in zeolites in comparison with Ag/Al₂O₃.

It can be summarized that well dispersed Ag cationic species in alumina (Ag^+ ions, Ag_2O species and Ag-aluminate) are better stabilized with respect to their reduction to metallic $\text{Ag}_n^{\delta+}$ clusters compared to MFI containing exclusively Ag^+ in charge balanced in cationic sites.

4.1.3 Interaction of silver with the supports

A decrease in intensities of bridging OH groups of the parent MFI zeolite and no changes in intensity of Si-OH groups clearly evidences that Ag^+ ions in AgNH_4 -MFI zeolite (see Fig 3-4) are at exchanged sites. A significant difference in intensity of the hydroxyl bands of parent Al_2O_3 and $\text{Ag}/\text{Al}_2\text{O}_3$ -1.3 at $7,320\text{ cm}^{-1}$ and $7,200\text{ cm}^{-1}$ indicated that silver in alumina interacted predominantly with most basic and acidic OH groups (Fig. 3-5). However, a similar intensity of the hydroxyl bands for $\text{Ag}/\text{Al}_2\text{O}_3$ samples with higher Ag loading indicates that the interaction proceeds only to limited extent. This finding is not in contradiction with conclusions on Ag in alumina given in the literature [28].

The data of acetonitrile uptake (Fig 3-7 and Tab 3-2) indicate the heterogeneity of Lewis acid centers on the surface of alumina. There is clear evidence that silver interacts predominantly with strong acid Lewis sites and to less extent with weak Lewis sites (Fig.3-7 and Tab. 3-2). But it should be noted that also silver cations deposited on alumina could reflect themselves as weak Lewis sites with respect to acetonitrile and provide interaction with CN groups with the same characteristic vibration. Accordingly, the small decrease in the 2313 cm^{-1} band intensity can be apparent. The IR spectra after adsorption of acetonitrile showed also bands of surface acetamide species formed by a hydrolytic process most probably with participation of basic OH groups [73] and formation of bands of OD and CD_2CN^- carbanion that could indicate presence of additional type of basic sites on alumina (O^{2-} anions). A substantial decrease of the number of basic OH groups after Ag^+ ions introduction onto alumina is also shown in NIR spectra (Figs. 3-5). According to the obtained results the amount of the surface acetamide species is substantially higher on alumina than that on silver alumina catalyst. Due to possible migration of all these products the intensity of their bands can hardly be used for determination of the number of the basic sites. Nevertheless, it is seen that the number of the basic sites is higher on parent alumina than that on silver alumina catalysts.

It could be concluded that Ag^+ ions in alumina are stabilized by different interactions between them in contrary to these cations in the zeolite. Ag^+ ions in the MFI zeolite are exchanged and coordinated to bridging oxygen atoms, while in alumina they interact predominantly with strong acid Lewis sites and a part of them with basic and acidic OH groups.

4.1.4 Relationships among the Ag state, interaction with the support and reducibility of silver species

Silver in oxidized $\text{Ag}/\text{Al}_2\text{O}_3$ and Ag -MFI zeolites studied exhibits various reducibility depending on the type of silver species and their interaction with the supports. Ag^+ ions in MFI zeolites are coordinated to framework bridging oxygen atoms and can be easily and completely reduced to $\text{Ag}_n^{\delta+}$ clusters relatively highly stabilized by negative framework charge and metallic silver particles. The interaction of silver with alumina, occurs with the strong and weak acid Lewis sites and basic and acidic OH groups. We suggest formation of various Ag^+ specie: atomically dispersed Ag^+ ions, very small silver oxide clusters and silver aluminate species, population of which depends on silver loading of $\text{Ag}/\text{Al}_2\text{O}_3$. The atomically dispersed Ag^+ and those in very small oxide clusters are reduced at relatively low temperatures, while silver aluminate species are reducible only at high temperatures.

4.2 Selective catalytic reduction of NOx by decane over silver catalysts

4.2.1 General features of the SCR-NOx reactions over silver alumina catalysts

Typical temperatures of diesel engine exhaust gases, determining operating temperature for selective catalytic reduction, are in the temperature window 470-720 K. However, the $\text{Ag}/\text{Al}_2\text{O}_3$ catalysts generally exhibit sufficient activity in SCR of NO to N_2 only at temperatures above 620 K. Thus catalytic activity of $\text{Ag}/\text{Al}_2\text{O}_3$ in the whole temperature range of 470-720 K should be considered as being of great importance.

The mechanism of SCR-NOx over silver catalysts is very complex and, although that numerous studies based on FTIR spectroscopy have been done, it has not been so far fully elucidated. Nevertheless, a general picture of the most significant steps of the reaction has been drawn [51,52,55]. It is assumed that the SCR-NOx reaction starts with formation of adsorbed

nitrate via oxidation of NO by O₂ and formation of acetate (formate) species by partial oxidation of a hydrocarbon with NO_x and O₂. The acetates (formates), which can act as surface reductants, reduce nitrates via several steps to N₂. One of the most important steps is formation of Ag⁺-CN species and their transformation into -NCO via organo-nitrogen species [12,50]. It is supposed that Ag⁺-NCO and -CN adspecies react further with another N-containing compound to -NH containing species and finally to N₂, [51,52,55]. Non-selective oxidation of hydrocarbon occurs in addition to SCR-NO_x. Thus, in order to achieve effective Ag/Al₂O₃ catalyst it has to possess high selectivity in hydrocarbon utilization in the SCR-NO_x reaction.

4.2.2 Activity of silver catalysts

The rate of N₂ formation at SCR-NO over Ag/Al₂O₃ is much higher than that over Ag-MFI catalyst in terms of NO_x conversion per catalyst weight and TOF values per Ag atom. Moreover, the Ag-MFI catalyst suffers of deactivation by coking. We suppose that this coking originates from transformation of olefins formed by decane cracking, oligomerization and aromatization over strong acid sites of the zeolite.

The highest activity in the terms of conversion and TOF values exhibits medium loaded Ag/Al₂O₃-1.8 catalyst (Figs. 3-8a, 3-8b). These results correspond to those found in the literature Refs [14,18,28,29,31,32,47]. The Ag/Al₂O₃-1.8 catalyst proved also long-term stable performance with respect to NO-N₂ at the SCR-NO_x process (Fig. 3-16). Values of TOF for Ag/Al₂O₃ show that ca 2 wt.% Ag was an optimum Ag loading for C₁₀H₂₂-SCR-NO_x with maximum exploitation of single Ag⁺ ions. The lower activity of silver alumina at higher silver loading could be connected with the state of silver. At higher loadings exceeding about 2 wt.% clustering of silver ions and their easier reduction have been indicated. It is known that metallic silver activates both molecular oxygen and hydrocarbons providing conditions for hydrocarbon oxidation. Thus decreasing SCR-NO_x activity with silver loading over ca 2 wt.% has been attributed to formation of metallic Ag particles and high rates of C₃H₆ oxidation with O₂, at the expense of its reaction with NO in Refs. [14,45,46]. The formation of large metallic particles has been attributed to the detrimental effect of increasing of the particle size of silver oxide entities with increasing loading, yielding entities easily reducible to Ag⁰ particles [14]. However, in Refs. [14,45,46] the activity of highly active Ag/Al₂O₃ (2 wt.%) was compared only with highly loaded

Ag/Al₂O₃ (ca 6 wt.% Ag) catalyst. On the other hand, the analysis of NO_x and C₁₀H₂₂ conversions obtained in this study for Ag/Al₂O₃ catalysts containing 1.8 and 2.9 wt.% Ag shows that C₁₀H₂₂ conversion is lower for Ag/Al₂O₃-2.9. Hence, the decrease of activity in NO_x reduction to N₂ cannot be only attributed to a substantial decrease in concentration of a hydrocarbon resulting from its higher non-selective combustion. Oxidation of hydrocarbons at SCR-NO_x over Ag/Al₂O₃-1.8 is predominantly connected with activity at NO_x reduction to N₂ (cf. C₁₀H₂₂ + O₂ and C₁₀H₂₂ + O₂ + NO). At Ag/Al₂O₃-2.9 is formed higher number of metallic silver than that at Ag/Al₂O₃-1.8 at SCR-NO_x. However, the reason why the de-NO_x activity decreases with higher silver loading could be more complex. It has been shown that small part of Ag⁺ ions interacts with support via hydroxyl group (Fig 3-5) and substantial part of Ag⁺ ions could interact by different route at least with acid Lewis or/and basic site on alumina surface (Fig 3-6). Bethke and Kung [14] supposed that the activity of the Ag/Al₂O₃ catalysts might not result solely from Ag, but Al₂O₃ itself may be involved in the reaction. They supposed that a similar mechanism as observed for Co/Al₂O₃ [82] and a mixture of Pt/SiO₂ with Al₂O₃ [83] occurred over Ag/Al₂O₃. The conversions of NO over the Pt/SiO₂-Al₂O₃ mixture were higher than the sum of the conversions over the individual components. It was suggested that this synergic effect resulted from a spillover or gas phase transfer of a short-lived intermediate, possibly a partially oxidized or activated hydrocarbon species. On the basis of these results, it could be expected a mechanism, where surface migration of a reaction intermediate from Ag species to surface of Al₂O₃ or vice versa occurs.

In conclusion the medium loaded Ag/Al₂O₃-1.8 catalyst exhibits the highest reduction activity at SCR-NO_x by decane. It is suggested that a specific local structure of silver ion species localized in a surrounding Al₂O₃ is responsible for the high reduction activity of NO_x. Nevertheless, the activity is low at low temperature region, which is essential for NO_x abatement in diesel engine exhausts.

4.2.3 Effect of reactant composition on SCR-NO_x over silver alumina

It was clearly shown (Tab. 3-3) that the conversion of NO_x to N₂ in SCR-NO_x over Ag/Al₂O₃-1.8 employing relatively high concentrations of NO₂ in NO/NO₂ inlet mixtures is lower compared to that if NO is used. It indicates some negative effect of NO₂ on the SCR-NO_x

reaction. On the other hand, formation of ad-NO_x (NO₂, NO₃) species on the surface sites is proposed to be the first reaction step. Nevertheless, the effect of NO₂ on the reduction of NO_x to nitrogen over Ag/Al₂O₃ catalysts is reported controversially in the literature. Both a positive [14] as well as a negative effect [20,48] of NO₂ was found compared to NO. Bethke and Kung [14] have shown that enhancement of the conversion of propane-SCR-NO_x by NO₂ also depends on the Ag loading on alumina. The different results are connected with the type of a hydrocarbon and reaction conditions used. The observed lower NO_x conversions with NO₂ at low temperature might be explained by strong adsorption of nitrates and thus blocking of active sites [60].

Similarly to the case of NO, many authors have proposed formation of surface acetate and/or formate species by partial oxidation of hydrocarbons with O₂ as the first reaction step [16,50,51]. It is to be noted that NO₂ is a stronger oxidant compared to molecular oxygen. Accordingly, conversion of NO to N₂ at SCR-NO_x over Ag/Al₂O₃-1.8 was enhanced by higher concentration of both decane and oxygen in the reaction stream (Figs 3-30 and 3-31). Molecular oxygen plays, besides NO_x a key role as oxidant at the SCR-NO_x process over Ag/Al₂O₃ due to its participation in the several steps of the complex process. Oxygen takes part in formation of intermediates like acetate (formate) and NCO surface species [12,16,50]. In addition, oxygen is essential for both keeping the catalyst in high oxidation state and cleaning the surface from carbonaceous deposit. The increasing O₂ concentration promotes not only the rate of total oxidation but also the rate of partial oxidation of hydrocarbon. If the oxidation activity is too low, the generation of the intermediates is slow and the rate of NO_x-reduction becomes low.

Contrary, when CO was added to the reactant mixture beside decane (Fig. 3-21), to investigate whether another reductant could have a similar function to hydrocarbons, no promotion of the SCR-NO_x over Ag/Al₂O₃-1.8 was observed. Thus Ag/Al₂O₃ cannot catalyse reduction of NO_x in oxidizing conditions.

4.2.4 *Decane-SCR-NO_x enhanced by hydrogen assistance*

Although the positive effect of hydrogen over Ag/Al₂O₃ for the CH_x-SCR-NO_x reactions was demonstrated for a spectrum of hydrocarbons, for methane, C₂ and C₃ paraffins and olefins, isobutane [20,48,58,67], octane [8,64], and ammonia [61], it is worthwhile to point out that with decane, as the main component of diesel engine exhausts, a similar hydrogen effect has been

observed. Among the Ag/Al₂O₃ catalysts studied, the Ag/Al₂O₃-1.8 catalyst exhibited the highest activity in NO_x to N₂ reduction also in reduction of NO_x by a mixture of decane and hydrogen. The conversion of NO to nitrogen was enhanced dramatically, at low temperature range (470-620 K) as well as at extremely high space velocities (shown up to 240,000 h⁻¹); (Figs. 3-10, 3-13, 3-15). Both these ranges of conditions are essential for NO_x abatement in diesel engine exhausts. A slight decrease in NO conversion at high temperatures (>673 K) at lower space velocities (30,000 h⁻¹) is due to a lack of hydrocarbon in the reaction mixture (Fig. 3-13). This observation is quite typical for lean NO_x reduction catalysts. During the H₂-assisted C₁₀H₂₂-SCR-NO_x reaction, the presence of high excess of water vapor in the gas stream is beneficial with respect to the long-term catalyst operation as, without water vapor presence, a substantial decrease in the NO_x conversion to nitrogen with time occurs (see Fig. 3-16). This is due to formation of deposits adsorbed on the catalyst surface. These deposits can be represented by olefin-type intermediates, as decane readily cracks with formation of olefins, which have tendency to oligomerize and further transform to high-molecular coke-like products.

Contrary to the highly beneficial effect of hydrogen on NO conversion, its presence slightly increases yields (up to 10%) of undesired N₂O and CO, especially at low temperatures (470-570 K); Fig. 3-10, 3-11. Generally, formation of N₂O is increased at conditions leading to increasing concentration of NO₂, i.e. at increasing hydrogen or oxygen concentration in the feed at SCR-NO_x, while variation of decane concentration has no effect on the N₂O yield. This finding might indicate incomplete reduction of NO_x to nitrogen.

However, without any doubt hydrogen enhances the rate of oxidation of NO to NO₂ at low temperatures (470-520 K) (Fig. 3-20, and ref. [48]) and thus leads to an increased concentration of NO₂ in the gas phase, and a pool of nitrates on the surface. But as the high concentration of NO₂ in the feed results in lower N₂ yields, the positive effect of hydrogen on the NO_x conversion to nitrogen in the C₁₀H₂₂-SCR-NO₂ reaction (Table 3-3) could not generally be accounted for by enhancement of the reaction of oxidation of NO to NO₂. Thus, another function of hydrogen, reflected rather in hydrocarbon oxidation, could contribute to the enhanced SCR-NO_x activity.

The mechanistic cause of enhancement of C₁₀H₂₂-SCR-NO activity by addition of H₂ over Ag/Al₂O₃ was also investigated with *in-situ* FT-IR spectroscopy in our laboratory [84,85]. It has been shown that formation of surface species during oxidation of NO or decane is greatly

affected by the presence of hydrogen. Surface monodentate nitrates are formed preferentially and are more reactive compared with the bidentate species. Oxidation of decane mostly yields surface acetates, and the presence of NO_x favours the formation of formates (acrylates). The reaction steps most enhanced by the addition of hydrogen to the SCR-NO_x reaction are the transformations of the intermediate -CN species into -NCO and oxidation of the hydrocarbon to formates (acrylates).

4.3 State of silver at the reaction conditions

4.3.1 Analysis of Ag species by UV-Vis spectra

Diffuse reflectance UV-Vis spectra monitoring during calcination and the decane-SCR-NO_x reaction over Ag/Al₂O₃ catalyst and that reaction co-assisted by H₂ or CO (as well as during oxidation of NO and H₂ by molecular oxygen) at the identical parameters of the micro-reactor when the reaction kinetics was studied provided *in-situ* information on the catalyst structure at real conditions of the catalytic reactions. The studies and information obtained at such a level represent a dramatic step ahead for understanding of catalyst structure and its operation during catalytic reactions. Nevertheless, the application of UV-Vis spectroscopy for analysis of the state of Ag in Ag/Al₂O₃ brings about also some limitations. A surprising absence of a significant decrease in the spectrum intensity of Ag⁺ ions between 40,000 - 50,000 cm⁻¹ when Ag_n^{δ+} clusters are formed at oxidation of H₂ by molecular oxygen (Fig. 3-24 and 3-25) could be explained most probably by very high differences in extinction coefficients for Ag⁺ ions and Ag_n^{δ+} clusters, as follows from Fig. 3-23, but to some extent possibly also and by the occurrence of the Ag⁺ 4d → 5s transitions of some Ag⁺ species exclusively above 50,000 cm⁻¹. The high difference in the extinction coefficients of Ag⁺ ions and Ag_n^{δ+} clusters follows from a comparison of the intensity of the broad band of small Ag_n^{δ+} clusters when a quarter of Ag⁺ ions was reduced (Fig. 3-23) with that monitored during the SCR-NO_x reaction. This shows that roughly only < 5% of the total amount of Ag⁺ ions was reduced. However, determination of extinction coefficients of Ag_n^{δ+} clusters could not be done, as a spectrum of clusters of various nuclearities are formed. This finding on the very low amount of Ag⁺ ions reduced might support speculation on the presence of silver in Ag/Al₂O₃ in the form of Ag₂O, as suggested in Ref. [20]. Low concentration of Ag₂O

could be hardly seen by a broad absorption, which is characteristic for bulk and thin layers of Ag_2O [81].

In conclusion, the UV-Vis spectra cannot provide complete quantitative picture on the behaviour of all the Ag^+ ions in $\text{Ag}/\text{Al}_2\text{O}_3$ under the reaction conditions. Nevertheless, the results of UV-Vis spectroscopy with the H_2 -TPR experiments suggest (i) assignment of the UV absorption bands at 41,600 and 46,600 cm^{-1} to Ag^+ ions in an oxygen ligand environment, vast amount of which does not undergo changes in the valence state at the conditions of the investigated SCR- NO_x process, and (ii) semiquantitative analysis of formation of $\text{Ag}_n^{\delta+}$ clusters at real reaction conditions depending on the reaction mixture composition. Low number of silver clusters is suggested to be formed either from the Ag^+ ions detected by absorption bands at 41,600 and 46,600 cm^{-1} but it cannot be excluded that some of them originate from undetected Ag^+ ions, such as represented by single Ag^+ ions or very small Ag_2O species.

On contrary, the UV-Vis spectra of $\text{Ag}/\text{Al}_2\text{O}_3$ have provided some insight into the development of small $\text{Ag}_n^{\delta+}$ clusters depending on the reaction conditions, although assignment of the individual absorptions below 40,000 cm^{-1} to $\text{Ag}_n^{\delta+}$ clusters of distinct nature and size is still under discussion (see Table 4-1).

The bands found with $\text{Ag}/\text{Al}_2\text{O}_3$ at 34,000 – 36,000 cm^{-1} and 25,000 – 27,000 cm^{-1} were attributed to small Ag_n clusters ($n = 2-7$) [43]. The absorption observed for the $\text{Ag}/\text{Al}_2\text{O}_3$ sample in the 30,000 – 32,000 cm^{-1} region can be attributed to $\text{Ag}_8^{\delta+}$ clusters, as these were monitored by direct-mass spectrometric experiments, in aqueous solutions [42] and in the confined space of zeolites [48, 79]. The presence of $\text{Ag}_8^{\delta+}$ clusters is supported by the fact that Ag clusters exhibiting the same UV-Vis spectrum contain Ag atoms with three nearest neighbours in the first coordination sphere, i.e. represent $\text{Ag}_4^{\delta+}$ clusters with tetrahedral symmetry or $\text{Ag}_8^{\delta+}$ clusters with cubic symmetry. Presence of $\text{Ag}_8^{\delta+}$ clusters is more probable due to their significantly higher stability (magic clusters) compared to $\text{Ag}_4^{\delta+}$ clusters, which are extremely unstable [86].

However, the observations of silver clusters at conditions of SCR- NO_x suffer due to presence of absorption bands of NO_x species at the UV-Vis spectrum. In Ref [66] it was derived from the volumetric experiments that a substantial part of silver in $\text{Ag}/\text{Al}_2\text{O}_3$ is finally converted into silver nitrate at presence of NO_2 in the reaction stream. Therefore, the band at 33,400 cm^{-1} in the *in-situ* diffuse reflectance UV-Vis spectrum during NO_2 adsorption experiment (Fig 3-27) is ascribed to silver nitrate. The assignment of the band at 26,600 cm^{-1} is less evident [66]. It is

speculated that it is connected with the coordination of Ag^+ with NO_2 preceding the formation of nitrate, which would explain its transient appearance. The intensities of the bands at 26,600 and 33,400 cm^{-1} are low due to low extinction coefficients of the NO_x species. The great difference between extinction of the bands of the absorbed NO_x species in this region and silver clusters enables to observe the silver clusters on the silver alumina catalysts at the reactant stream containing nitrogen oxides. Contrary, the bands of NO_x species above 40,000 cm^{-1} have high intensity. An analysis of the individual NO_x species and the bands of Ag^+ ions cannot be made due to their overlap.

The assignment of the individual bands to silver species given in the literature and suggested in this study is summarized in Table 4-1.

4.3.2 *Ag species under the reaction conditions of oxidation of H_2 and NO by molecular oxygen*

At very mild reduction of silver in the $\text{Ag}/\text{Al}_2\text{O}_3$ sample under vacuum, as well as at low hydrogen pressure at RT, the bands monitored at 28,000 and 34,000 cm^{-1} can be ascribed to the $\text{Ag}_n^{\delta+}$ clusters. Under the conditions of the $\text{H}_2 + \text{O}_2$ reaction over $\text{Ag}/\text{Al}_2\text{O}_3$ -1.8, these two characteristic bands were no longer resolved and the existence of a broad band ranging from 20,000 to 40,000 cm^{-1} (Fig. 3-22) indicated the presence of several types of small $\text{Ag}_n^{\delta+}$ clusters, which can hardly be defined with respect to their nuclearity. Bearing in mind the relatively high stability of silver clusters with $n = 8$ [86], the observed local maximum of absorption around 31,000 cm^{-1} , can probably be ascribed to the presence $\text{Ag}_n^{\delta+}$ clusters predominantly with $n = 8$. With the $\text{NO}-\text{NO}_2$ reaction using similar NO and H_2 concentrations as those in the $\text{C}_{10}\text{H}_{22}$ -SCR- NO_x reaction, only a very low intensity band of NO_x species or/and insignificant concentration of $\text{Ag}_n^{\delta+}$ clusters was formed, although the conversion of NO was increased dramatically (Figs. 3-26 and 3-20). We supposed that this extremely low number of $\text{Ag}_n^{\delta+}$ clusters is not sufficient for enhancement of the $\text{NO}-\text{NO}_2$ reaction rate and the hydrogen function in the $\text{NO}-\text{NO}_2$ reaction is not connected with the function of these $\text{Ag}_n^{\delta+}$ clusters. In Ref. [20], dissociation of oxygen on small Ag clusters was assumed, but without giving the experimental evidence. We speculate that the HO_2 radicals formed (see below par. 4.6) are responsible for NO to NO_2 oxidation at

hydrogen or hydrocarbon presence (cf. enhancement of NO-NO₂ oxidation by both hydrogen and decane, see Figs. 3-20 and 3-8c, resp.).

4.3.3 *Ag species under the decane-SCR-NO_x reaction and that co-assisted by hydrogen and carbon monoxide*

The shape of the UV-Vis bands in the region from 20,000 to 40,000 cm⁻¹ of Ag_n^{δ+} clusters forming an envelope and observed during the C₁₀H₂₂-SCR-NO_x reaction or that co-assisted by hydrogen at various reactant/product compositions is rather complex. Nevertheless, as the shape of this broad band is not significantly varied depending on reaction conditions and reactant compositions, it can be inferred that more or less similar Ag_n^{δ+} species are present. It should be pointed out that, under the reaction conditions investigated (with stable NO_x conversions for many hours), we did not observe formation of large metallic Ag⁰ particles, which should be manifested in strong absorption in the Vis spectrum.

Based on the *ex-situ* UV-Vis spectra and EXAFS studies, analysing the state of silver in the Ag-MFI zeolite catalyst after the H₂/propane-SCR-NO_x reaction [49,65], the authors suggested that the positive "hydrogen effect" is caused by formation of small Ag_n^{δ+} clusters with n = 2-4 and, therefore, these species represent active sites. Without co-assistance of hydrogen they did not report occurrence of Ag_n^{δ+} clusters. However, our results indicate that already during the decane-SCR-NO_x reaction over Ag/Al₂O₃ the Ag_n^{δ+} clusters are definitively, and the most populated, besides clusters of other nuclearity, are probably Ag₈^{δ+} clusters.

It follows from a comparison of the UV-Vis spectra of Ag/Al₂O₃-1.8 in the H₂/C₁₀H₂₂-SCR-NO_x reactions at various feed compositions (cf. Figs. 3-28, 3-29, 3-30) that in both the presence and absence of hydrogen as co-reactant, small Ag_n^{δ+} clusters are present in the catalyst. Their number clearly increases with increasing conversion of NO to nitrogen, regardless of whether this conversion increase is achieved by the increasing concentration of hydrogen or decane. This finding implies that there is some obvious relationship (although not quantitative) between the conversion of NO to N₂ and the number of small Ag_n^{δ+} clusters in the catalyst. Hence the conversion of NO to N₂ also depends on the catalyst activity in oxidation of NO and CH_x by molecular oxygen, and CH_x by NO_x, the relationship between the Ag structure and SCR-NO_x activity could be hardly established.

However, such apparent correlation between the NO_x-N₂ conversion and amount of Ag_n^{δ+} clusters is not in agreement with the immediate responses of the system (completely reversibly) to hydrogen addition and removal followed by increased and decreased NO conversion, respectively. The responses in the changes in the number of small charged Ag_n^{δ+} clusters were substantially much slower (particularly at hydrogen removal from the reactant feed, see Fig. 3-32). It implies that the Ag_n^{δ+} clusters are not formed exclusively as a result of hydrogen addition, but that their number during the SCR-NO_x reaction could be also controlled by the accumulation of surface organic intermediates. This conclusion is supported by the observation, obtained in our laboratory by IR spectra monitoring of surface species at *in-situ* conditions of the reaction, that enhancement of the NO-N₂ reaction by hydrogen is accompanied by a substantial increase of surface reaction intermediates [84].

To confirm the suggestion that Ag_n^{δ+} clusters are not a real active sites CO was added to the reactant mix to investigate whether another reductant could have a similar effect to hydrogen. Clearly, carbon monoxide does not promote the SCR-NO_x reaction (Fig. 3-21). Although CO has no direct effect on the rate of NO_x conversion, *in-situ* UV-Vis spectra show that it promotes, similarly to hydrogen, the formation of small Ag_n^{δ+} clusters during the CO/decane-SCR-NO_x reactions as well as CO oxidation. The extent of Ag_n^{δ+} cluster formation when CO is added is less than that observed for hydrogen addition, but is nevertheless significant. Thus Ag_n^{δ+} cluster are not responsible for high activity of Ag/Al₂O₃ in SCR-NO_x.

Consistently with those findings Breen et al. [63] reported just in 2005 that the enhanced activity found in the presence of hydrogen is thought to be due to a chemical effect and not the result of a change in the structure of the active site, as they concluded from the *in-situ* EXAFS study. Nevertheless, the EXAFS indicates that small silver clusters are formed to small extent during the SCR-NO_x process particularly if H₂ or CO is co-fed.

Therefore, the number of small Ag_n^{δ+} clusters can be related to the reducing environment of reaction atmosphere present over the catalyst surface during the SCR-NO_x reaction in both cases, i.e. in the presence and absence of hydrogen. Thus, the number of Ag_n^{δ+} clusters is predominantly a result of reducing effect of adsorbed surface intermediates.

It should be also mentioned that the enhancing effect of H₂ on the SCR-NO_x reaction was reported only over Ag/Al₂O₃, much less over Ag-MFI (see Fig. 3-12), but not over other silver based catalysts. The NO-N₂ activity over Ag/TiO₂, Ag/ZrO₂, Ag/SiO₂, and Ag/Ga₂O₃ was

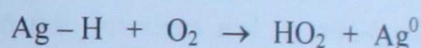
reported to be very low in both the presence and absence of H_2 [48], and thus no positive hydrogen-effect occurred. Although the process of SCR- NO_x is very complex, it could be found some connection (not quantified) between the $NO-N_2$ conversion over Ag based catalysts and reducibility of Ag^+ ions on these supports. It seems that the trend of the $NO-N_2$ activity of Ag on various supports $Ag/Al_2O_3 < Ag-MFI < Ag/ZrO_2 < Ag/SiO_2$ is reverse to that of Ag^+ ions reducibility (see Refs. [14,47,65] and H_2 -TPR results – Fig. 3-3). This implies that there is additional support for the conclusion that with the increasing stability of the Ag^+ oxidation state increases $NO-N_2$ activity of the Ag based catalysts. Analogous trend is seen for the enhancement of the SCR- NO_x reaction co-assisted by hydrogen.

Table 4-1 Band positions for various silver species in UV-Vis spectra

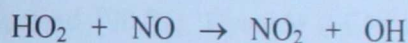
Wavenumber (cm ⁻¹)	Ag species	Comments	Refs.
32,300	Ag ₂ ⁺	Mordenite	79
37,700	Ag ₄ ²⁺	Mordenite	79
39,200; 32,800	Ag ₄ ²⁺	ZSM-5	65
30,300	Ag ₅ ⁰	Mordenite	79
34,500	Ag ₇ ^{δ+} or Ag ₈ ^{δ+}	Mordenite	79
30,800	Ag ₈ ^{δ+}	Solution, magic cluster	86
31,300	Ag ₈ ⁰	Mordenite	79
28,200	(Ag ₄ ⁺) ₂	Mordenite	79
25,600-27,000	Ag _n ^{δ+} (n=2-7)	γ-Al ₂ O ₃ , SiO ₂	43
34,500-37,000	Ag _n ^{δ+} (n=2-7)	γ-Al ₂ O ₃ , SiO ₂	43
42,600; 47,600	Ag ⁺	ZSM-5	65
44,400; 47,600; 52,100	Ag ⁺	Ag(H ₂ O) ₄	42
41,700	Ag ⁺	γ-Al ₂ O ₃ , SiO ₂	43
44,600; 47,200; 51,000	Ag ⁺	ZSM-5	31
52,600	Ag ⁺	ZSM-5	80
from NIR to UV region	Ag ₂ O	bulk	81
41,600; 46,600	Ag ⁺	γ-Al ₂ O ₃	this study
27,000; 28,000; 30,000; 31,000,	Ag _n ^{δ+} (n ≤ 8)	γ-Al ₂ O ₃	this study
34,000; 38,000			
ca < 26,000	Ag agglomerates	γ-Al ₂ O ₃	this study

4.6 Function of hydrogen at SCR-NO_x over silver alumina catalyst

The number of small Ag_n^{δ+} clusters over Ag/Al₂O₃ can be related to the reducing environment present on the catalyst surface formed by the SCR-NO_x reaction in both cases, i.e. in the presence and absence of hydrogen. Also the increased activity in NO-NO₂ oxidation under presence of hydrogen is not accompanied with a significant increase of the number of Ag_n^{δ+} clusters. Accordingly, the presence of Ag_n^{δ+} clusters is likely not the reason for the enhanced NO-N₂ activity of Ag/Al₂O₃, but hydrogen itself has to take part in the reaction. In Refs. [87, 88] it was shown that hydrogen dissociates when adsorbs on Ag⁺ in zeolites and generates acidic protons and silver-hydride. Methane also dissociates on silver with formation of CH₃^{δ+} and silver-hydride [87]. Similar processes of hydrogen dissociation as well as hydrogen atom abstraction from a hydrocarbon might occur at SCR-NO_x over Ag/Al₂O₃. We speculate that silver-hydride at the SCR-NO_x reaction mixture immediately reacts with oxygen to form hydroperoxy radicals (HO₂)



Hydroperoxy radical, which is highly active oxidant [89], readily react with NO to NO₂ and hydroxy radical [89,90] according to the following reaction



Both these radicals can react with hydrocarbons to their oxo/nitro derivatives [89]. We suppose that hydrogen addition enhances formation of silver-hydride and thus support radical-type reactions. Such mechanism of hydrogen (and hydrocarbon) functioning is in accordance with the experimental observations obtained in this study that both hydrogen and decane enhances NO-NO₂ oxidation, hydrogen enhances all the SCR-NO_x reaction steps, and that occurrence of gas phase radical-type transformations behind the catalyst bed was observed at octane-SCR-NO_x (without hydrogen) over Ag/Al₂O₃ catalyst [56].

The effect of hydrogen on SCR-NO_x is likely very complex. The low activity of Ag/Al₂O₃ at temperatures below 573 K was also ascribed to inhibition of active sites by strongly adsorbed nitrates [21]. It has been recently shown that addition of hydrogen into reactant stream enhances, but also limits decomposition, of stable nitrate species [60,66]. This limitation of amount of adsorbed nitrates could explain higher NO_x to N₂ activity at H₂/C₁₀H₂₂-SCR-NO_x compared with H₂O₂/C₁₀H₂₂-SCR-NO_x.

It was also speculated that silver is in the presence of hydrogen in SCR reactant stream reduced to atomic Ag^0 and that they are the species responsible for high catalytic activity [20]. However, atomic Ag^0 species were not observed in the $\text{Ag}/\text{Al}_2\text{O}_3$ catalyst under reaction conditions and CO added to the reactant mix also promote Ag^+ reduction but does not promote the SCR reaction [85].

4.7 Enhancement of SCR-NO_x over silver alumina catalyst by hydrogen peroxide

The observed enhanced rate of oxidation of NO to NO_2 and NO_x reduction to N_2 by addition of hydrogen peroxide to SCR-NO_x mixture supports the suggestion that the initial step in the mechanistic pathways of SCR-NO by hydrogen peroxide consists in generation of highly reactive hydroxy and hydroperoxy radical species. Hydrogen peroxide decomposition is a well-known process generating hydroxy and hydroperoxy radicals; however, competition between H_2O_2 consumption in the oxidation reactions and its non-productive decomposition could be expected in the SCR-NO_x process. Simultaneous presence of nitrogen oxides, hydrocarbons and radicals results in high complexity of the reaction mechanism. Hydroxy alkyl radical and oxo/nitro radical species are formed [90,91]. Cyanide ($-\text{CN}$) and isocyanate ($-\text{NCO}$) species were found to be important intermediates in the formation of molecular nitrogen in the SCR-NO_x process over $\text{Ag}/\text{Al}_2\text{O}_3$ [21]. Thus, the function of H_2O_2 in the SCR-NO_x reaction is specifically based on the activation of relatively stable reactants as well as more reactive intermediates.

Therefore, the enhanced conversion of NO to NO_2 and N_2 , accompanied by the increase in the decane oxidation, caused by the addition of hydrogen peroxide to the SCR-NO_x reactants, supports our previous suggestion that the initial step and the role of hydrogen in the mechanistic pathways of the $\text{H}_2/\text{CH-SCR-NO}$ reaction might consist generation of the highly reactive hydroxy and hydroperoxy radical species. If hydrogen peroxide is used as a co-reactant with hydrocarbons, higher yields of NO_2 are obtained compared to the reaction in which hydrogen is used. It should be mentioned that the increased formation of NO_2 does not increase the degree of reduction of NO_x to nitrogen over $\text{Ag}/\text{Al}_2\text{O}_3$, but that the opposite effect was found (see Tab. 3-3).

It can be suggested that the positive effect of hydrogen peroxide addition at the SCR-NO_x process could be also utilized to boost the SCR-NO_x process; this procedure might be especially important for applications to reduce emissions in the exhaust gases of mobile diesel engines.

4.8 Active site at SCR-NO_x over silver alumina catalyst

The discovery of the promotion effect of hydrogen on SCR-NO_x [58] opened a discussion about the role of small silver clusters in SCR-NO_x over silver catalysts. The formation of small Ag_n^{δ+} clusters was related to the increased NO_x to N₂ reduction activity and, therefore, the positive effect of added hydrogen on the SCR-NO_x reaction was attributed exclusively to the formation of small charged metallic Ag_n^{δ+} clusters [48,49,58,65,67].

In this study, it was clearly shown by *in-situ* monitoring of the structure of Ag/Al₂O₃ catalyst at real conditions of the SCR-NO_x catalytic process in both steady-state and transition conditions (with respect to hydrogen concentration) that only a small part of very reactive Ag⁺ (estimated to be < 5%) is reduced to metallic charged Ag_n^{δ+} clusters ($n \leq 8$) during both the decane- and H₂/decane-SCR-NO_x reactions. The number of Ag_n^{δ+} clusters formed depends mainly on the level of NO conversion to nitrogen, but it is to be stressed that regardless of whether the conversion level is attained by the addition of hydrogen or by an increased concentration of decane or oxygen in the feed. The time-resolved responses of NO_x-N₂ conversion and of the number of Ag_n^{δ+} clusters to the addition/removal of hydrogen from the reactants indicate that the Ag_n^{δ+} clusters are mainly formed because of the reducing effect of adsorbed CH_xO-containing reaction intermediates. A comparison of the function of added H₂ and CO into the feed also showed that although both carbon monoxide and hydrogen promoted formation of Ag_n^{δ+} clusters during the SCR-NO_x reaction, but only hydrogen increased NO_x-N₂ conversion, in contrast to carbon monoxide, which had not a significant effect on NO to N₂ reduction. This clearly demonstrates that the enhanced activity due to the addition of hydrogen to the NO_x-SCR mixture cannot be attributed to the formation of Ag_n^{δ+} clusters. It was proposed that hydrogen itself participates directly in the reaction mechanism via its dissociation, formation of silver hydride and initiation radical reactions. The relationship between the activity of silver alumina catalysts and the state of silver clearly shows that the Ag⁺ centre are the active sites participating in the SCR-NO_x over silver alumina catalyst. Active Ag⁺ ions are suggested to be

represented by a single Ag^+ ions and/or very small Ag_2O species stabilized on alumina by strong mutual interaction.

5 Conclusions

Selective catalytic reduction of NO_x to nitrogen with decane (decane-SCR-NO_x), individual reaction steps (NO-NO₂, decane + O₂), and these reactions enhanced by co-fed hydrogen over silver alumina were investigated with the aim to bring an insight into behaviour of silver at these reactions and to contribute to application of the SCR-NO_x process for abatement of NO_x from exhaust gases of diesel engines. The main goal of the study has been a complex picture of the highly positive effect of hydrogen addition on SCR-NO_x over Ag/Al₂O₃ catalyst. Multi-technique approach, consisting of UV-Vis-NIR, FTIR spectroscopy and H₂-TPR technique, was used for structural analysis. The structural analysis of the state of silver was attempted to provide information under the real reaction conditions in the steady-state and transient modes by *in-situ* UV-Vis spectroscopy.

Under simulated conditions of diesel engine exhaust composition, i.e. low concentration of NO_x and high concentration of oxygen and water vapor, and using decane as main diesel fuel component, Ag/Al₂O₃ and Ag-MFI catalysts showed activity in C₁₀H₂₂-SCR-NO_x. The activity of Ag/Al₂O₃ was superior to that of Ag-MFI. The optimum Ag/Al₂O₃ with 1.8 wt.% Ag exhibited the highest NO to N₂ reduction activity among the studied catalysts. The SCR-NO_x over the Ag/Al₂O₃ catalyst is promoted by increasing concentration of oxygen and/or decane in the reactant stream [84], whereas is not affected by CO [85]. Nevertheless, at temperatures below 620 K the activity of Ag/Al₂O₃ is very low for its application at diesel engine exhausts.

Addition of hydrogen into reactant stream, like for SCR-NO_x with low chain paraffins reported in the literature, dramatically increased the conversion of NO to N₂ with decane in the temperature region 470-720 K and at very high space velocities (60,000–240,000 h⁻¹), important for reduction of NO_x at diesel engine exhausts. Also oxidation of NO or decane by oxygen over Ag/Al₂O₃ was greatly increased by the presence of hydrogen. As we have found that at low temperatures the increasing concentration of NO₂ in the reactant mixture had a negative effect on the SCR-NO_x reaction due to strong adsorption of nitrates on surface catalyst, the positive effect of hydrogen on SCR-NO_x is not based on the promotion of NO to NO₂ oxidation [84].

In calcined catalysts silver was in a form of Ag⁺ ions in both Ag/Al₂O₃ and Ag-MFI catalysts. All Ag⁺ ions were coordinated to bridging oxygen in Ag-MFI catalysts. Ag⁺ ions in Ag/Al₂O₃ catalyst were stabilised mainly on the account of the Lewis acid and basic sites and a

part of silver was exchanged with protons. Alumina support provided high dispersion and stabilization of single Ag^+ ions and small Ag_2O species.

For the first time we monitored redox changes of silver occurring during the real SCR-NO_x reaction performance [84]. Formation of small metallic charged $\text{Ag}_n^{\delta+}$ clusters (with $n \leq 8$) from Ag^+ species during the decane-SCR-NO_x reaction occurred in both cases of the absence and presence of hydrogen in a reactant stream. Moreover, it has been found that formation of $\text{Ag}_n^{\delta+}$ clusters follows increasing conversion of NO to nitrogen, regardless of whether this conversion increase is achieved by an increase in the concentration of hydrogen or decane or even oxygen. The number of $\text{Ag}_n^{\delta+}$ clusters formed under the SCR-NO_x reaction has been estimated to be low, <5% of the total content of Ag in highly active $\text{Ag}/\text{Al}_2\text{O}_3$ catalyst. The time-resolved responses of NO_x-N₂ conversion and the number of $\text{Ag}_n^{\delta+}$ clusters to the addition/removal of hydrogen from the reactants feed clearly indicated that the number of $\text{Ag}_n^{\delta+}$ clusters did not straightforwardly correlate with the NO to N₂ conversion [84]. Finally, it is to be mentioned that CO added into the reactants also increased the number of the $\text{Ag}_n^{\delta+}$ clusters, but on contrary, did not increase NO_x-N₂ conversion [85].

So far in the literature, the highly positive effect of hydrogen on SCR-NO_x activity has been ascribed to formation of $\text{Ag}_n^{\delta+}$ clusters and these have been suggested as highly active centers in the H₂/CH_x-SCR-NO_x process. However, we provided a completely different picture on the function of silver in $\text{Ag}/\text{Al}_2\text{O}_3$. On contrary, in this study we have evidenced that the active centers for the SCR-NO_x reaction are Ag^+ ions (either single cations or small Ag_2O species). In fact the presence of hydrogen (or increased concentration of decane or oxygen) is accompanied by the increased number of small $\text{Ag}_n^{\delta+}$ clusters. $\text{Ag}_n^{\delta+}$ clusters are suggested to be formed as a result of an increased formation of oxygenates from hydrocarbons strongly adsorbed and reducing the catalyst surface [84,85].

All this implies that the enhancement of SCR-NO_x over $\text{Ag}/\text{Al}_2\text{O}_3$ by hydrogen is due to a chemical effect of hydrogen and not the result of a change in the structure of the Ag^+ active site. The acceleration of the SCR-NO_x reaction by hydrogen is suggested to originate mainly from the increased rate of oxidation of hydrocarbons and important intermediates. It is supposed that hydrogen itself participates in the SCR-NO_x reaction by its dissociation on Ag^+ ions with formation of Ag-hydride and proton sites. Ag-hydride is oxidized with NO_x with formation of

hydroperoxy and hydroxy radical species. These radical species might dramatically enhance propagation of the SCR-NO_x reaction [78,84,85].

This suggested pathway for a function of hydrogen is supported by application of H₂O₂ as ad-mixture at decane-SCR-NO_x. Hydrogen peroxide as an additive over Ag/Al₂O₃ increased significantly conversion of NO-NO₂ and yield of N₂ [78]. These results, therefore, support the suggestion that the initial step in the mechanistic pathways of the activation of SCR-NO_x by hydrogen might consist generation of highly reactive hydroxy and hydroperoxy radical species.

The thesis represents a substantial part of the European research project "Advanced nanostructured metal/metal-oxo/matrix catalysts for redox processes. Application for NO_x reduction to nitrogen" coordinated through 2001-2004 years by the J. Heyrovský Institute of Physical Chemistry, Prague. On the basis of the knowledge obtained by this thesis further extended cooperation within the EU cooperative research is in progress.

References

- [1] Encyclopedia WIKIPEDIA [online]. c2001, last revision 4 October 2005 [cit. 10 October 2005]. <<http://www.wikipedia.org/>>.
- [2] U.S. Environmental Protection Agency [online]. Last revision 10 October 2005, [cit. 10 October 2005]. <<http://www.epa.gov/>>.
- [3] R. Burch, J.P. Breen, F.C. Meunier, *Appl. Catal. B* 39 (4) (2002) 283.
- [4] F. Garin, *Catal. Today* 89 (2004) 255.
- [5] R.M. Heck, *Catal. Today*, 53 (1999) 519.
- [6] S. Sillman, *Atmospheric Environment* 33(12) (1999) 1821.
- [7] R. Burch, *Catal. Reviews* 46(3-4) (2004) 271.
- [8] M. Koebel, M. Elsener, M. Kleemann, *Catal. Today* 59 (2000) 335.
- [9] G. M. Tonetto, M. L. Ferreira and D. E. Damiani, *J. Mol. Catal. A: Chem.* 193(1-2) (2003) 121.
- [10] M. Iwamoto, H. Yahiro, N. Mizuno, *Nippon Kagaku Kaishi* 5 (1991) 574.
- [11] A. Keshavaraja, X. She, M. Flytzani-Stephanopoulos, *Appl. Catal. B* 27 (2000) L1.
- [12] F.C. Meunier, J.P. Breen, V. Zuzaniuk, M. Olsson, J.R.H. Ross, *J. Catal.* 187 (1999) 493.
- [13] N. Aoyama, K. Yoshida, A. Abe, T. Miyadera, *Catal. Lett.* 43 (1997) 249.
- [14] K.A. Bethke, H.H. Kung, *J. Catal.* 172 (1997) 93.
- [15] K. Shimizu, A. Satsuma, T. Hattori, *Appl. Catal. B* 25 (2000) 239.
- [16] K. Shimizu, J. Shibita, H. Yoshida, A. Satsuma, T. Hattori, *Appl. Catal. B* 30 (2001) 151.
- [17] H. Hamada, Y. Kintaichi, M. Sasaki, T. Ito, T. Yoshinari, *Appl. Catal. A* 88 (1992) L1.
- [18] T. Miyadera, *Appl. Catal. B* 2 (1993) 199.
- [19] X.Y. Shi, C.B. Zhang, H. He, *Chin. J. Catal.* 26(1) 2005 69.
- [20] M. Richter, U. Bentrup, R. Eckelt, M. Schneider, M.-M. Pohl, R. Fricke, *Appl. Catal. B* 51 (2004) 261.
- [21] A. Satsuma, K. Shimizu, *Progr. Energy Comb. Sci.* 29 (2003) 71.
- [22] C. Morterra, G. Magnacca, *Catal. Today* 27 1996 497.
- [23] C. Paze, G. Gubitosa, S.O. Giacone, G. Spoto, F.X. Llabres I Xamena, A. Zecchina, *Topics in Catal.* 30/31 (2004) 169.

- [24] International Zeolite Association [online], last updated: 27 September 2005 [cit. 30 September 2005]. <<http://topaz.ethz.ch/IZA-SC/StdAtlas.htm>>
- [25] Z. Gabelica, E.G. Derouane, N. Blom, *Appl. Catal.* 5(1) 1983 109.
- [26] H.van Bekkum, M. Flanigen, J.C. Jansen, *Stud. Surf. Sci. Catal.* 58 (1991) 359.
- [27] E. Seker, J. Cavataio, E. Guari, P. Lorpongpaiboon, S. Osuwan, *Appl. Catal. A* 183 (1999) 121.
- [28] A. Martinez-Arias, M. Fernandez-Garcia, A. Iglesias-Juez, J.A. Anderson, J.C. Conesa, J. Soria, *Appl. Catal. B* 28 (2000) 29.
- [29] A. Iglesias-Juez, A.B. Hungria, A. Martínez-Arias, A. Fuerte, M. Fernández-García, J.A. Anderson, J.C. Conesa, J. Soria, *J. Catal.* 217 (2003) 310.
- [30] H.-W. Jen, *Catal. Today* 42 (1998) 37.
- [31] Ch. Shi, M. Chenga, Z. Qua, X. Baoa, *Appl. Catal. B* 51 (2004) 171.
- [32] K. Masuda, K. Tsujimura, K. Shinoda, T. Kato, *Appl. Catal. B* 8(1) (1996) 33.
- [33] E.F. Iliopoulou, A.P. Evdou, A.A. Lemonidou, I.A. Vasalos, *Appl. Catal. A* 274 (2004) 179.
- [34] T. Nakatsuji, R. Yasukawa, K. Tabata, K. Ueda, M. Niwa, *Appl. Catal. B* 17 (1998) 333.
- [35] H. Beyer, P.A. Jacobs, J. B. Uytterhoeven, *Chem. Soc., Faraday Trans.* 72 (1976) 674.
- [36] T.E. White Jr., *Catalysis Rev.* 8 (1973) 117.
- [37] D. R. Brown, L. Kevan, *J. Phys. Chem.* 90 (1986) 1129.
- [38] M. Narayana, L. Kevan, *J. Phys. Chem.* 83 (1985) 2556.
- [39] T. Baba, Y. Tohjo, T. Takahashi, H. Sawada, Y. Ono, *Cat. Today* 66 (2001) 81.
- [40] A. Gedeon, R. Burmeister, R. Grosse, B. Boddenberg and J. Fraissard, *Chem. Phys. Lett.* 179 (1991) 191.
- [41] M. Richter, M. Langpape, S. Kolf, G. Grubert, R. Eckelt, J. Radnik, M. Schneider, M.-M. Pohl, R. Fricke, *Appl. Cat. B* 36 (2002) 261.
- [42] J. Texter, J.J. Hastreiter, J.L. Hall, *J. Phys. Chem.* 87 (1983) 4690.
- [43] A.N. Pestryakov, A.A. Davydov, *J. Electr. Spectr. Rel Phenom.* 74 (1995) 195.
- [44] V.S. Gurin, N.E. Bogdanchikova, V.P. Petranovskii, *Mater. Sci. Eng. C* 18 (2001) 37.
- [45] N. Bogdanchikova, F.C. Meunier, M. Avalos-Borja, J.P. Breen, A. Pestryakov, *Appl. Catal. B* 36 (2002) 287.
- [46] F.C. Meunier, R. Ukropec, C. Stapleton, J.R.H. Ross, *Appl. Cat. B* 30 (2001) 163.
- [47] T. Furusawa, K. Seshan, J.A. Lercher, L. Lefferts, K. Aika, *Appl. Catal. B* 37 (2002) 205.

- [48] S. Satokawa, J. Shibata, K. Shimizu, A. Satsuma, T. Hattori, *Appl. Catal. B* 42 (2003) 179.
- [49] J. Shibata, Y. Takada, A. Shichi, S. Satokawa, A. Satsuma T. Hattori, *J. Catal.* 222 (2004) 368.
- [50] A. Obuchi, C. Wogerbauer, R. Koppel, A. Baiker, *Appl. Catal. B* 19 (1998) 9.
- [51] S. Kameoka, T. Chafik, Z. Ukisu, T. Miyadera, *Catal. Lett.* 55 (1998) 211.
- [52] C. Li, K.A. Bethke, H.H Kung, M.C. Kung, *J. Chem. Soc., Chem. Commun.* 813 (1995).
- [53] A.D. Cowan, N.W. Cant, B.S. Haynes, P.F. Nelson, *J. Catal.* 176 (1998) 329.
- [54] J. Eng, C.H. Bartholomew, *J. Catal.* 171 (1997) 127.
- [55] H. He, Ch. Zhang, Y. Yu, *Catal. Today* 90 (2004) 191.
- [56] K. Eranen, L.-E. Lindfors, F. Klingstedt, D. Yu. Murzin, *J. Catal.* 219 (2003) 25.
- [57] K. Arve, E.A. Popov, M. Rönholm, F. Klingstedt, J. Eloranta, K. Eränen, D.Yu. Murzin, *Chem. Engineering Science* 59 (2004) 5277.
- [58] S. Satokawa, *Chem. Lett.* (2000) 294.
- [59] J. Shibata, Y. Takada, A. Shichi, S. Satokawa, A. Satsuma, T. Hattori, *Appl. Catal. B* 54 (2004) 137.
- [60] U. Bentrup, M. Richter, R. Fricke, *Appl. Catal. B* 55 (2005) 213.
- [61] M. Richter, R. Fricke, R. Eckelt, *Catal. Lett.* 94 (2004) 115.
- [62] K. Arve, E.A. Popov, F. Klingstedt, K. Eränen, L.-E. Lindfors, J. Eloranta, D.Yu. Murzin, *Catal. Today* 100 (2005) 229.
- [63] J.P. Breen, R. Burch, Ch. Hardacre, Ch.J. Hill, *J. Phys. Chem. B* 109(11) (2005) 4805.
- [64] K. Eränen, F. Klingstedt, K. Arve, L.-E. Lindfors, D.Yu. Murzin, *J. Catal.* 227 (2004) 328.
- [65] J. Shibata, K. Shimizu, Y. Takada, A. Shichi, H. Yoshida, S. Satokawa, A. Satsuma, T. Hattori, *J. Catal.* 227 (2004) 367.
- [66] R. Brosius, K. Arve, M.H. Groothaert, J. A. Martens, *J. Catal.* 231 (2005) 344.
- [67] J. Shibata, K. Shimizu, S. Satokawa, A. Satsuma, T. Hattori, *Phys. Chem. Chem. Phys.* 5 (2003) 2154.
- [68] R. Burch, J.P. Breen, C.J. Hill, B. Krutzsch, B. Konrad, E. Jobson, L. Ciderc, K. Eränen, F. Klingstedt, L.-E. Lindfors, *Topics in Catal.* 30/31 (2004) 19.
- [69] K. Arve, F. Klingstedt, K. Eränen, D. Yu. Murzin, L. Čapek, P. Sazama, J. Dědeček, B. Wichterlová, K. Svennerberg, L. R Wallenberg, J.-O. Bovin, *Phys. Chem. Chem. Phys.*, submitted.

- [70] W. Hanke, K. Möller, *Zeolites* 4 1984 244
- [71] G. Busca, V. Lorenzelli, V. Sanchez Escribano, R. Guidetti, *J. Catal.* 131 (1991) 167.
- [72] A. A. Stolov, A. I. Morozov and A. B. Remizov, *Spectrochim. Acta, Part A* 54(4) (1998) 589.
- [73] E.E. Platero, M. P. Mentrui, C. Morterra, *Langmuir* 15 (1999) 5079.
- [74] H. Knözinger, H. Krietenbrink, *J. Chem. Soc., Faraday Trans. 1* 71 (1975) 2421.
- [75] C. Thomas, L. Vivier, A. Travert, F. Maugé, S. Kasztelan, G. Pérot, *J. Catal.* 179 (1998) 495.
- [76] T. Baba, Y. Tohjo, T. Takahashi, H. Sawada, Y. Ono *Catal. Today* 66 (2001) 81.
- [77] L. Čapek, K. Novoveská, Z. Sobalík, B. Wichterlová, *Stud. Surf. Sci. Catal.* in press.
- [78] P. Sazama, B. Wichterlová, *Chem. Comm.* (2005) 4810.
- [79] N.E. Bogdanchikova, V.P. Petranovskii, R. Machorro, Y. Sugi, V.M. Soto, S. Fuentes, *Appl. Surf. Sci.* 150 (1999) 58.
- [80] W.-S. Ju, M. Matsuoka, K. Iino, H. Yamashita, M. Anpo, *J. Phys. Chem. B* 108 (2004) 2128.
- [81] A.J. Varkey, A.F. Fort, *Solar Energy Mater. Solar Cells* 29 (1993) 253.
- [82] H. Hamada, Y. Kintaichi, M. Inaba, M. Tabata, T. Yoshinari, H. Tsuchida, *Catal. Today* 29 (1996) 53.
- [83] M. Inaba, Y. Kintaichi, H. Hamada, *Catal. Lett.* 36 (1996) 223.
- [84] P. Sazama, L. Čapek, H. Drobná, Z. Sobalík, J. Dědeček, K. Arve, B. Wichterlová *J. Catal.* 232(2) (2005) 302.
- [85] B. Wichterlová, P. Sazama, J.P. Breen, R. Burch, C.J. Hill, J. Čapek, Z. Sobalík *J. Catal.* 235 (2005) 195.
- [86] B.G. Ershov, E. Janata, A. Henglein, A. Fojtik, *J. Phys. Chem* 97 (1993) 339.
- [87] T. Baba, H. Sawada, T. Takahashi, M. Abe, *Appl. Catal. A* 231 (2002) 55.
- [88] T. Baba, Y. Abe, *Appl. Catal. A* 250 (2003) 265.
- [89] J. Park, C.G. Jongsma, R. Zhang, S.W. North *J. Phys. Chem. A* 108 (2004) 10688.
- [90] J. Zhang, T. Dransfield, N.M. Donahue, *J. Phys. Chem. A* 108 (2004) 9082.
- [91] J. Smith, J. Phillips, A. Graham, R. Steele, A. Redondo and J. Coons, *J. Phys. Chem. A* 101 (1997) 9157.

Index to abbreviations and symbols

A/F	air/fuel ration
c_i	concentration of the reactant i after outlet of the reactor
c_i^0	concentration (ppm) of the reactant i before inlet of the reactor
$C_{10}H_{22}$ -SCR-NO _x	selective catalytic reduction of NO _x by decane
$C_{10}H_{22}$ -SCR-NO	selective catalytic reduction of NO by decane
$C_{10}H_{22}$ -SCR-NO ₂	selective catalytic reduction of NO ₂ by decane
DTGS	deuterated triglycine sulfat
EPA	Environmental Protection Agency
ESR	electron spin resonance
EURO	European emissions requirements
EXAFS	extended X-ray absorption fine structure
FID	flame ionisation detector
FTIR	Fourier-Transform infrared
$F(R_\infty)$	spectroscopic absorption defined by Kubelka and Munk
GC	gas chromatograph
GHSV	gas hourly space velocity h^{-1}
HC	hydrocarbons
HC-SCR-NO _x	selective catalytic reduction of NO _x by hydrocarbons
HP	Hewlett Packard
H ₂ -TPR	temperature-programmed reduction by hydrogen
IIC	Institute of Inorganic Chemistry
IUPAC	International Union of Pure and Applied Chemistry
M_n	cation of valency n
MAS NMR	magic angle spinning nuclear magnetic resonance
MFI	zeolite structure of ZSM-5 according to IUPAC
MOR	zeolite structure of mordenite according to IUPAC
MRP	member ring pore
NH ₃ -SCR-NO _x	selective catalytic reduction of NO _x by ammonia
NIR	near infrared

NO _x	nitrogen oxides
NSR	NO _x storage-reduction technique
PM	particulate matter
QC	quartz cell
R _∞	diffuse reflectance from a semi-infinite layer
RT	room temperature
SCR	selective catalytic reduction
SCR-NO _x	selective catalytic reduction of NO _x
TCD	thermal conductivity detector
TOS	time on stream
TWC	three-way catalyst
urea-SCR-NO _x	selective catalytic reduction of NO _x by urea
UV	ultraviolet
v _j	number of <i>j</i> atoms in the corresponding molecule
Vis	visible
x _i	conversion of the reactants <i>i</i>
XPS	X-ray photoelectron spectroscopy
XRD	X-ray diffraction
y _j	yield of component <i>j</i>

List of publications

Publications in International Scientific Journals

1. P. Sazama, B. Wichterlová:

Selective catalytic reduction of NO_x by hydrocarbons enhanced by hydrogen peroxide over silver/alumina catalyst.

Chemical Communications (2005) 4810 - 4811.

2. P. Sazama, L. Čapek, H. Drobná, Z. Sobalík, J. Dědeček, K. Arve, B. Wichterlová:

Enhancement of decane-SCR-NO_x over Ag/alumina by hydrogen. Reaction kinetics and in-situ FTIR and UV-Vis study.

Journal of Catalysis 232(2) (2005) 302-317.

3. O. Bortnovský, P. Sazama, B. Wichterlová:

Cracking of pentenes to C₂-C₄ light olefins over zeolites and zeotypes. Role of topology and acid site strength and concentration.

Applied catalysis A: General 287(2) (2005) 203-213.

4. B. Wichterlová, P. Sazama, J.P. Breen, R. Burch, C.J. Hill, J. Čapek, Z. Sobalík:

An *in-situ* UV-Vis and FTIR spectroscopy study of the effect of H₂ and CO during the selective catalytic reduction of nitrogen oxides over a silver alumina catalyst

Journal of Catalysis 235 (2005) 195-200.

5. L. Čapek, L. Vradman, P. Sazama, M. Herskowitz, B. Wichterlová, R. Zukerman, R. Brosius, J.A. Martens:

Kinetic experiments and modeling of NO oxidation and SCR of NO_x with decane over Cu- and Fe-MFI catalysts.

Applied catalysis B: Environmental, submitted.

Patents

1. P. Sazama, B. Wichterlová, L. Čapek, Z. Sobalík:

Proces katalytické redukce oxidů dusíku s použitím směsi uhlovodíků a peroxidu vodíku.

Patent application PV 2005-296.

Papers Presented at International Conferences

1. P. Sazama, B. Wichterlová, Z. Sobalík, J. Dědeček:

Ag active site, surface intermediates and hydrogen function at decane-SCR-NO_x over Ag/alumina.

5th Tokyo Conference on Advanced Catalytic Science and Technology, Tokyo, Japan, 23–28 July 2006, submitted.

2. P. Sazama, B. Wichterlová, Z. Sobalík, J. Dědeček:

A complex view on the role and nature of silver species operating at selective catalytic reduction of NO over silver alumina. Second International Congress on Operando Spectroscopy, Toledo, Spain, 23–27 April 2006, submitted.

3. P. Sazama, B. Wichterlová, Z. Sobalík and J. Dědeček:

Enhancement of selective catalytic reduction of nitrogen oxides over silver alumina catalyst. XXXVII Symposium on Catalysis, Prague, Czech Republic, 8-9 November 2005, Book of abstracts.

4. P. Sazama, L. Čapek, H. Drobná, Z. Sobalík, J. Dědeček, B. Wichterlová:

Hydrogen-effect in enhancement of HC-SCR-NO_x over Ag/alumina.

7th European Congress on Catalysis, Sofia, Bulgaria, 28 August – 1 September 2005, Book of abstracts.

5. P. Sazama, J. Dědeček, B. Wichterlová:

In-situ UV-Vis study of the nature and role of silver in the enhanced effect of hydrogen on SCR-NO_x over silver/alumina catalysts.

XXXVI Symposium on Catalysis, Prague, Czech Republic, 8-9 November 2004, Book of abstracts.

6. P. Sazama, B. Wichterlová:

In-situ UV-Vis-NIR spectroscopy study of the nature and role of Ag/alumina catalyst in the selective catalytic reduction of nitrogen oxides by decane and hydrogen.

EFCATS 3rd School on Catalysis, Ustroń, Poland, 21-26 September 2004, Book of abstracts.

7. P. Sazama, H. Drobná, Z. Sobalík, J. Dědeček, B. Wichterlová:
In-situ UV-Vis and FTIR study of the enhanced effect of hydrogen on SCR-NO_x over Ag/alumina catalyst.
7th Pannonian International Symposium on Catalysis, Smí, Czech republic, 12–16 September 2004, Book of abstracts.
8. B. Wichterlová, P. Sazama, L. Čapek, J. Dědeček, H. Drobná, Z. Sobalík, D. Kaucký:
A complex view on the enhanced effect of hydrogen on SCR-NO_x over Ag/alumina catalyst. In-situ UV-Vis and FTIR study at reaction conditions.
13th International Congress on Catalysis, Paris, France, 10–16 July 2004, Book of abstracts.
9. O. Bortnovsky, P. Sazama, B. Wichterlová:
Cracking of pentenes to C₂-C₄ light olefins over zeolites and zeotypes. Role of topology and acid site concentration and strength.
EuropaCat VI. Innsbruck, Austria, 31 August - 4 September 2003, Book of abstracts.

Papers Presented at Local Conferences

1. P. Sazama, B. Wichterlová:
Selective catalytic reduction of nitrogen oxides by decane and hydrogen over Ag/alumina. In-situ UV-Vis-NIR study.
Student seminar, Třešť, Czech Republic, 22–24 June 2004.
2. P. Sazama, F. Baitolow, L. Svoboda:
DSC and TG study of water adsorption on H-MFI zeolites.
Calorimetric seminar, Suchá Rudná, Czech Republic, 26-30 May 2003, Book of abstracts p.189-192.
3. P. Sazama, B. Wichterlová:
Decane-SCR-NO_x over Ag/alumina - promotion effect of H₂ on the low temperature activity.
Student seminar, Třešť, Czech Republic, 3-5 June 2003.

4. G. Franková, P. Sazama:

Study of hydration enthalpy of zeolites and bentonites.

International Czech and Slovak Calorimetric seminar, Račkova Dolina, Slovakia, 28 May – 1 June 2001, Book of abstracts p. 43.

5. G. Franková, E. Hynková, L. Svoboda, P. Sazama:

Determination characteristic properties of bentonites.

CHISA 2001, Srní, Czech Republic, 15-18 October 2001, Book of abstracts p.138.

6. G. Franková, E. Hynková, P. Sazama:

Corrosive effect of bentonites.

53. Zjazd chemických spoločností, Banská Bystrica, Slovakia, 3–6 September 2001, Book of abstracts p. 359.

7. G. Franková, E. Hynková, P. Sazama:

Calorimetric study of zeolites.

53. Zjazd chemických spoločností, Banská Bystrica, Slovakia, 3–6 September 2001, Book of abstracts p. 312.